A Study of Catalytic Carbon Dioxide Methanation Leading to the Development of Dual Function Materials for Carbon Capture and Utilization

Melis S. Duyar

Submitted in partial fulfillment of the
requirements for the degree of
Doctor of Philosophy
in the Graduate School of Arts and Sciences

COLUMBIA UNIVERSITY

2015

ABSTRACT

A Study of Catalytic Carbon Dioxide Methanation Leading to the Development of Dual Function Materials for Carbon Capture and Utilization

Melis S. Duyar

The accumulation of CO_2 emissions in the atmosphere due to industrialization is being held responsible for climate change with increasing certainty by the scientific community. In order to prevent its further accumulation, CO_2 must be captured for storage or conversion to useful products. Current materials and processes for CO_2 capture rely on the toxic and corrosive methylethanolamine (MEA) absorbents and are energy intensive due to the large amount of heat that needs to be supplied to release CO_2 from these absorbents. CO_2 storage technologies suffer from a lack of infrastructure for transporting CO_2 from many point sources to the storage sites as well as the need to monitor CO_2 against the risk of leakage in most cases. Conversion of CO_2 to useful products can offer a way of recycling carbon within the industries that produce it, thus creating processes approaching carbon neutrality. This is particularly useful for mitigation of emissions if CO_2 is converted to fuels, which are the major sources of emissions through combustion. This thesis aims to address the issues related to carbon capture and storage (CCS) by coupling a CO_2 conversion process with a CO_2 capture process to design a system that has a more favorable energy balance than existing technologies.

This thesis presents a feasibility study of dual function materials (DFM), which capture CO_2 from an emission source and at the same temperature (320^{o}C) in the same reactor convert it to synthetic natural gas (SNG), requiring no additional heat input. The conversion of CO_2 to

SNG is accomplished by supplying hydrogen, which in a real application will be supplied from excess renewable energy (solar and/or wind). The DFM consists of Ru as methanation catalyst and nano dispersed CaO as CO_2 adsorbent, both supported on a porous γ-Al_2O_3 carrier. A spillover process drives CO_2 from the sorbent to the Ru sites where methanation occurs using stored H_2 from excess renewable power. This approach utilizes flue gas sensible heat and eliminates the current energy intensive and corrosive capture (amine solutions) and storage processes without having to transport captured CO_2 or add external heat.

The catalytic component (Ru/γ-Al_2O_3) has been investigated in terms of its suitability for a DFM process. Process conditions for methanation have been optimized. It has been observed that the equilibrium product distribution for CO_2 methanation with a H_2:CO_2 ratio of 4:1 can be attained at a temperature of 280^{o}C with a space velocity of 4720 h^{-1}. TGA-DSC has been employed to observe the sequential adsorption and reaction of CO_2 and H_2 over Ru/γ-Al_2O_3. It was shown that H_2 only reacts with a CO_2-saturated Ru/γ-Al_2O_3 surface but does not adsorb on the bare Ru surface at 260^{o}C, consistent with an Eley-Rideal type reaction. In this rate model CO_2 adsorbs strongly on the catalyst surface and reacts with gas phase H_2. Kinetic tests were employed to confirm this observation and demonstrated that the rate dependence on CO_2 and H_2 was also consistent with an Eley-Rideal mechanism. A rate expression according to the Eley-Rideal model at 230^{o}C was developed.

Activation energy, pre-exponential factor and reaction orders with respect to CO_2, H_2, and products CH_4, and H_2O were determined in order to develop an empirical rate equation in a range of commercial significance. Methane was the only hydrocarbon product observed during

CO_2 hydrogenation. The activation energy was found to be 66.084 kJ/g-mole CH_4. The empirical reaction order for H_2 was 0.88 and for CO_2 0.34. Product reaction orders were essentially zero.

Table of Contents

List of Figures:

List of Tables

Acknowledgements:

I would like to thank my PhD advisor and mentor Prof. Bob Farrauto for all his guidance, motivation and support. Bob has given me countless opportunities to pursue new ideas as well as supervise researchers and his enthusiasm for teaching has always inspired me. I have been very lucky to have his constant support during my PhD, and to share his passion for the research we have done.

I would also like to thank my committee members Prof. Tuncel Yegulalp, Prof. Alissa Park, Prof. Klaus Lackner and Dr. Michel Deeba for following my research over the years and always offering vital feedback for my research. I would like to thank Prof. Yegulalp in particular for introducing me to my first research project at Columbia and for his patience and guidance during my Master's. I would like to thank Prof. Park for showing interest in my work from the beginning and for inspiring a brand new path for my research during my Qualifying exam. Prof. Lackner's insight has taught me so much over the years and will be a source of motivation as I continue academic research on CO_2 capture and utilization. I would like to thank Dr. Deeba for all his help, challenging questions, and industry insight over the span of our meetings at BASF and Columbia.

I would like to thank all the past and present members of the Catalysis for a Sustainable Environment research group for making the PhD a very enjoyable experience. I would especially like to thank Dr. Christiane Janke for not only the amazing foundation she helped develop for the CO_2 hydrogenation project, but also for being a great friend. I owe a great amount of my enthusiasm for research to Dr. Amanda Simson for always taking the time to teach me something new, and for all the reactor dance playlists. I have really enjoyed both working and hanging out with everyone in the CO_2 project, and would like to thank Mikayla Hoskins, Martha Arellano, Arvind Ramachandran, Christine Wang for all their hard work and contribution. I would like to thank Emi Leung, Angela Zhang, Yannis Valsamakis, and Federico Carneiro among the many wonderful people I have met at CSE.

I started out my research in the Combustion and Catalysis Laboratory and I would like to thank everyone I've met during my Master's. I would like to thank Prof. Marco Castaldi for trusting me to fix a broken gas turbine with two wrenches and for his insight and guidance on laboratory work. I would like to thank Tim Sharobem for failing to fix the gas turbine with me, teaching me squash and for encouraging me to rant about everything. I would like to thank Alexsandra Guerra for the dance parties in 933, Robyn Smith, Garrett Fitzgerald, McKenzie Kohn, Naomi Klinghoffer, Mariam Gadjiko among everyone else I've met.

In addition to all the wonderful people with whom I was lucky enough to work , I would also like to thank all my friends, specifically those around Columbia: Ece Erturk, Aslihan Saygili, Aysegul Yilmaz, Yasemin Uyar, Beyza Bulutoglu, Harun Ferit Ozbakir, Max Stonor, Constantine Spanos, Rob Van Haaren, Kyle Fricker, Samet Ozturk. I also appreciate Deniz Tortum for being there during this madness and all the long-distance support I've received over the years from Nazli Cem, Gulsah Mursaloglu, Goksin Ugur and Elif Naz Kayran. I would like to thank Marc Porosoff for his valuable contributions to my research and life.

My brother Suleyman and my sister in law Irem have always been there for me. I'm grateful to them for making my life in New York amazing and I hope I can make up for all the times I have postponed meeting them while writing this thesis.

Finally I would like to thank my parents Melahat Tosunoglu and Ahmet Duyar for inspiring my fascination with science and art. Their constant love, encouragement and support have made me believe in myself and there are no words to describe the love and appreciation I feel for them.

To my parents Melahat and Ahmet

Chapter 1 : Introduction

1.1 Motivation

Energy is a fundamental need in our modern society, and its consumption is projected to rise further with expected population and economic growth. This ever-increasing energy demand poses a number of challenges for the prosperity of individual nations as well as the global population. Global energy infrastructure relies heavily on fossil fuels. Fossil fuel feedstocks have varying compositions as well as an uneven geographical distribution across the world, which has resulted in both technological and political challenges. In accommodating the growing global population's energy needs, a great technological challenge lies in managing the environmental consequences of expanding use of an increasingly diverse supply of fossil fuels.

A particularly demanding task is to mitigate the effects of rising greenhouse gas emissions resulting from combustion of fossil fuels. According to the Intergovernmental Panel on Climate Change, there is widespread agreement within the scientific community that the rising concentrations of anthropogenic CO_2 in the atmosphere are responsible for increasing global average temperatures and climate change[1]. The effects of increasing atmospheric CO_2 concentrations are expected to be long lasting due to the complexity of climate feedback systems. The International Energy Agency reports that energy consumption is responsible for 69% of greenhouse gas emissions among all human activities[2]. CO_2 constitutes 90% of the greenhouse gases released from energy consumption[2]. The effort to mitigate CO_2 emissions requires both a global commitment to an emissions reduction target, as well as a concerted scientific effort in developing the necessary carbon neutral or carbon negative technologies for the global energy infrastructure.

A switch to renewable energy sources such as wind or solar energy for heat and power generation constitutes an important part of approaching carbon neutrality on a global scale. Solar energy technologies hold enormous potential to supply the world's energy needs because solar radiation provides enough energy to the Earth in 1 hour to supply the global yearly demand[3]. One challenge lies in making solar cells more efficient at harnessing this tremendous source of energy. Due to the intermittent nature of solar and wind energy, even highly efficient technologies will require viable energy storage solutions before they can be implemented on a wider scale. Non-emitting transportation solutions such as fuel cell vehicles or high energy density renewable/carbon neutral fuels for conventional vehicles are also major technological challenges along the way to a renewable energy powered society. Hence the transition to carbon neutral systems on a global level requires a tremendous collaborative effort for a wide range technological innovations.

CO_2 capture, utilization and storage (CCUS) will also need to be implemented while the world transitions towards a low carbon based energy supply. Immediate benefits of such technologies will be to slow down or prevent the accumulation of CO_2 in the atmosphere while non-emitting energy sources are developed and implemented. However, these technologies should not only be viewed as short-term solutions. If efficient CO_2 capture and utilization technologies can be developed, CO_2 can become a significant and widely available feedstock for chemical and fuel production. Renewable energy can be used to convert CO_2 to chemicals and fuels in a carbon neutral way. Widespread production of renewable fuels from CO_2 can allow existing industrial processes to function in the context of a carbon neutral economy.

The concept of utilizing CO_2 as a feedstock is also attractive because widespread implementation of CCUS technologies can be an equalizer amongst nations with varying degrees of access to fossil fuel reserves. The control of fossil fuel supply is a major force affecting economic development, and this creates political challenges on a local and global scale. Development of technologies that "recycle" carbon by converting captured CO_2 to chemicals or fuels will reduce dependence of the global economy on fossil fuel producing nations. For instance, this holds particular significance for European countries that are currently importing natural gas. Hence CCUS is a key part of tackling the climate change problem in conjunction with the further development and deployment of renewable energy technologies.

Existing technology for CO_2 capture mainly exploits the absorption of CO_2 by amine based solvents. This technology is currently being used in commercial processes such as production of ammonia and beer fermentation. The absorbent, monoethanolamine (MEA) is toxic and corrosive, and needs to be diluted with water and used as a 20-30% aqueous solution by weight[4]. The absorbent is regenerated by heating to 100-120^{o}C to release the captured CO_2[4]. The aqueous nature of the MEA absorbent causes the process to consume significant amounts of heat during regeneration due to the high heat of vaporization of water. This creates unfavorable process economics in a carbon dioxide capture and storage process. CO_2 capture constitutes the most expensive step accounting for 70-80% of the full cost of CCS [5, 6].

This thesis focuses on addressing the issues of state of the art CCUS technologies by designing a novel system for CO_2 capture and conversion. The central focus of this work is to design and develop dual function materials (DFMs) that can both capture CO_2, and at the same temperature and in the same reactor convert it to a useful product. The concept involves coupling an exothermic reaction with the endothermic CO_2 desorption step. This is demonstrated by developing materials that contain a methanation catalyst (Ru) and a reversible CO_2 solid adsorbent (nano dispersed CaO on γ-Al_2O_3). The dual function material first captures CO_2 from flue gas at a sufficiently high temperature until it is completely saturated with CO_2. The dual function material is then exposed to renewable hydrogen at the same temperature as adsorption, which methanates the CO_2 over the Ru catalyst. The methanation reaction is exothermic, and therefore generates sufficient heat to cause the CO_2 molecules adsorbed on the dispersed CaO sites to spillover to the Ru sites, where they are further methanated. Hence a completely new approach to CO_2 capture and utilization is explored by combining an exothermic and endothermic process in dual function materials to produce an energy efficient means of CO_2 capture from flue gas, while generating fuel to be recycled to the front end of the process.

1.2 Thesis Structure

This work aims to present a completely new approach to CO_2 capture and utilization. A unique dual function material concept is developed for both capturing CO_2 from an emissions source and then converting it in the same reactor at the same temperature to a useful product. This thesis focuses specifically on the proof of concept as well as optimization of dual function materials that convert captured CO_2 to synthetic natural gas (i.e. methane), so that the product stream can be recycled to the front end of the process as fuel.

The case for the development of dual function materials is made in Chapter 2. An overview of the background and existing literature is presented to summarize the issues related to increasing atmospheric CO_2 concentrations and to highlight weaknesses of the state of the art CO_2 capture, utilization and sequestration (CCUS) technologies. The role of renewable energy technologies in CCUS schemes is also explained and an argument is made to develop a joint solution to CCUS and renewable energy storage issues. Based on scientific consensus on the need to address climate change as well as the shortcomings of existing CCUS and intermittent renewable energy technologies, the dual function material concept is developed as a possible solution. While in theory dual function materials can be designed to make a variety of chemicals from captured CO_2, synthetic natural gas (SNG) is chosen as a reasonable starting point based on maturity of methanation technologies and the significant worldwide demand for natural gas as industrial and household fuel. For the proof of concept of DFMs, $Ru/\gamma\text{-}Al_2O_3$ is identified as a starting methanation catalyst, and nano dispersed $CaO/\gamma\text{-}Al_2O_3$ is chosen as an adsorbent for its suitability for operation at expected temperatures for catalytic methanation of captured CO_2.

The experimental methods used to investigate catalysis over $Ru/\gamma\text{-}Al_2O_3$ and for the development of a novel dual function material capable of capturing CO_2 and subsequently converting it to methane are presented in Chapter 3. The chapter outlines the methods used to prepare the catalyst and adsorbent materials as well as their combinations, which are then screened for suitability for the DFM concept. A thorough explanation of all catalytic experiments as well as proof of concept and characterization methods are presented in Chapter 3.

The thermodynamic limitations for CO_2 methanation are established in Chapter 4 and Ru/γ-Al_2O_3 is examined in terms of its activity and selectivity. In this chapter, reaction parameters such as temperature, gas hourly space velocity (GHSV), pretreatment conditions and the effects of catalyst reduction at different temperatures are investigated. Optimum conditions for the operation of Ru/γ-Al_2O_3 for CO_2 methanation are identified.

Chapter 5 focuses on testing the stability of the catalyst during cyclic reducing and oxidizing conditions as well as cyclic CO_2 capture and hydrogenation conditions experienced over long periods of time. The results presented are important in view of dual function material applications because the DFM is expected to experience both oxidizing (flue gas) and reducing (hydrogenation) conditions in a realistic power plant effluent. Therefore the effects of repeated oxidation and reduction and CO_2 capture and hydrogenation on Ru/γ-Al_2O_3 are examined separately to predict the stability of the catalyst. A brief investigation into how CO_2 is adsorbed on Ru/γ-Al_2O_3 at various temperatures is presented in Chapter 6.

A rate model for CO_2 methanation is developed in Chapter 7. Results from TGA-DSC and reactor experiments suggest that CO_2 and H_2 react via an Eley Rideal mechanism where CO_2 adsorbs on the catalyst and is hydrogenated by gas phase H_2. An Eley Rideal rate expression is developed to describe the kinetics of reaction for varying concentrations of CO_2 in the feed.

Kinetics of CO_2 methanation over Ru/γ-Al_2O_3 are discussed in Chapter 8. The effects of reactant and product concentrations are determined along with the apparent activation energy for methanation. An empirical rate law is developed and its implications for the design of processes using dual function materials are discussed.

Chapter 9 presents a summary of key findings in the previous chapters focusing on Ru/γ-Al_2O_3 and their implications on designing a dual function material containing Ru as methanation catalyst. This is followed in Chapter 10 with a discussion of the operation of the CaO/γ-Al_2O_3 adsorbent. Chapter 10 presents the results from previous work on CO_2 adsorption and desorption by CaO/γ-Al_2O_3 from steam and CO_2 mixtures which are relevant to the DFM application.

In Chapter 11 the preliminary TGA-DSC experiments suggesting the feasibility of DFMs consisting of nano dispersed CaO/γ-Al_2O_3 as an adsorbent and Ru as a supported catalyst are presented. Furthermore, the DFM concept is demonstrated using a physical mixture of CaO/γ-Al_2O_3 and Ru/γ-Al_2O_3 via cyclic CO_2 capture and hydrogenation experiments in a flow reactor. Results presented in Chapter 11 constitute the proof-of-concept for dual function materials for CO_2 capture and conversion.

Dual function materials consisting of Ru and nano dispersed CaO are optimized in Chapter 12 through investigation of different preparation methods and ratios of catalyst and solid adsorbent. The incipient wetness impregnation method is optimized for the preparation of dual function materials. An optimum dual function material is identified under idealized conditions where CO_2 is captured from a dilute binary gas mixture. The optimum DFM is then tested under accelerated realistic conditions where the CO_2 capture feed contains both air and steam, simulating power plant effluent. It is evaluated under these highly oxidizing conditions, where sintering of both the CaO and Ru may occur. It is demonstrated that it can withstand realistic flue gas conditions, while converting most of the captured CO_2 to synthetic natural gas. The DFM is characterized before and after accelerated cyclic tests to understand the effects of aging on the material.

It is recognized that the DFM performance can be further optimized by using other catalytic and adsorbent components. Chapter 12 investigates the possibility of using other catalytic metals in the DFM for methanation of captured CO_2. Activity tests are performed on catalysts containing Ni, Co, Rh, Pd, and Pt within the range of temperatures favorable for methanation. After comparing the activities of these precious and base metals to Ru, Rh is identified as a superior methanation catalyst. DFMs consisting of Rh and nano dispersed CaO are prepared and tested in cyclic CO_2 capture and methanation experiments. An optimum material is identified and is observed to outperform the optimum Ru CaO/γ-Al_2O_3 DFM. However, the economics of Rh use, given it expense, must be factored into the final material design.

Finally, Chapter 13 presents the conclusions of the present work. The areas of improvement and future work are identified and the DFM concept is evaluated for its suitability for real CO_2 capture and utilization projects.

Chapter 2 Background and Literature Review

2.1 Climate change and the need for carbon neutral and carbon negative solutions

Rising CO_2 levels in the atmosphere have created concerns about climate change due to greenhouse gas emissions resulting from fossil fuel based power generation and other industrial activities[5, 7, 8]. Approaches for lowering emissions of anthropogenic CO_2 in the atmosphere include switching to carbon free sources of electricity from renewable energy sources in combination with a hydrogen economy, using biomass as feedstock for chemicals, CO_2 capture from emissions sources as well as direct air capture of CO_2 from the atmosphere[5, 8-12]. It is likely that a combination of solutions will be needed to reduce CO_2 emissions across all areas of energy use, since all suggested technologies have their respective limitations.

When developing solutions to stabilize greenhouse gas concentrations in the atmosphere, it is highly unlikely that there exists a single technological innovation that will lead the world to the correct course of action. Tackling such a complex problem on a political and technological level requires the implementation of many different strategies that complement each other on the way to a carbon neutral or carbon negative economy. While the development and widespread deployment of non-emitting power generation technologies such as solar panels and wind turbines is an essential part of any course of action targeting reduced greenhouse gas emissions, there is an immediate need for carbon dioxide capture, utilization and storage technologies to reduce the risk of catastrophic climate change.

2.2 Carbon dioxide capture technologies

CO_2 capture is the first step to mitigating CO_2 emissions from existing electricity generation and industrial activities. Post-combustion CO_2 capture is the most widely studied scheme for CCUS systems although pre-combustion CO_2 capture and oxy-combustion schemes have also been proposed. Post-combustion CO_2 capture is performed on gases exiting a process and therefore enables the control of emissions without changing the process itself. Pre-combustion CO_2 capture schemes aim at designing new processes that contain an integrated CO_2 capture component prior to fuel combustion to prevent the release of CO_2 to the atmosphere. Pre-combustion CO_2 removal technologies are usually applicable to integrated gasification combined cycle (IGCC) plants, where CO_2 is produced through gasification and water gas shift reactions[10, 13]. Oxy-combustion refers to the use of pure oxygen to combust fuels, which results in a concentrated CO_2 stream at the exit of the process[14]. Post-combustion CO_2 capture techniques offer the most flexibility in terms of application and can be implemented for existing applications.

Post combustion CO_2 capture requires a sorbent capable of efficiently capturing CO_2 from a 4-14% (volume based) mixture[5]. The low concentration of CO_2 in post-combustion flue gas streams forms a significant kinetic constraint for developing capture technologies. The most common CO_2 capture technology employs liquid phase amine absorbents to scrub CO_2 from flue gas. Technologies in development mostly focus on absorbents, adsorbents and membranes.

Conventional post-combustion CO_2 capture relies on the absorption of CO_2 from a gas stream to a liquid stream. Absorption can be a physical or chemical phenomenon, driven respectively by either the solubility gradient that exists within the absorbent liquid or chemical bond formation between CO_2 and the absorbent. CO_2 scrubbing by aqueous amine solvents is the most developed of the post-combustion CO_2 capture technologies and has been used industrially since 1930 [4]. In this process, CO_2 is absorbed into an aqueous amine solution near ambient temperature[4]. The amine solution is regenerated by stripping with water vapor at 100-120^{o}C, after which the water is condensed to yield pure CO_2 [4]. Commonly used absorbents include monoethanolamine (MEA), diethanolamine (DEA) and potassium carbonate. MEA has been found to be the most efficient and widely used of the amine based absorbent options for CO_2 capture [4, 6, 15]. MEA is typically used as a baseline when comparing the performance of new absorbents or adsorbents for CO_2 capture [16]. A typical MEA solution contains 20-30% MEA in water [4, 10], the latter necessary to minimize corrosion. However, conventional absorbent technologies for CO_2 capture suffer from major drawbacks, which has led to research in the development of alternative materials. These drawbacks include the low cyclic CO_2 capture capacity of the absorbents, the corrosive nature of amine absorbents, high energy requirement for absorbent regeneration, significant losses of absorbent due to evaporation and absorbent degradation in the presence of oxygen [5].

Adsorption of CO_2 is viewed as a feasible alternative to scrubbing by absorbents. Adsorption involves the adhesion of molecules from a gas or liquid phase to a solid surface [5]. The adhesion of molecules on a solid surface instead of a liquid is what distinguishes adsorbents from absorption systems discussed earlier. The absence of water in solid adsorbents make the sorbent regeneration step less energy intensive compared to absorption technologies. Moreover, the use of a solid adsorbent eliminates the corrosion problem associated with amine-based scrubbing systems. Adsorbents can be divided into physical sorbents and chemisorbents, depending on the strength of the bond between the solid material and CO_2.

Physical adsorbents exploit the van der Waals, pole-ion or pole-pole attractions between CO_2 molecules and the solid adsorbent surface [10]. Activated carbons, carbon molecular sieves, carbon nanotube based sorbents, zeolites and metal organic frameworks (MOFs) are among the physical sorbents being investigated for their CO_2 capture properties [10]. The weak physical attraction between CO_2 and physisorbents allows for the CO_2 to be released under mild conditions. However, due to weak bond formation between CO_2 and adsorbent, physical sorbents all suffer from low selectivity for CO_2, especially in the presence of water as in the case during post-combustion CO_2 capture. Among physisorbents activated carbons possess useful properties such as being low cost, possessing high internal surface area and requiring low regeneration energy, but they nevertheless suffer from low selectivity for CO_2 adsorption due to competitive adsorption by H_2O [10]. Metal organic frameworks have also been investigated within a post-combustion CO_2 capture context[17].

Since flue gas from combustion contains air and water as well as trace impurities such as SO_x and NO_x, a post-combustion CO_2 adsorbent needs to have a high affinity for CO_2, resulting in high selectivity for CO_2 over all other components. Selectivity over water is particularly important because adsorption of water will decrease CO_2 capacity and add an energy penalty during desorption which can offset its benefits over aqueous absorbents[18]. Supported amine adsorbents have been widely investigated for their good CO_2 capture performance under humid conditions [12, 19-24]. Recent developments in adsorbents also include the integration of amine sites into metal organic frameworks to achieve a stronger chemisorption bond and therefore higher selectivity for CO_2 capture[25-27].

While solid adsorbent materials offer advantages over aqueous amine absorbents, there is still a need for further development before they can compete with MEA scrubbing. Material regeneration and working capacity of adsorbents need to be improved, their operation under flue gas conditions demonstrated and their production scaled up before they can become a technology that can be deployed. Regeneration of the sorbent inflicts an energy penalty on all existing CO_2 capture processes. Furthermore, once the sorbent releases pure or concentrated CO_2, there is a need for additional transportation and processing of the CO_2 to produce chemicals, or compression and injection into underground repositories for the prevention of its release to the atmosphere.

2.3 Storage of captured CO_2

The cost and energy intensiveness of CO_2 capture technologies are not the only obstacles limiting large-scale CCUS projects. Once CO_2 has been captured from emissions sources, it must be prevented from being released into the atmosphere. Hence a critical precondition for implementing CO_2 capture into any process is the existence of suitable technologies for handling and sequestering the captured CO_2. One widely investigated option for managing CO_2 is to find suitable reservoirs that can contain a large volume of it for a long time. CO_2 storage methods aim to contain the CO_2 to mitigate the effects of climate change until less carbon intensive industrial practices can be adopted. CO_2 sequestration can be a 'quick fix' to manage captured CO_2, thus facilitating the immediate deployment of carbon capture technologies. However, CO_2 storage methods suffer from technical and infrastructure-related issues that render their implementation inconvenient and effectiveness dubious.

Geological storage, the injection of CO_2 below non-permeable rock formations, is one way of sequestering captured CO_2. There is significant technical experience with injecting CO_2 into underground repositories as part of enhanced oil recovery (EOR) projects. However, in the case of EOR, it has not been demonstrated with any certainty that the CO_2 will stay underground for long periods of time[28]. For geological storage, the main locations under consideration are depleted hydrocarbon reservoirs, deep coal seams and saline aquifers[29]. However, if CO_2 storage is to be adopted as a major climate change mitigation strategy, it becomes clear that saline aquifers are the only geological formations capable of storing the necessary amounts of CO_2 [28].

Mineral trapping is another option explored for storage of captured CO_2. This approach involves the conversion of CO_2 into a solid mineral carbonate such as calcite ($CaCO_3$) or magnesite ($MgCO_3$) for long-term storage. Since carbonate is the most stable form of carbon, this is the most environmentally safe option for geological storage and offers the advantage of not requiring monitoring[30-32]. Tectonically exposed portions of the Earth's upper mantle, such as the ophiolites in Oman, Papua New Guinea, New Caledonia and coastal regions in the Adriatic Sea are suggested as suitable sites for mineral carbonation[33]. According to a study by

Kelemen and Matter in 2008, there are enough magnesium ions in the Samail ophiolite in Oman to contain all the CO_2 in the atmosphere in the form of magnesite[33]. Some works suggest that by performing the carbonation reactions in-situ by drilling into such geological formations, it can be possible to sustain high reaction rates due to the heat generated from carbonation[31, 33, 34].

While a variety of storage options have been proposed, the two most likely approaches are geological storage and mineral trapping. Geological storage technologies are easiest to implement because of the existing experience and technical maturity of enhanced oil recovery (EOR) projects. The Weyburn oil field in Canada[35] and Sleipner gas field in the North Sea[36] are some of the EOR sites where CO_2 storage and monitoring have been demonstrated on a large scale. This storage method nevertheless suffers from two critical issues. The CO_2 needs to be compressed, transported to the site of disposal and injected underground. Assuming that CO_2 capture is established at all point sources of emissions, this requires a pipeline infrastructure connecting all sites to a geological storage facility. This infrastructure does not currently exist, thus posing a major challenge for this technology[37]. A second technical problem faced by geological storage is to establish standards and technologies to accurately monitor the stored CO_2 to prevent leakage[37]. Accidental release of CO_2 will be devastating not only for climate change reasons but also for human health. A natural disaster in Lake Nyos in Cameroon has previously caused a rapid release of CO_2, which due to its high density sank to a nearby valley, killing 1700 people[32]. Mineral trapping is attractive because there is little risk of CO_2 leakage. However, the lack of infrastructure is also an issue because for in-situ carbonation, CO_2 captured from point sources needs to be transported to the site of disposal. Moreover, if in-situ carbonation technology cannot be scaled up in a feasible way, then mineral trapping will require mining and processing large amounts of minerals for ex-situ carbonation, which is an even more complicated technology to establish.

2.4 CO_2 utilization as a chemical feedstock and its conversion using renewable hydrogen

The problems associated with CO_2 storage can be avoided completely if CO_2 could be converted back to useful chemicals. Current industrial processes rely on some form of fossil fuel to supply either heat or raw materials for the necessary chemical reactions. In theory, renewable energy could be used to convert captured CO_2 to synthetic fuels or chemicals, thus resulting in carbon neutral industrial processes. Every fuel or chemical made from CO_2 would substitute for a fossil based fuel or chemical, thus preventing CO_2 release. This would form a type of carbon recycling scheme that decreases the need for fossil fuels for energy and raw material needs. This scheme can allow countries dependent on foreign oil and gas to secure their own energy and raw materials. Moreover, by converting CO_2 to valuable products, it would be possible to generate some revenue that can offset the cost of CO_2 capture.

Currently, CO_2 is used as feedstock in the synthesis of urea for fertilizers, salicylic acid in the pharmaceutical industry and polycarbonates for plastics[38]. When converting captured CO_2 to useful products, the price of the final product plays an important role in creating the necessary incentive for substituting CO_2 as raw material rather than petroleum based reactants such as synthesis gas. If the product has significant value it may justify the costs associated with capture. However, for purposes of climate change mitigation, the demand for the products made from

CO_2 plays an even greater role; in order for CO_2 utilization to be a viable climate change mitigation strategy the products made from CO_2 must have a large enough market to absorb a significant portion of the world's emissions. Hence a straightforward approach to tackling the world's CO_2 emissions would be to devise processes for converting CO_2 to bulk chemicals or fuels. Methanol is an important example in this respect because it can be used as additive to fuels in addition to its role in various chemical industries as a reactant[39]. Since CO_2 is mostly produced from the combustion of fuels, converting CO_2 to synthetic fuels can facilitate the recycling of a significant amount of carbon, thus allowing processes to approach carbon neutrality. However, CO_2 conversion to fuels will require a supply of energy. Hence such processes will have to utilize renewable energy sources to either electrochemically reduce CO_2 or to produce hydrogen as a reactant for thermochemical conversion of CO_2.

Due to the inherent intermittency problems with renewable electricity and difficulties in scaling up battery systems for its storage, the expansion of renewable energy projects results in excess energy that cannot be sent to the electrical grid due to insufficient demand for it. Using this excess electricity to produce hydrogen via water electrolysis (Eq.1) is considered a renewable electricity storage option[40]. If such practices are implemented, this excess renewable hydrogen can be used as reactant to convert captured CO_2 to useful products.

$$2\ H_2O \rightarrow 2\ H_2 + O_2 \qquad \text{(Eq. 1)}$$

The use of synthetic fuels made from CO_2 as carriers for excess renewable electricity offers a solution to manage fluctuating output of renewable energy while mitigating CO_2

emissions[41]. Due to the large worldwide demand of natural gas and unequal global geographical distribution of its supply, synthetic natural gas from CO_2 provides a good starting point for the development of combined renewable storage and CO_2 utilization projects. The CO_2 methanation reaction also offers the advantage of being well established in terms of technology. It is thermodynamically favorable at lower temperatures and pressures, making the process more energy efficient, given a suitable catalyst.

2.5 CO_2 methanation: The Sabatier Reaction

Naturally occurring renewable energy sources can be utilized to generate H_2 by electrolysis of water. Carbon dioxide, captured from natural gas combustion and other sources, can be combined with H_2 and catalytically converted to synthetic natural gas (SNG) or methane. SNG as an energy carrier has advantages over H_2 because it can easily be handled and transported via the existing natural gas pipeline infrastructure. The CO_2 methanation reaction is shown in Eq. 2. This process concept utilizes CO_2 as a C_1 building block to produce SNG as fuel. Consequently, the amount of imported natural gas for power generation is reduced, saving operating costs, while simultaneously reducing green-house gas emissions and avoiding the waste of renewable energy [42]. Production of synthetic natural gas (SNG) from CO_2 and renewable H_2 (via Eq.2) has been demonstrated on an industrial scale in Audi motor company's "e-gas" facility in Werlte (Germany); this facility produces 1000 metric tons/year of SNG from concentrated CO_2 obtained from a nearby biogas plant [43, 44].

$$CO_2 + 4H_2 \leftrightarrow CH_4 + 2H_2O \qquad \Delta H^o = -164 \text{ kJ/mol} \qquad \text{(Eq. 2)}$$

CO_2 hydrogenation is strongly exothermic and thermodynamically favored at low temperatures, where reaction rates are low. Thus, heat management is crucial to avoid catalyst damage and to utilize the released heat effectively. Managing heat in a fixed bed reactor can be difficult due to the tendency of hot spot formation. A highly active catalyst is required for the reaction mainly because the thermodynamic equilibrium dictates that the catalyst is required to show high activity below 350^{o}C in order to maximize the yield of methane at 1 bar and at a stoichiometric H_2/CO_2 ratio of 4. At temperatures higher than 350^{o}C, steam reforming of methane becomes thermodynamically favorable resulting in limited amounts of methane and an increase in CO and CO_2. In addition to a high catalyst activity, the catalyst must be resistant towards deactivation caused by sintering or/and carbon deposition and must survive start-up/shut-down cycles with various time-on-stream (TOS). The start/stop requirement is based on intermittent solar or wind available to produce the H_2.

In the last three decades, studies of CO_2 methanation have intensively focused on various supported catalysts. Catalysts based on Ni [45, 46], Ru [47], Rh [48-50], Pd [51-53], Fe[54] or Co [55, 56] have been identified. Carrier or supports such as Al_2O_3 [57], SiO_2 [58], ZrO_2[59], CeO_2 [60], La_2O_3 [61], MgO [62], TiO_2 [63], carbon materials [64] and zeolites [65] have been used to support the active metals. Doping and promoting effects have been evaluated as well [66-68]. Among these catalytic systems, Ru was chosen as the catalytic component for developing and demonstrating the DFM concept due to its high activity per gram and relatively low cost compared to other precious metal alternatives. Furthermore, as will be shown later, its redox chemistry is consistent with the operation of DFM, which is not the case for most of the other metals.

Kinetics and mechanism of CO_2 hydrogenation to CH_4 over Ru catalysts have been investigated before by many researchers[69-79]. Particular emphasis was placed on the hydrogenation of CO_2 in CO_2/CO mixtures, due to the possible implications on using methanation for CO removal in reformate gas streams[69-71, 78]. The reaction intermediate for CO_2 hydrogenation has been widely discussed in the literature. There has generally been disagreement between studies identifying the intermediate surface species as an adsorbed formate, and those that have claimed that the intermediate is adsorbed CO resulting from the dissociative adsorption of CO_2[69]. For instance, Eckle et al. have concluded via DRIFTS that CO_2 dissociatively adsorbs on the surface of Ru/Al_2O_3 to form $CO_{(a)}$ and $O_{(a)}$, which are then hydrogenated[69]. This work also rules out any redox mechanism for the conversion of CO_2 to $CO_{(a)}$ and $O_{(a)}$ because of the irreducible nature of the support[69]. Through DRIFTS and mass spectrometry Marwood et al. have also determined that for Ru/TiO_2 adsorbed CO is the key intermediate that leads to methane formation[72]. However, they argue that CO is formed from a formate species, resulting from the reaction of adsorbed CO_2 with H_2 dissociated on metal sites[72]. The role of the hydrogen has also been under considerable debate. For the methanation of CO_2 over Ru/TiO_2, Marwood et al. have suggested a mechanism whereby H_2 is dissociated on the metal and reacts with adsorbed CO_2 to form a formate species which decomposes to CO[72]. In another study on Ru/TiO_2, Marwood et al. have determined through DRIFT spectroscopy that through the reverse water gas shift reaction H_2 facilitates the dissociation of CO_2 to $CO_{(a)}$, and that $CO_{(a)}$ formation is the rate determining step of methanation [73].

While there exists a large volume of work investigating the kinetics and mechanism of CO_2 methanation, there is still debate on the nature of the key and spectator surface species as well as the rate determining step for methanation. This thesis investigates the adsorption of reactants and kinetics of reaction over Ru/γ-Al_2O_3 focusing specifically on the interpretation of results in light of CO_2 utilization and renewable energy storage applications. A particular emphasis is placed on the development of dual function material (DFM), where CO_2 is adsorbed onto the catalyst from a dilute stream and then hydrogenated with a subsequent exposure to H_2, in two consecutive steps.

2.6 Design of a dual function material for CO_2 capture and catalytic conversion

The shortcomings of the existing CO_2 capture technologies, lack of infrastructure to transport captured CO_2, and uncertainties regarding storage schemes constitute the main motivations behind the present work. There is a need for energy efficient CO_2 capture processes and this can be achieved by replacing the thermal swing process (adsorption of CO_2 at a low temperature and its separation at a higher temperature) with one that operates isothermally. The necessary heat for the desorption of CO_2 can be supplied by coupling it to an exothermic reaction for the conversion of CO_2 to methane. The dual function material concept is inspired by the need to simplify our approach to CO_2 capture and utilization. The simplicity of design comes from using an isothermal process for capturing CO_2 and from releasing CO_2 as a product (methane) for which the transportation and industrial infrastructure is present on a global scale.

Furthermore, the output of the process is synthetic natural gas, which is indistinguishable from the widely used natural gas fuel for industrial and household applications. This means CO_2 is not only recycled effectively back to the sources of its production, but also that there is a revenue stream to be generated from selling the synthetic natural gas.

The principal goal of the present work is to design and optimize dual-function materials (DFM) that offer a unique renewable energy storage solution by producing SNG directly from industrial flue gas (dilute CO_2), while eliminating the energy requirement, corrosion and transportation issues associated with existing CCUS technologies. The DFM process utilizes H_2 produced via electrolysis using renewable electricity (wind, hydro, geothermal and/or solar) to make synthetic natural gas catalytically via the methanation reaction. Hence DFMs can be used to devise a carbon recycling scheme within combustion based (or other CO_2-generating) industries while integrating more renewable energy into the grid.

The total dual function conceptual process for CO_2 capture and utilization is shown in Figure 2.1. The DFM process operates at a temperature below 350°C to maximize conversion of CO_2, using heat recovered from the flue gas, eliminating the need for externally added energy. It is housed inside one reactor, which adsorbs CO_2 until saturation and subsequently converts it to synthetic natural gas (SNG) catalytically with Ru by the addition of stored renewable H_2 . Both adsorption of CO_2 and its methanation are conducted in the same reactor at the same temperature simplifying the entire process of capture and product production. The resultant SNG + H_2O product is compressed, dried and the methane recycled to the front end of the process or the natural gas grid.

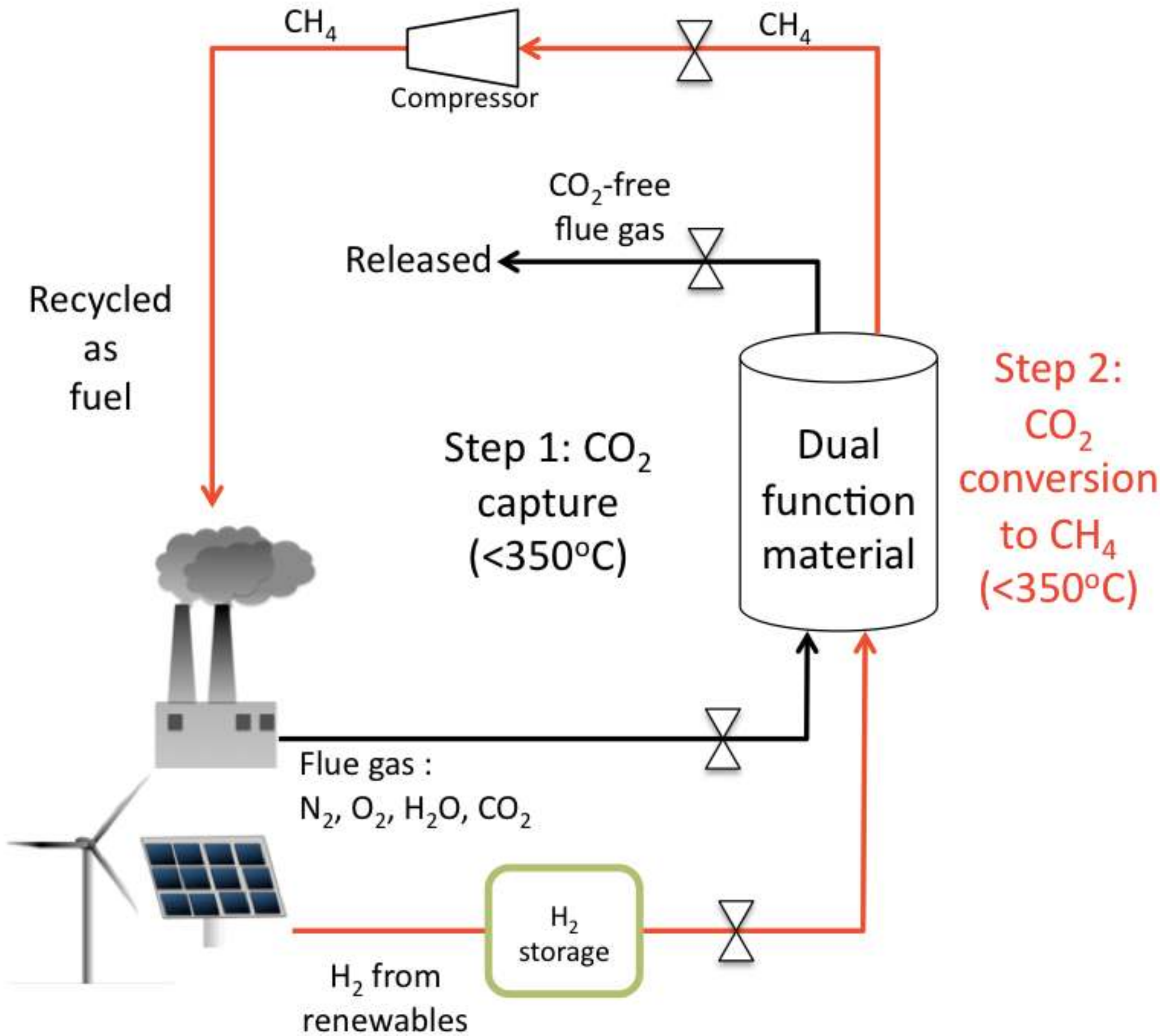

Figure 2.1: Process diagram for CO_2 capture and recycle as synthetic natural gas (CH_4) to an industrial facility. The CO_2 saturating the adsorber is methanated to CH_4 (SNG) in the same reactor. While this is shown as two separate process steps, they both occur in the same reactor and at the same temperature.

A theoretical process where CO_2 is captured directly from ambient air using a K_2CO_3/Al_2O_3 composite sorbent and catalytically methanated at a higher temperature using renewable H_2 has been suggested in the literature[80]. In their publication, Veselovskaya et al. calculated the theoretical energy storage efficiency for their suggested process as 52%, based on energy requirements for thermal swing and water electrolysis[80]. This idea is also mentioned in the work by Derevschikov et al., which focuses on direct air capture using K_2CO_3/Y_2O_3 sorbents [81]. Xie et al. have developed and experimentally demonstrated the use of conjugated microporous polymers for CO_2 capture and subsequent conversion under ambient conditions to propylene carbonate, a chemical used in the pharmaceutical industry[82]. Yang et al. have reviewed the use of CO_2 as C1 feedstock and suggested the direct conversion of captured CO_2 to commodity chemicals within amine based absorbent or adsorbents as a means of overcoming current problems associated with CCS[83]. Although the chemical conversion of CO_2 as a means to offset the costs of CO_2 capture has previously been considered in the literature, this thesis presents the first experimental demonstration of a simple isothermal CO_2 capture and methanation process that operates in a single reactor at the same temperature. Moreover, by producing synthetic natural gas the DFM process ideally approaches carbon neutral power generation.

Since synthetic natural gas is produced through the exothermic CO_2 methanation reaction, it supplies the necessary energy for CO_2 desorption from the sorbent component of the DFM. Hence when the DFM is saturated with CO_2 and exposed to H_2, a spillover process occurs, which drives the chemisorbed CO_2 to catalytic sites for further methanation. In this way the DFM is regenerated at the end of each cycle.

2.7 $CaO/\gamma\text{-}Al_2O_3$ as reversible CO_2 adsorbent for combined CO_2 capture and catalytic conversion

Calcium oxide offers good CO_2 capture capacity and kinetics at high temperatures by undergoing the reversible carbonation reaction.

$$CaO(s) + CO_2(g) \leftrightarrow CaCO_3(s) \qquad \text{(Eq. 3)}$$

The carbonation reaction is initially fast, where it is controlled by chemical kinetics. As the reaction proceeds, the product layer (i.e. $CaCO_3$) on the surface of CaO particles imposes a diffusion limitation which slows the rate of reaction[84]. Thus the formation of $CaCO_3$ prevents most of the CaO from contacting CO_2 and lowers the CO_2 capture efficiency. Decomposition of $CaCO_3$ to CaO is thermally intensive (~800^{o}C), and is believed to cause sintering, which reduces the available pore area for reaction and reduces the activity of sorbent after multiple cycles of capture and regeneration[85].

A unique adsorbent has previously been developed for use in in-situ CO_2 capture applications by dispersing CaO on a $\gamma\text{-}Al_2O_3$ carrier in an effort to overcome the limitations associated with bulk CaO [85-87]. The "nano dispersed CaO" ($CaO/\gamma\text{-}Al_2O_3$) behaves radically different compared to bulk or unsupported CaO. Its dispersion onto a carrier creates nano-sized islands of CaO, which reversibly chemisorb CO_2, capturing and releasing it at moderate temperatures (~300^{o}C). This is a very significant improvement compared to bulk CaO, which forms carbonates that decompose at ~800^{o}C[86, 87]. The high dispersion of CaO particles on the γ-Al_2O_3 support minimizes sintering allowing the dispersed CaO sorbent to maintain a stable CO_2 capture capacity over many cycles of capture and release[86].

It has previously been shown that CaO dispersed as nano-particles (~ 3 nm) on γ-Al_2O_3 provides some novel properties which make this material suitable for in situ capture of CO_2 during the catalytic water gas shift reaction. CaO/γ-Al_2O_3 is an attractive sorbent because it consists of one of the most abundant oxides in nature supported on an inexpensive and ubiquitous catalyst support[86]. Moreover, it is prepared via a common incipient wetness impregnation technique employed by the catalyst industry and therefore can easily be integrated into catalytic production systems. The alumina support also allows this material to be thermally stable in a cyclic CO_2 capture and regeneration operation[86]. CaO/γ-Al_2O_3 has also shown stable performance as a washcoat in monolithic systems for in-situ CO_2 capture to enhance the water gas shift reaction[87]. Moreover, the adsorbent can be regenerated in a partial pressure swing operation; once saturated with CO_2, CaO/γ-Al_2O_3 can release CO_2 at low temperatures (~350-500^{o}C) when CO_2 is removed from the feed stream.

Based on its reversible adsorption characteristics, good performance in the presence of steam, and ease in implementation in catalytic production systems, CaO/γ-Al_2O_3 was deemed appropriate for the demonstration of the dual function material concept. It is also a critical advantage that reversible adsorption/desorption of CO_2 over CaO/γ-Al_2O_3 has already been demonstrated at temperatures high enough to allow for catalytic reactions with CO_2 to proceed [86, 87]. The unique properties of nano dispersed CaO/γ-Al_2O_3 make it an excellent reversible

CO_2 adsorbent for use at temperatures between 300 and 650^oC, which is a perfect range for performing catalytic reactions with CO_2[86].

Chapter 3 : Experimental Methodology

3.1 Material synthesis

3.1.1 Preparation of Ru/γ-Al_2O_3 catalyst

Ru/γ-Al_2O_3 was supplied by BASF and was synthesized by incipient wetness impregnation of γ-Al_2O_3 with an aqueous solution of Ruthenium (III) nitrosyl nitrate. The Ru-loading was adjusted to 10 wt.%. The impregnated powder was dried at 120^oC and calcined in air at 250^oC for 2 hours to decompose the precursor salt. The calcination temperature of 250^oC was chosen to prevent the formation of volatile ruthenium oxides, which become favorable at higher temperatures. The catalyst was used either as received or exposed to a pre-reduction protocol as indicated for each experiment. The internal surface area of the fresh catalyst was determined as 51 m^2/g via single-point BET analysis.

3.1.2 Preparation of CaO/γ-Al_2O_3 adsorbent

The adsorbent used for the cyclic CO_2 capture and utilization studies was a nano dispersed CaO/γ-Al_2O_3. CaO was dispersed on a high surface area γ-Al_2O_3 support (SBA 150 from SASOL) using the incipient wetness technique. The γ-Al_2O_3 support was impregnated using $Ca(NO_3)_2$ as CaO precursor. The powdered sample was then dried in air for 3 hours at 200^oC and calcined in air for 4 hours at 500^oC. A loading of 10% (by mass) CaO on γ-Al_2O_3 was used for the thermogravimetric analysis (TGA) experiments.

For flow through reactor experiments demonstrating CO_2 adsorption and desorption in the presence of steam, 8.4% $CaO/\gamma\text{-}Al_2O_3$ was supported on Corning ceramic monoliths 0.75 inches in diameter with cell densities of 400 cells/in^2. Each monolith was washcoated with adsorbent to achieve a thin, uniform coating on the walls of the monolith channels. This process involves dipping the monolith in an aqueous slurry removal of excess slurry with a purge of air and heat treatment to ensure adhesion. The adsorbent slurry was prepared using a 25% (by weight) solution of ethanol as a base and a solids ($CaO/\gamma\text{-}Al_2O_3$) content of 26.7%. The adsorbent slurry was ball milled overnight. In each case the slurry was milled for 24 hours and the particle size distribution was measured using laser diffraction. Slurries with average particle size below 10 µm showed good adhesion on monoliths. The monoliths were dried in air at 180^{o}C for 3 hours. If multiple washcoats were needed to achieve a higher loading of adsorbent on the monolith, the latter was dipped in slurry again after drying. Once all coatings had been applied, a final calcination was performed for 5 hours in air at 550^{o}C to fix the washcoats on the monolith. The weight loading was determined by subtracting the weight of the uncoated monolith from the coated sample.

3.1.3 Preparation of Ru $CaO/\gamma\text{-}Al_2O_3$ dual function materials

Ru and CaO based dual function materials were prepared by incipient wetness impregnation of either $Ru(NO)(NO_3)_2$ on 10 wt.% $CaO/\gamma\text{-}Al_2O_3$ or of $Ca(NO_3)_2$ on 10 wt.% $Ru/\gamma\text{-}Al_2O_3$. A naming convention was adopted for these samples to indicate which impregnation order was followed. Samples prepared by impregnation of $Ru(NO)(NO_3)_2$ on 10% $CaO/\gamma\text{-}Al_2O_3$ are referred to as x% Ru 10% $CaO/\gamma\text{-}Al_2O_3$, where x denotes the loading of Ru (by weight) in the sample. Samples prepared by impregnation of $Ca(NO_3)_2$ on 10% Ru/γ-Al_2O_3 are referred to as y% CaO 10% Ru/γ-Al_2O_3 where y denotes the loading of CaO in the sample by weight.

All samples were dried in air at 120°C for 1 hour and calcined in air at 250°C for 2 hours. This pretreatment ensured the decomposition of $Ru(NO)(NO_3)_2$ to Ru. The DFMs received in-situ pre-reduction in 4%H_2/N_2 at 320°C for 2 hours at the beginning of each reactor test to ensure decomposition of $Ca(NO_3)_2$ to CaO and reduction of any oxides of Ruthenium.

3.1.4 Preparation of supported Pt, Rh, Pd, Ni and Co catalysts

To compare the catalytic activity of Ru/γ-Al_2O_3 with other potential catalysts, several precious and base metals were supported on γ-Al_2O_3 (SBA-150). All catalysts were prepared using the incipient wetness technique and the metal loading in all catalysts was 10% by weight. Pt/γ-Al_2O_3 was prepared using a proprietary water soluble Pt salt provided under a secrecy agreement from BASF. Rh/γ-Al_2O_3, Pd/γ-Al_2O_3, Ni/γ-Al_2O_3, Co/γ-Al_2O_3 were prepared using Rhodium (III) nitrate, Palladium (II) nitrate, Nickel (II) nitrate, Cobalt (II) nitrate precursors respectively. All catalysts were dried in air at 120°C for 2 hours and calcined in air at 250°C for 2 hours. This preparation method resulted in catalysts with similar BET surface areas, as shown in Table 3.1.

Table 3.1: BET surface areas for supported precious and base metal catalysts prepared through incipient wetness impregnation

Catalyst	BET surface area (m^2/g)
10% Pt/Al_2O_3	117.4
10% Rh/Al_2O_3	105.4
10% Pd/Al_2O_3	118.7
10% Ni/Al_2O_3	102.9
10% Co/Al_2O_3	109.1

3.1.5 : Preparation of Rh $CaO/\gamma\text{-}Al_2O_3$ dual function materials

Rh and CaO based dual function materials were prepared by incipient wetness impregnation of varying amounts of Rhodium (II) nitrate on 10 wt.% $CaO/\gamma\text{-}Al_2O_3$. All samples were dried in air at 120°C for 1 hour and calcined in air at 500°C for 2 hours. This pretreatment ensured the decomposition of the rhodium precursor to rhodium metal. The DFMs received in-situ pre-reduction in 4%H_2/N_2 at 320°C for 2 hours at the beginning of each reactor test to ensure decomposition of $Ca(NO_3)_2$ to CaO and reduction of any oxides of rhodium.

3.2 Standard Characterization Methods

3.2.1 BET Surface Area

A ChemBET Pulsar TPR/TPD unit (Quantachrome) was used to measure single-point BET surface area for fresh and spent catalyst samples. The sample was placed inside the U shaped sample holder of the ChemBET Pulsar TPR/TPD unit and degassed for 1 hour to remove any adsorbed vapors in the sample. The BET surface area was subsequently measured at 77 K. Three measurements were made for each sample.

3.3 Characterization of Ru/γ-Al_2O_3

3.3.1 CO Chemisorption on Ru/γ-Al_2O_3

CO chemisorption was performed using a ChemBET Pulsar TPR/TPD unit (Quantachrome). The sample was placed inside the U shaped sample holder of the ChemBET Pulsar TPR/TPD unit and degassed to remove any adsorbed vapors from the sample. Subsequently, the sample was reduced in-situ, in 4 % H_2/N_2 (60 mL/min). When analyzing fresh Ru/γ-Al_2O_3, the effect of reduction at different temperatures was investigated by maintaining the temperature during in-situ reduction at either 250, 320, 350, or 550^{o}C for 1 h. For spent catalyst samples collected from various catalytic tests, a fixed reduction temperature of 320^{o}C was chosen as an optimum temperature based on TPR studies. Following reduction, the sample was brought to room temperature in helium. CO (100% purity) chemisorption of pretreated samples was performed at RT.

3.4 Characterization of Dual Function Materials

3.4.1 H_2 Chemisorption on Dual Function Materials

The dispersion of the catalyst metal component in DFMs was determined via H_2 chemisorption. H_2 Chemisorption experiments were performed using a ChemBET Pulsar

TPR/TPD unit (Quantachrome). The fresh or spent 5%Ru 10%CaO/γ-Al_2O_3 sample was placed inside the U shaped sample holder of the ChemBET Pulsar TPR/TPD unit and degassed to remove any adsorbed vapors in the sample. Subsequently, the sample was reduced in-situ, in 4 % H_2/N_2 (60 mL/min) at a temperature of 320^oC for 2 h. Following reduction, the sample was cooled to room temperature in helium. H_2 (100% purity) chemisorption of pretreated samples was performed at room temperature.

3.4.2 CO_2 Chemisorption on Dual Function Materials (Ru CaO/γ-Al_2O_3)

The dispersion of CaO in DFMs was determined via CO_2 chemisorption. CO_2 Chemisorption experiments were performed using a ChemBET Pulsar TPR/TPD unit (Quantachrome). The fresh or spent 5%Ru, 10%CaO/γ-Al_2O_3 sample was placed inside the U shaped sample holder of the ChemBET Pulsar TPR/TPD unit and degassed to remove any adsorbed vapors in the sample. Subsequently, the sample was reduced in-situ, in 4 % H_2/N_2 (60 mL/min) at a temperature of 320^oC for 2 h. Following reduction, the sample was cooled to room temperature in helium. CO_2 (100% purity) chemisorption of pretreated samples was performed at room temperature.

CO_2 chemisorption was also performed on a sample of γ-Al_2O_3 as background to correct dispersion measurements for CO_2, which may be adsorbed on the support. It was assumed that each CO_2 adsorbed on one Ru site. It was assumed that H_2 chemisorption takes place only on Ru sites and that each H_2 molecule occupies 2 Ru sites. CO_2 chemisorption was used to calculate the total Ru and CaO sites, as well as sites associated with the support. CaO dispersions were calculated by subtracting from the total number of sites those of Ru (determined by H_2 chemisorption) and support sites (determined by CO_2 chemisorption on γ-Al_2O_3).

3.4.3 Temperature Programmed Desorption (TPD)

TPD was performed on spent DFM samples (from the cyclic test described in section 3.7.5) using a ChemBET Pulsar TPR/TPD unit (Quantachrome) to determine the retention of CO_2 on the DFM. The spent dual function material was heated from room temperature to a final temperature of 1000°C in a flow of helium (100 mL/min) with a heating rate of 5°C/minute. The thermal conductivity of gases released was measured via a thermal conductivity detector (TCD). A cold trap placed upstream from the TCD was used to condense the any water liberated from the sample. A calibration was performed separately where known volumes of CO_2 were injected (at room temperature) and TCD signals recorded. This calibration data was used to convert the thermal conductivity signal (in units of mV) to volume of CO_2 released. The TCD used for these experiments is capable of measuring thermal conductivity with less than 1% relative error.

3.5 Catalytic and adsorption tests on Ru/γ-Al_2O_3

3.5.1 Catalytic activity testing in a flow reactor

Catalytic tests were performed in a fixed bed quartz reactor with an inner diameter of 12 mm at 1 bar. The catalyst was pressed to pellets and crushed and sieved to obtain a particle fraction of 610-700 μm in diameter. The reactor was loaded with 1 volume catalyst to 1.25

volumes of quartz to maintain uniformity of temperature and isothermal conditions. The space velocity GHSV, was varied from 4720 h^{-1} to 84 000 h^{-1}. The temperature at the exit of catalyst bed was measured and is defined as hydrogenation reaction temperature. The diluent should insure isothermal conditions in the bed. The temperature of the furnace was controlled by an additional thermocouple, placed at the inlet of the catalyst bed. A reaction mixture of 4 Vol.-% CO_2, 16 Vol.-% H_2 (4 H_2/1 CO_2) with He as the balance was used. The flow was controlled by a rotameter. Water was condensed at the reactor exit to allow measurement of product gases (CH_4, CO, CO_2, and H_2) by micro GC . The water level in the cold trap was low enough to prevent absorption of any gases. The reaction mixture was heated to the desired inlet temperature varied from 160°C to 320°C. A blank test with only quartz beads showed no conversion of H_2 or CO_2. Analysis of the product distribution was performed on-line with a micro GC (GC 3000 A, Agilent) equipped with a Molsieve column to measure H_2, He, CH_4 and CO concentrations. A Plot U column was used to detect CO_2. An OV-1 column and alumina column was used to monitor the formation of light hydrocarbons and olefins. Neither olefins nor C_1+ hydrocarbons were detected under any reaction conditions. Helium was used as an internal standard for all GC measurements. Results in this work are given in Vol.-% on a dry basis including the He concentration.

3.5.2 Kinetic testing in a differential reactor

A fixed bed quartz reactor with an inner diameter of 12 mm was used at a pressure of 1 atm. The catalyst was pressed to pellets and crushed and sieved to obtain a particle fraction of 610-700 μm in diameter. The reactor was loaded with 0.1 mL catalyst and 0.1 mL quartz.

Catalytic tests were operated with low conversions to ensure differential conditions and minimize temperature increases in the bed. Quartz is an inert solid and was used to dilute the catalyst to further absorb the heat produced and to prevent hot spots. The gas hourly space velocity (GHSV) was adjusted to maintain differential conditions (<10% conversion) and varied between 90 000 - 262 920 hr^{-1}. The temperature of the furnace was monitored by a K-type thermocouple (Omega), placed at the inlet of the catalyst bed, and controlled using an Omega CN 7800 series temperature controller. Mixtures of H_2, CO_2 and He were used to determine the order of reaction with respect to H_2 and CO_2. The products CH_4 and H_2O were also mixed into the feed to determine their kinetic influence. Flow rates of all gas phase species were controlled by mass flow controllers (Aalborg). Water was introduced using a syringe pump (KD Scientific) into a heated line kept above 100°C and connecting to the furnace. In all experiments water was condensed at the exit to allow measurement of product gases (CH_4, CO, CO_2, and H_2) using a micro GC. The water level in the cold trap was low enough to minimize absorption of species. Analysis of the product distribution was performed on-line with a micro GC (Agilent Quad) equipped with a Molsieve column to measure H_2, He, CH_4 and CO concentrations. A Plot U column was used to detect CO_2. No CO was detected during these tests. Carbon balances were calculated for each data point using helium as internal standard and were consistently between 99 and 101%.

3.5.3 Cyclic temperature programmed oxidation/reduction (TPO/TPR) via TGA-DSC

The cyclic temperature-programmed-oxidation-reduction studies, a combination of alternating TPO and TPR cycles were performed with fresh 10% Ru/γ-Al_2O_3 powder in a Jupiter

STA 449 F3 instrument (Netsch). Typically, 50 mg of the catalyst powder was placed into an alumina crucible and a blank test performed prior to the measurement with an empty cell under the experimental reaction condition. The sensitivity calibration for the DSC mode was performed in a flow of N_2 using In, Sn, Bi, Zn and Al as the calibration standard.

For the cyclic TPR/TPO study, the fresh sample was exposed first to 2 % H_2/N_2 and the temperature was raised with a ramp of 5 K/min to 320°C (TPR). After cooling in N_2 to room temperature the catalyst was exposed to 1 % O_2/N_2 and the temperature was raised to 320°C (TPO) with 5 K/min. The TPO and TPR tests were applied consecutively 3 times each (6 cycles in total) to the catalyst to obtain information about the redox-properties and indirectly the sintering resistance of the catalyst.

3.3.2 Cyclic CO_2 adsorption/hydrogenation tests via TGA-DSC

The cyclic hydrogenation test in CO_2/N_2 and H_2/N_2 was performed isothermally in a thermogravimetric analysis and differential scanning calorimetry (TGA-DSC) instrument from Netszch (STA449 F3 Jupiter). After treating the 10% Ru/γ-Al_2O_3 sample at 320°C in 2 % H_2/N_2, the catalyst was exposed initially to 0.5 % CO_2/N_2 at 260°C for 90 min, followed by a purge in pure N_2 for 30 min and finally to 2 % H_2/N_2 for 90 min. One full hydrogenation cycle consists of CO_2 adsorption and subsequent H_2 treatment (methanation) with a N_2 purge in-between. 20 cycles were conducted consecutively. The weight loss and gain in the thermogram and the exothermic signals in the heat flux function from the DSC mode were used as an indication of hydrogenation activity. The WHSV in this cyclic test was 14.4 $Lh^{-1}g^{-1}$. For comparison catalytic activity in the fixed bed reactor over $Ru/\gamma\text{-}Al_2O_3$ particulates, the highest space-velocity (84 000 h^{-1}) corresponds to a WHSV of 88.6 $Lh^{-1}g^{-1}$ and the lowest (4720 h^{-1}) to a WHSV of 5.1 $Lh^{-1}g^{-1}$.

In addition, inter-cycle reduction at 320°C in $2\%H_2/N_2$ was performed between each hydrogenation cycle. This was done to investigate whether the Ru sites were oxidized due to dissociation of adsorbed CO_2. Since RuO_x is not active for CO_2 methanation, this inter-cycle reduction is considered a method of catalyst regeneration.

The CO_2 uptake capacity for each cycle relative to the capacity in the first cycle was calculated to judge the success of the inter-cycle reduction (at 320°C in 2% H_2/N_2). It was derived from Eq. 4 shown below:

$$\text{Relative } CO_2 \text{ uptake capacity} = (\Delta w_n/\Delta w_1) * 100\% \qquad \text{(Eq. 4)}$$

where Δw_n is the weight gain during CO_2 introduction in cycle n and Δw_1 is the weight gain during CO_2 introduction in the first cycle. Weight gains observed during CO_2 introduction periods were assumed to be associated only with the chemisorption of CO_2 on the catalyst.

3.6 CO_2 adsorption/desorption studies with $CaO/\gamma\text{-}Al_2O_3$

3.6.1 Thermogravimetric analysis (TGA) of CO_2 adsorption and desorption

Thermogravimetric analysis was performed on powdered samples of $CaO/\gamma\text{-}Al_2O_3$ containing 10% CaO by mass using a Netsch STA449 F3 Jupiter type TGA. In all experiments, the sample was first heated to 350°C in nitrogen. In the experiment aimed at determining the optimum temperature for regenerating the sorbent, CO_2 capture was initiated at a temperature of 350°C from a feed consisting of 10% CO_2 and balance N_2 by volume. After 30 minutes the feed was switched to 100% N_2 under isothermal conditions. After being exposed to pure nitrogen at 350°C for 30 minutes, the temperature was increased using a ramp of 5K/min up to 600°C to determine the temperature at which all captured CO_2 is released. In the experiments where the effect of exposure to steam on CO_2 capture was investigated, the sample first received either a 'steam treatment' in a flow of 10% steam (balance N_2) or no treatment (100% N_2), both at 350°C for 30 minutes. This was followed by a period of CO_2 capture from a 10% CO_2/N_2 mixture at 350°C for 60 minutes. At the end of each test the sample was cooled to room temperature in N_2.

3.6.2 CO_2 adsorption and desorption in a flow reactor using $CaO/\gamma\text{-}Al_2O_3$//monolith samples

A laboratory scale flow-through reactor was used to test the adsorption/desorption behavior of CO_2 on $CaO/\gamma\text{-}Al_2O_3$ monoliths. Monoliths (Corning, 400 cells per square inch) were housed inside a quartz tube and temperature inside this reaction zone was controlled using a tube furnace (Thermocraft) connected to a variable transformer. Steam was generated by means of a syringe pump (KD Scientific) injecting distilled water into a heated (~130°C) reactant stream. Product analysis was performed using a micro-GC (Agilent Quad). Steam in the product mixture was condensed prior to entering the micro-GC. Pre-heating of the reactants prior to entering the furnace and the products prior to entering the condenser was achieved using heat tape (Omega STH101-040) controlled by variable transformers.

The reactor was operated in two cycles, which are referred to in this study as 'capture' and 'regeneration'. Only the reactor feed was changed when the cycle was switched; during 'capture', the waschoated monoliths were exposed to a mixture of carbon dioxide, nitrogen and steam, whereas during 'regeneration' the carbon dioxide flow was shut off while the nitrogen and steam flow rates remained unchanged. In all 'capture' cycles, the CO_2 concentration was maintained at 10% in the reactant mixture, whereas steam concentrations varied from 0 to 28%. In 'regeneration' cycles, steam content in the feed varied from 0 to 48%.

During the 'capture' cycles, the adsorption capacities of $CaO/\gamma\text{-}Al_2O_3$ coated monoliths were tested under conditions with varying steam concentration at a temperature of 350^oC. This was a preliminary test to understand how process conditions such as temperature and steam concentration would affect the performance of the adsorbent. 'Regeneration' cycles enabled detection of the CO_2 released in response to decreasing CO_2 partial pressure to zero. Desorption of CO_2 at 350^oC under various steam concentrations was examined.

3.7 CO_2 capture and methanation studies with DFMs

3.7.1 Proof of concept studies for DFM in a flow reactor

A reactor identical to the one described in section 3.5.1 was used to demonstrate proof of concept for dual function materials. A physical mixture of 10 wt.% $CaO/\gamma\text{-}Al_2O_3$ and 10 wt.% $Ru/\gamma\text{-}Al_2O_3$ was packed into a fixed bed reactor. The mixture contained 0.4255 g $CaO/\gamma\text{-}Al_2O_3$

and 0.4008 g Ru/γ-Al_2O_3. The reactor was operated in a cyclic manner; 5 cycles each were performed at 260 and 320^oC. Each cycle consisted of a 'CO_2 capture' period where a 10% CO_2 in N_2 mixture with a total flow rate of 10.3 mL/min was introduced to the reactor. This was followed by a 'methanation' period, where the CO_2/N_2 was discontinued and a mixture of pure H_2 with a flow rate of 4 mL/min and pure He with a flow rate of 6.1 mL/min was introduced into the reactor .The test included a pre-reduction step (at reaction temperature) only before the first cycle. An additional pre-reduction was not performed before the other cycles because the H_2 -rich stream during methanation was sufficient to reduce the catalyst prior to the next cycle of CO_2 capture based on experiments. The reactor was purged with He between each cycle (CO_2 capture + methanation).

3.7.2 Cyclic CO_2 adsorption/hydrogenation tests via TGA-DSC

A physical mixture of 10% CaO/γ-Al_2O_3 and 10% Ru/γ-Al_2O_3 was used to capture CO_2 from a dilute stream (0.5%CO_2 in N_2) and to subsequently generate CH_4 from the adsorbed CO_2 by flowing H_2 (2% in N_2) under isothermal conditions. CaO/γ-Al_2O_3 and Ru/γ-Al_2O_3 were mixed in equal weights. 50 mg of sample was used for each experiment. Experiments were performed in the TGA/DSC apparatus (Netszch Jupiter) where the catalyst/adsorbent mixture was kept at 350^oC, a temperature where the Ru catalyst could easily be maintained in a reduced state. Two tests were performed. In both tests a fresh sample was exposed initially to 0.5 % CO_2/N_2 at 350^oC for 90 minutes, followed by a purge in pure N_2 for 30 minutes and finally to 2 % H_2/N_2 for 90 minutes. The first test involved no pretreatment of the catalyst whereas the second test contained a pre-reduction segment prior to CO_2 adsorption and hydrogenation segments. The pre-reduction was performed at 350^oC in a flow of 2%H_2/N_2. The weight loss and gain in the thermogram and the exothermic signals in the heat flux function from the DSC mode were used as an indication of hydrogenation activity.

3.7.3 Cyclic temperature programmed oxidation/reduction (TPO/TPR) via TGA-DSC

The cyclic temperature-programmed-oxidation-reduction studies, a combination of alternating TPO and TPR cycles were performed with fresh 10% CaO 10% Ru/γ-Al_2O_3 powder in a Jupiter STA 449 F3 instrument (Netsch). Typically, 50 mg of the DFM powder was placed into an alumina crucible and a blank test was performed prior to the measurement with an empty cell under the experimental reaction condition. The sensitivity calibration for the DSC mode was performed in a flow of N_2 using In, Sn, Bi, Zn and Al as the calibration standard.

For the cyclic TPR/TPO study, the fresh sample was exposed first to 2 % H_2/N_2 and the temperature was raised with a ramp of 5 K/min to 320^oC (TPR). After cooling in N_2 to room temperature the catalyst was exposed to 1 % O_2/N_2 and the temperature was raised to 320^oC (TPO) with 5 K/min. The TPO and TPR tests were applied consecutively 3 times each (6 cycles in total) to the sample to obtain information about the redox-properties and indirectly the sintering resistance of the catalyst.

3.7.4 Optimization of DFM composition using the Quantachrome chemisorption unit as a microreactor

These tests were performed in a ChemBET Pulsar TPR/TPD unit (Quantachrome) to optimize the compositions of both Ru $CaO/\gamma-Al_2O_3$ DFMs as well as the Rh $CaO/\gamma-Al_2O_3$ DFMs investigated later. Approximately 100 mg of powdered dual function material was loaded into a quartz U-tube and then placed in the micro-reactor furnace (Quantachrome unit). The sample was first reduced for 2 hours at 320°C in 4% H_2/N_2 (flow rate of 26 mL/min). For Ru $CaO/\gamma-Al_2O_3$ DFMs this ensured that all the precursor salts (calcium nitrate and ruthenium (III) nitrosyl nitrate) decomposed to CaO and Ru, and ensured that RuO_x was completely reduced to Ru^0. For Rh $CaO/\gamma-Al_2O_3$ DFMs the same prereduction protocol was followed to decompose the precursor salts (calcium nitrate and Rhodium (III) nitrate) and to reduce any oxides of Rhodium to Rh^0.

Following pre-reduction protocol, the sample was exposed to a 10% CO_2/N_2 mixture (30 mL/min) at 320°C for 30 minutes. This constituted the "CO_2 capture" step. Following this was a "methanation" step, which consisted of 4%H_2/N_2 (26 mL/min) being introduced into the reactor for 2 hours. Online monitoring of gas compositions at the exit of the reactor was performed using an Enerac portable emissions analyzer, capable of continuously monitoring CO_2 and CH_4 concentrations. Sampling time of the Enerac was 1 second. Following the hydrogenation cycle the reactor was cooled to room temperature in He. It was observed that the measurements during the CO_2 capture step were unreliable due to the fact that measured CO_2 concentration differences were much smaller than the error in measurement (~4%) of the Enerac's CO_2 detector. Hence

DFM performances were judged based on the amounts of methane released, which could be measured precisely (±4 ppm).

3.7.5 Accelerated cyclic testing in a packed bed reactor:

Powder 5%Ru 10%CaO/γ-Al_2O_3 was packed inside a quartz tube housed in a furnace. Gas analysis was performed on-line via an Enerac, which is an IR based gas analyzer also used for combustion applications. The DFM was pre-reduced in-situ at 320^{o}C for 2 hours using 5% H_2/N_2 (46.3 mL/min). Cyclic tests were all performed at 320^{o}C. Each cycle consisted of a CO_2 capture step and a methanation step.

In the first cyclic test the CO_2 capture capability of 1.001g of 5% Ru, 10%CaO/γ-Al_2O_3 from a source of 10% CO_2 /air over 20 cycles of CO_2 capture and methanation was evaluated. Ruthenium (Ru) will oxidize when exposed to air in the capture mode and will subsequently be reduced during methanation. A feed gas of 90% air contains O_2 (~ 18%) well in excess of the 6-8% O_2 in a power plant effluent and thus this test should be considered accelerated to stress the materials. During CO_2 capture 10% CO_2/air was introduced to the reactor at a flow rate of 17.4 mL/min for 20 minutes. The reactor was then purged with He until CO_2 and O_2 could no longer be detected at the exit. This was followed by methanation, which involved flowing 5%H_2/N_2 at 89.5 mL/min for 20 minutes. A dilute source of H_2 was used in order to prevent methane formation from exceeding our limits of detection; pure H_2 would be used in a stoichiometric amount (i.e. 4:1) relative to CO_2 captured in a power plant application. The cyclic experiment was performed with the same volume of γ-Al_2O_3 as a background test. Methanation was not observed during the test with γ-Al_2O_3.

Chapter 4 : Optimization of process parameters and catalyst treatment procedures for CO_2 methanation over 10% Ru/γ-Al_2O_3

Catalyst activity and selectivity to the desired product (CH_4) depends on a number of factors including reaction conditions and prior treatment protocols. Understanding the behavior of the catalyst under conditions it will experience during the target application forms a key aspect of our efforts in development of commercially viable dual function materials. This chapter aims to identify the optimum pretreatment and reaction conditions as well as the limitations of only the catalytic methanation reaction using supported Ru. Particular emphasis is placed on identifying those conditions that will allow operation at the lowest possible temperature favoring thermodynamics as well as energy efficiency considerations. Pre-reduction of the catalyst is investigated as a potential means of increasing activity through its impact on catalyst structure.

4.1 Thermodynamics of CO_2 methanation at atmospheric pressure

Figure 4.1 displays the equilibrium distribution as a function of temperature at atmospheric pressure including H_2O, CH_4, CO_2, CO and C species. At higher temperatures, thermodynamic equilibrium favors steam reforming of methane and reverse water gas shift, both of which are endothermic processes. Hence both conversion and selectivity to methane decrease at temperatures greater than 350^{o}C. Exposure of the catalyst to high temperatures is also expected to result in deactivation due to sintering. From the equilibrium product distribution shown in Fig. 4.1 it can be seen that maintaining the temperature as low as possible through good heat management is critical to maintain favorable thermodynamics and hence increasing conversions to methane as well as maintaining 100% selectivity.

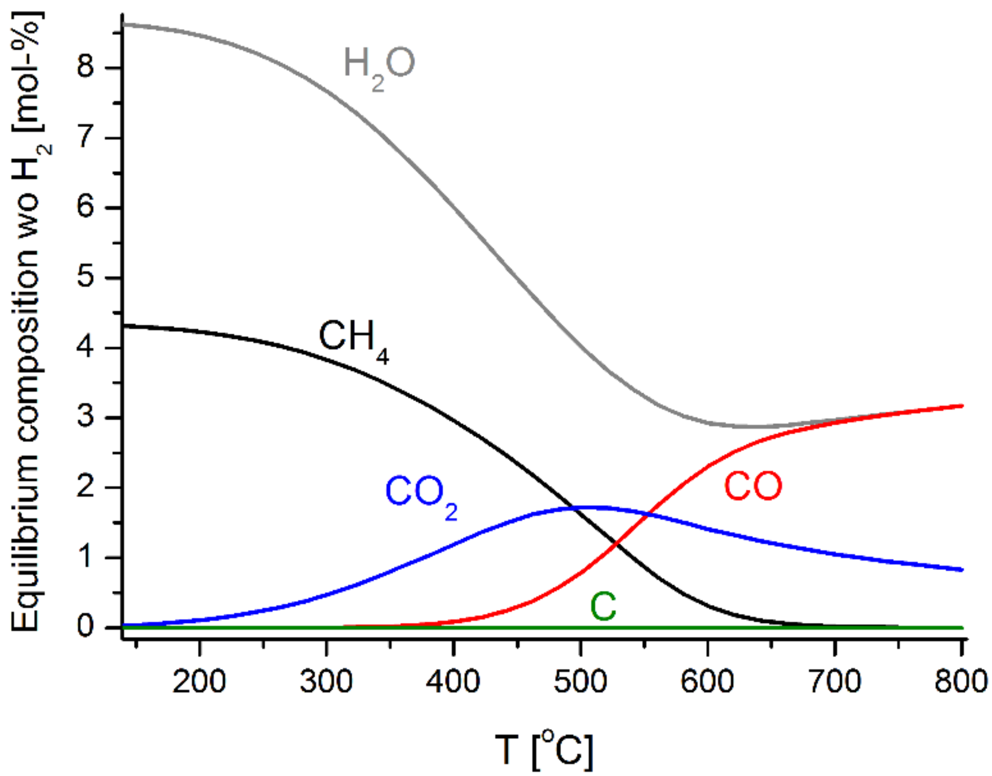

Figure 4.1: Equilibrium distribution at atmospheric pressure as a function of temperature, including water and amorphous carbon species.

4.2 Impact of reaction temperature and space velocity on Ru catalytic activity and selectivity

The catalytic performance as a function of the reaction temperature and GSHV is shown in Figure 4.2. The equilibrium composition is shown in red (solid line w/o data points) for CO_2, CH_4 and CO. It is clear that the space velocity and reaction temperature impact the product distribution significantly. At GHSV = 4720 h^{-1} thermodynamic equilibrium is almost reached at 280°C. However, increased GHSV results in lower CO_2 conversion with some CO formation.

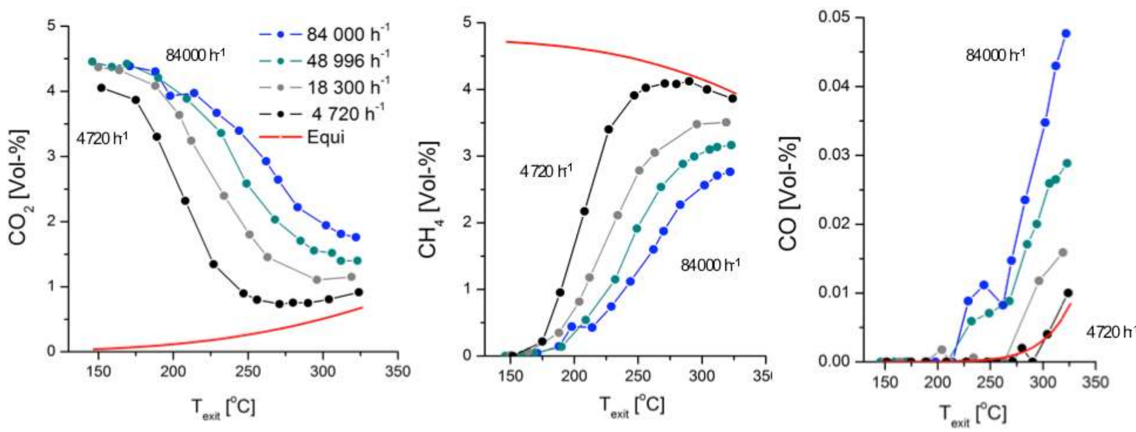

Figure 4.2: Catalytic performance for Ru/γ-Al_2O_3 particles in a fixed bed reactor as a function of the reaction temperature for different GHSV at 1 bar and H_2/CO_2 = 4 (H_2:CO_2:He = 16:4:80 (in Vol.-%), left plot: CO_2 concentration, middle plot: CH_4 concentration, right plot: CO concentration, solid line with no data points: dry equilibrium concentrations.

The increase in CO formation with increasing space velocity is accompanied by a decrease in CO_2 conversion and a shift of the maximum activity to higher reaction temperatures. In principle, CO formation can occur mostly by the reversed water gas shift (RWGS) reaction (Eq. 5) with a small contribution depending on temperature from steam reforming (SR) of methane (Eq. 6). Thus temperature control is essential for high selectivity to methane

$$CO_2 + H_2 \rightarrow CO + H_2O \qquad \text{(Eq. 5)}$$

$$CH_4 + H_2O \rightarrow CO + 3\ H_2 \qquad \text{(Eq. 6)}$$

In several publications it was reported that for CO and CO_2 containing feeds, CO hydrogenation occurs at lower temperatures than CO_2 over supported Ru-containing catalysts [88-90]. For instance, it has been shown that the CO methanation is favored kinetically over that of CO_2 below 300^{o}C for 0.5 % Ru/Al_2O_3, even when the CO_2 concentration was 15 times higher than the CO at CO_2/H_2 = 3.3 [89]. Considering these results, CO formation as a by-product is initially surprising. However, in agreement with our results, it has been also shown in this work [89] that with increasing temperature and space velocity the CO conversion to CH_4 decreases significantly relative to CO_2 conversion. The authors also attributed this to an increasing contribution from the RWGS reaction. Accordingly, the rate of the reverse water gas shift reaction is much faster than the rate of CO hydrogenation. In addition, it has been suggested in several publications that CO_2 hydrogenation is initiated by a dissociative adsorption of CO_2 (Eq. 7) to adsorbed CO and adsorbed O, followed by dissociation of the former species to C and O (Eq. 8) and successive hydrogenation of C to CH_4 [91, 92]. Other authors have proposed the formation of a formate intermediate at the metal-support interface, which decomposes to CO

(Eq. 9) and subsequently reacts with adsorbed hydrogen to form CH_4 [72, 93]. Hence CO is also an intermediate in the CO_2 hydrogenation reaction.

$$CO_{2(a)} \rightarrow CO_{(a)} + O_{(a)} \qquad \text{(Eq. 7)}$$

$$CO_{(a)} \rightarrow C_{(a)} + O_{(a)} \qquad \text{(Eq. 8)}$$

$$HCOO^{-}_{(a)} + H^{+}_{(a)} \rightarrow CO_{(a)} + H_2O_{(a)} \qquad \text{(Eq. 9)}$$

4.3 Impact of reduction temperature on metal dispersion in 10% Ru/γ-Al_2O_3

CO chemisorption was performed on the catalyst reduced at various temperatures in the range 250-550°C to determine the optimum reduction temperature for Ru dispersion. Table 4.1 displays Ru dispersion data for various pre-reduction temperatures. It can be seen that metal dispersion reaches its highest value of 19.24% at a reduction temperature of 320°C. The observed increase in dispersion (from 8.37 to 19.24%) as pre-reduction temperature was increased from 250 to 320°C suggests that Ru-containing compounds were not fully reduced to Ru^0 metal at 250°C.

Table 4.1: Metal dispersion for Ru/γ-Al_2O_3 samples following reduction at different temperatures.

Reduction temperature (°C)	Ru Dispersion (%)
250	8.37
320	19.24
350	11.54
550	6.93

A significant drop in dispersion is observed at pre-reduction temperatures exceeding 320°C. This is attributed to metal sintering. Sintering is first observed for a catalyst pre-reduced at 350°C, when the dispersion drops to 11.54%. For a pre-reduction temperature of 550°C, the metal dispersion is 6.93%. This demonstrates the sensitivity of the Ru/γ-Al_2O_3 catalyst to temperature and identifies metal sintering as a mode of catalyst deactivation for a reactor with poor temperature control; ensuring isothermal conditions for CO_2 hydrogenation will minimize this problem, provided the operating temperature is below 350°C.

Chapter 5 : Ru/γ-Al_2O_3 stability during cyclic TGA-DSC tests

The results presented in this chapter have been published in Applied Catalysis B: Environmental in a paper entitled "Catalytic and adsorption studies for the hydrogenation of CO_2 to methane".

This chapter employs thermogravimetric analysis and differential scanning calorimetry (TGA-DSC) to investigate the cyclic behavior of Ru/γ-Al_2O_3. Catalyst activity is also examined, employing cyclic conditions where CO_2 adsorption and hydrogenation of adsorbed CO_2 occur in two consecutive steps. Potential limitations and optimum conditions of cyclic operation of Ru/γ-Al_2O_3 are identified.

The results presented in this chapter also offer insight into the stability of dual function materials. The target application for dual function materials is CO_2 capture from an industrial flue gas stream and the subsequent hydrogenation of captured CO_2. Post-combustion flue gases will contain varying amounts of oxygen and steam while the feed during methanation will be pure hydrogen. Hence the reduction-oxidation behavior of the catalytic component of the DFM presents an important factor affecting CO_2 capture and conversion. The material must maintain its structural integrity under cyclic oxidizing (exhaust) and reducing (hydrogenation) conditions over many cycles. Hence the redox behavior of Ru/γ-Al_2O_3 is studied to guide DFM design and operation.

5.1 The effect exposure to reducing and oxidizing conditions on 10% Ru/γ-Al_2O_3

The fresh 10% Ru/γ-Al_2O_3 sample has been exposed to temperature programmed reduction and temperature programmed oxidation cycles (TPR/TPO), consecutively. The goal of this study was to further investigate the sintering and redox properties of the catalyst. It is expected that sintering in general will be accompanied by a loss of redox behavior. In Figure 5.1, the response of the TGA and DSC signal occurring upon reduction and subsequent re-oxidation are compared for three TPR/TPO cycles.

As can be seen in Figure 5.1, in the first applied temperature-programmed reduction cycle (TPR-1) almost no change of the mass is observed until 150^{o}C. A rapid decline of the mass (~5% mass loss) is seen at T > 150^{o}C. Simultaneously, the corresponding DSC function shows a minimum at T ≈ 200^{o}C indicating that the rapid mass change occurs due to an exothermic reaction. Re-oxidation in O_2/N_2 (TPO-1) results in 1.2% mass increase, which does not recover the mass lost during TPR-1. Hence the mass loss starting at 150^{o}C and the DSC function with minimum at 200^{o}C during TPR-1 are assigned to the decomposition of Ru-nitrate precursors in the catalyst sample which have not been fully decomposed during calcination. Calcination was deliberately performed at 250^{o}C to avoid forming RuO_x compounds. While this temperature is low enough to prevent the formation of volatile RuO_x species, it has likely not caused complete decomposition of the precursor salts. Note that also CO chemisorption studies as a function of pre-reduction temperature have shown that the metal dispersion is lower when the catalyst is reduced at 250^{o}C but increases as soon as the reduction temperature is 320^{o}C, also indicating that in the first TPR cycle mass loss and exothermic signal originates from decomposition of Ru-nitrate traces.

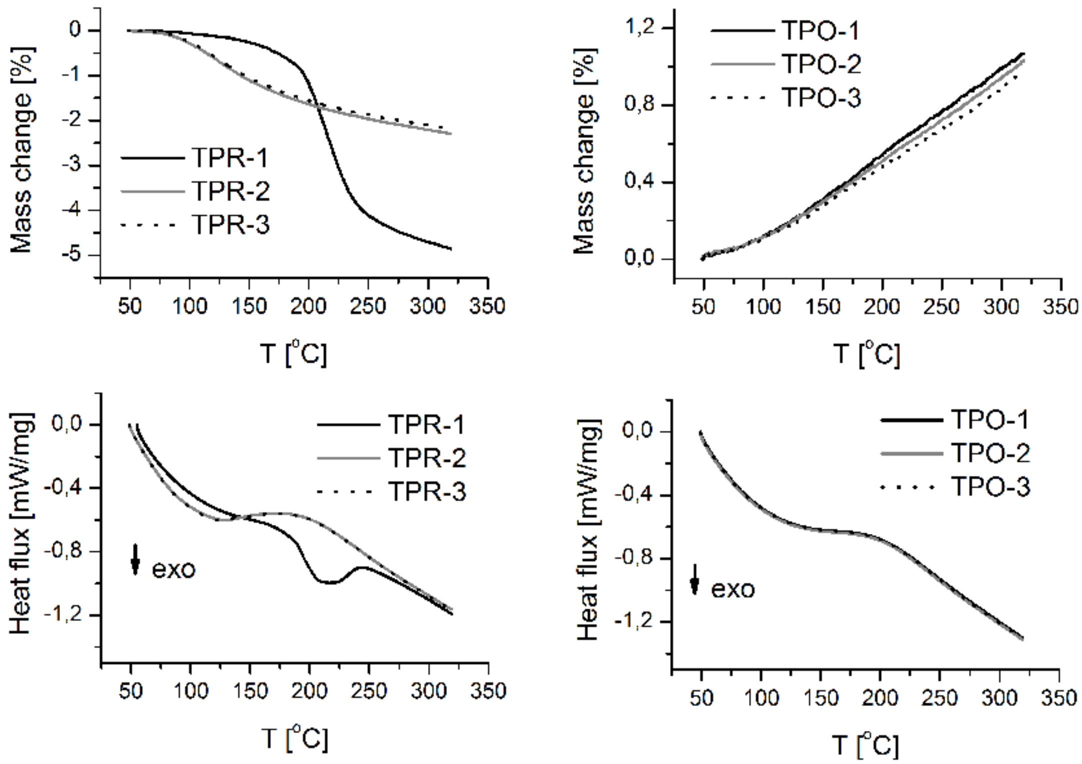

Figure 5.1: TGA response for temperature-programmed reduction (top, left) and re-oxidation (top, right) and DSC signals for temperature-programmed reduction (bottom, left) and subsequent re-oxidation (bottom, right) cycles.

The second and third applied TPR/TPO cycles show almost identical TGA and DSC responses, indicating that after the initial H_2 treatment almost the same amount of Ru sites can be reduced and re-oxidized reversibly. Hence, significant sintering of Ru/γ-Al_2O_3 in an oxidizing and reducing atmosphere up to 350°C is not expected.

5.2 Isothermal cyclic studies using CO_2 and H_2 (cyclic hydrogenation) over 10% Ru/γ-Al_2O_3

To obtain further information about the CO_2 hydrogenation stability of the 10% Ru/γ-Al_2O_3 catalyst, consecutive cyclic studies using TGA-DSC have been performed isothermally. The sample was exposed first to diluted CO_2 in N_2 and subsequently to diluted H_2 in N_2 at 260^{o}C for methanation. In between these treatments the sample was purged in pure N_2. This hydrogenation or methanation cycle, consisting of three gas treatments, was repeated 20 times. The TGA and DSC response is given for each cycle in Figure 5.2. In Figure 5.3 the first 3 cycles of this test are plotted separately to indicate the TG and DSC signals corresponding to different stages of the hydrogenation cycles. The changes of the TGA response and DSC signal are taken as a measure of the hydrogenation activity. Note that prior to this cycle study the catalyst had been reduced in H_2 at 320^{o}C, to avoid mass changes during the cyclic test in the TGA that may be induced by reduction or changes of the catalyst itself. That this is indeed important has been shown by the cyclic TPO/TPR treatment, discussed previously.

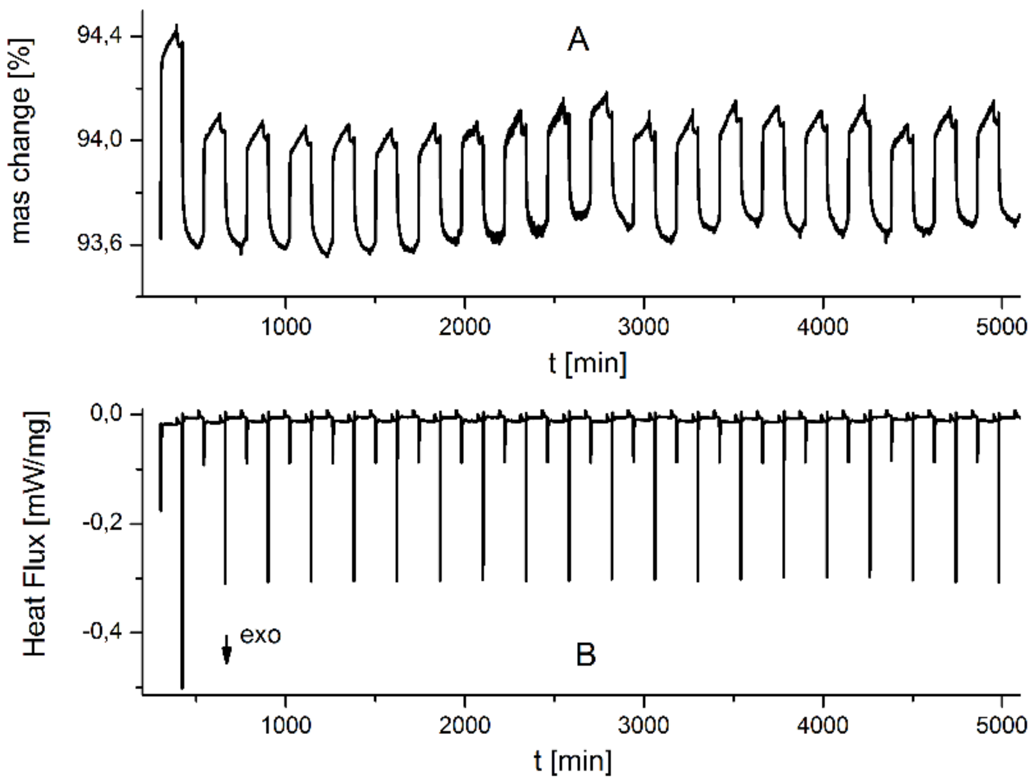

Figure 5.2: TGA response (A) and DSC response (B) for consecutive introduction of first a) CO_2/N_2, b) N_2 and c) H_2/N_2 at T = 260°C. Each treatment has been applied 20 times. One cycle is defined as CO_2/N_2 + N_2 + H_2/N_2 introduction.

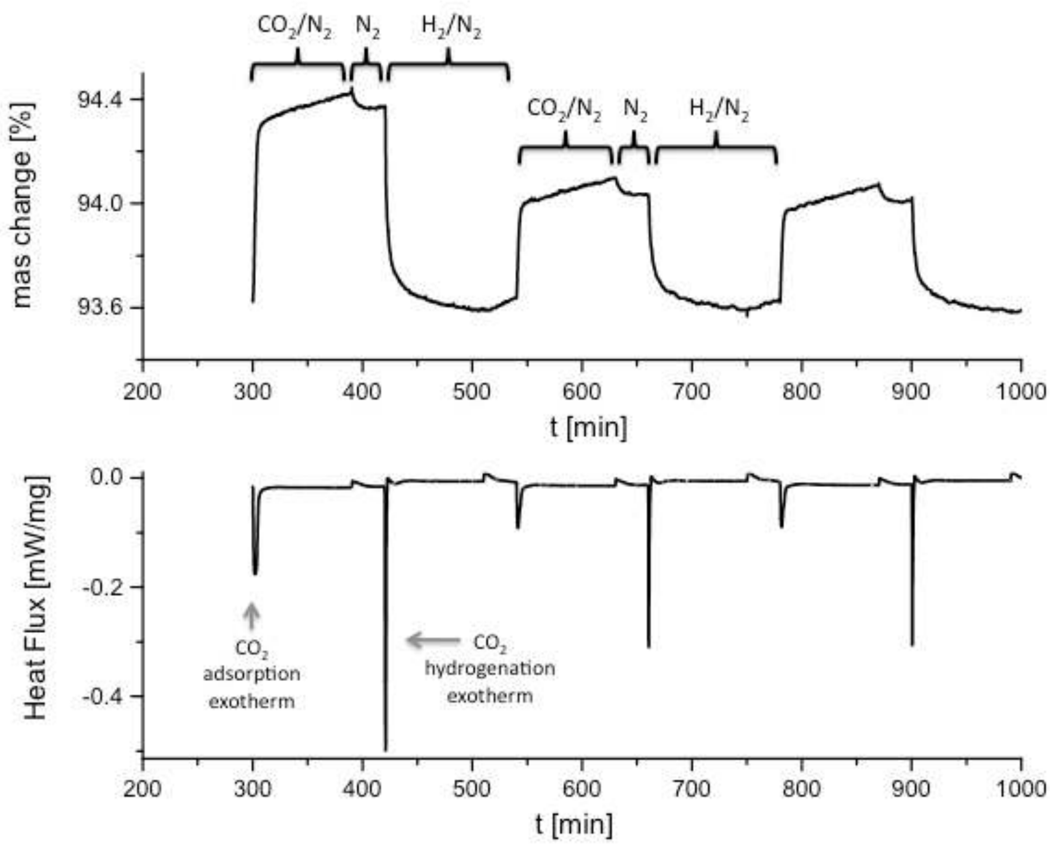

Figure 5.3: TGA and DSC responses for the first 3 cycles of hydrogenation for the 20-cycle TGA-DSC test on 10% Ru/γ-Al_2O_3. CO_2/N_2 + N_2 + H_2/N_2 introduction constitute a single cycle of hydrogenation

As expected, CO_2 treatment (at 260°C) causes a mass increase in the thermogram and an exothermic response in the DSC. Switching to N_2 reduces the mass slightly by desorbing a small amount of the weakly adsorbed CO_2. Switching to a H_2-containing stream also at 260°C gives rise to a mass decrease and a second even more intense exothermic DSC signal. Note that the mass loss induced by H_2 introduction is essentially equal to the mass gain recorded for the CO_2 treatment. Thus, the catalyst is most likely free of any CO_2 after H_2 introduction, indicating that hydrogenation has reached full conversion under these conditions. Interestingly, only signals for the first cycle differ significantly from those obtained for the other 19 subsequent cycles. As it is seen from the mass gain and intensity of the DSC signal, the catalyst is able to chemisorb larger amounts of CO_2 in the first cycle compared to the other 19 cycles. This chemisorbed CO_2 can be fully removed by the subsequent H_2-introduction. In addition, the DSC signal induced by H_2 introduction in the first cycle is much more intense than those for the other 19 DSC signals. Conclusively, the catalyst appears to have lost sites for CO_2 chemisorption and appears to have undergone about a 40% loss in activity

However, the catalytic performance is constant for the following 19 cycles, since the area of the exothermic CO_2 and H_2 signals are almost identical. This is also the case for the mass loss and mass gain in each thermogram although a baseline drift contributes to the TGA. Since less CO_2 is adsorbed in the second cycle, it seems reasonable, to assume that active sites for CO_2 adsorption/chemisorption are irreversibly lost after the first hydrogenation cycle. Since addition of H_2 in the first cycle recovers the initial catalyst mass, it is unlikely that CO_2, or CO stays on the catalyst surface, reducing CO_2 uptake in the subsequent cycle. It is possible that elemental carbon remains on the surface, causing masking of active sites. However, if significant carbon deposition occurs in the first cycle, it would be expected that the carbon would build up over the catalyst, causing further drop in CO_2 uptake in every cycle. Sintering of Ru-sites seems to be unlikely, since the reaction temperature is only 260^{o}C and the catalyst has been reduced in H_2 at 320^{o}C for 1 h prior the first cycle. It might also be possible that Ru-sites may migrate partially into the bulk, thus lowering the number of active sites for CO_2 chemisorption. However, TPO/TPR cycle studies suggest that the catalyst can be fully re-oxidized in O_2-containing feed following prior reduction; hence a movement of Ru sites into the bulk appears to be unlikely as well.

Partial re-oxidation of Ru^0 sites might be another explanation, assuming that Ru^0 sites are indispensable for CO_2 chemisorption and hydrogenation activity, respectively. Hydrogenation is assumed to be initiated by dissociation of CO_2 via the reverse water gas shift reaction (Eq. 10) or the dissociative adsorption of CO_2 (Eq. 11), which is a source of oxygen atoms.

$$CO_2 + H_2 \rightarrow CO + H_2O \qquad \text{(Eq. 10)}$$

$$CO_{2(a)} \rightarrow CO_{(a)} + O_{(a)} \qquad \text{(Eq. 11)}$$

Shalabi et al. have investigated the impact of H_2-pretreatment on the catalytic performance of Ni/γ-Al_2O_3 catalysts in CO hydrogenation and found that reduction in H_2 as a function of temperature and duration increases CO hydrogenation activity, suggesting indeed that Ni^0 and most likely Ru^0 is needed for high CO_2 methanation activity [94]. It should be noted that some publications suggest an alternative mechanism in which the adsorbed CO intermediate reacts directly with adsorbed hydrogen to form CH_4 [72, 93]. In our TGA/DSC work, O atom production through dissociation of CO_2 at 260°C was assumed to be responsible for oxidation of Ru sites because the observed 40% decrease in active sites (in the 2nd cycle) by adsorbed CO would have produced a noticeable mass gain relative to the original catalyst weight. Furthermore parametric studies show that CO_2 is hydrogenated to methane at 260°C while the dispersion of Ru (and its activity) is maximized only at 320°C. This led us to tentatively believe that some adsorbed species, possibly O----Ru, had to be removed to completely reduce the Ru species to the metallic state and regain essentially all of the activity. The catalyst was treated in H_2 at 320°C in-between each hydrogenation cycle to investigate whether re-oxidation of reduced Ru in the first cycle is responsible for the decline in CO_2 chemisorption and hydrogenation activity.

5.3 Isothermal cyclic studies over Ru/γ-Al_2O_3 using CO_2 and H_2 and the impact of inter-cycle H_2 treatment

Three isothermal hydrogenation cycles (including CO_2, N_2, and H_2 treatment at 260°C) have been performed with and without inter-cycle H_2-treatment at 320°C. It was assumed that the loss in CO_2 chemisorption and hydrogenation activity due to re-oxidation of Ru-sites after the first cycle can be suppressed by reducing the catalyst in-between each hydrogenation cycle.

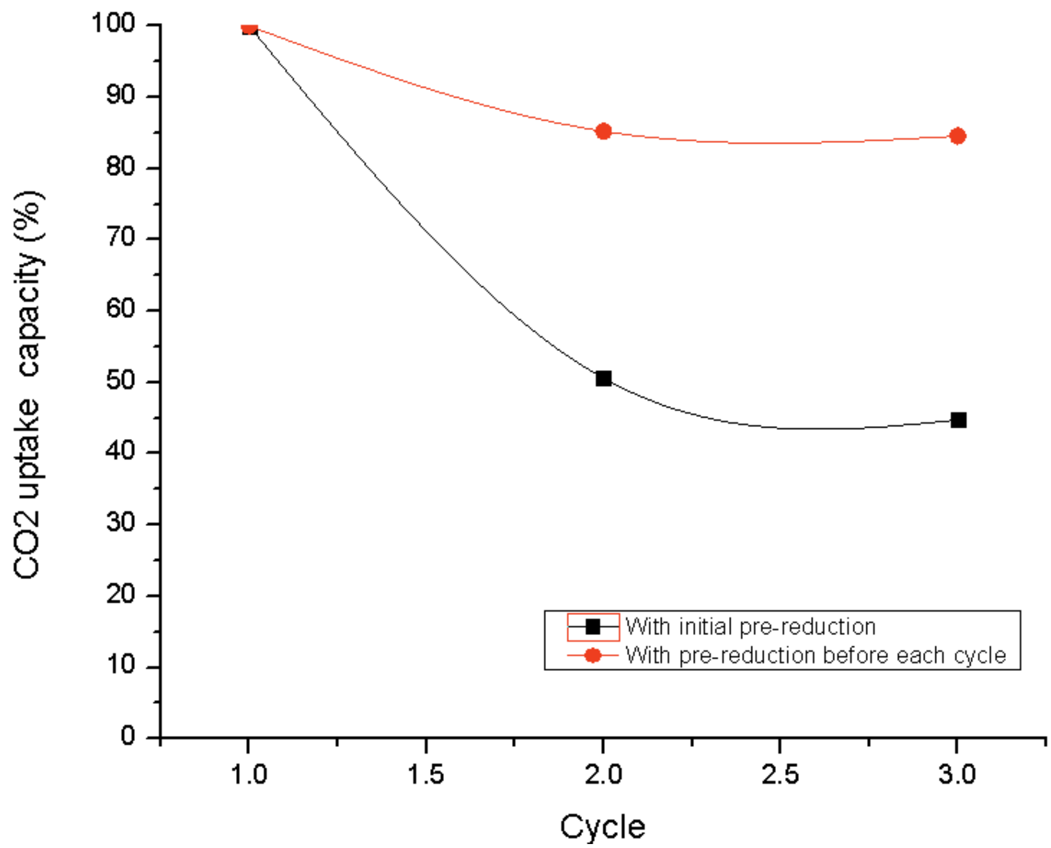

Figure 5.4: Impact of H_2/N_2 treatment at 320°C on percentage CO_2 uptake capacity at 260°C over Ru/γ-Al_2O_3. CO_2 uptake capacity has been calculated by assigning 100% capacity to the weight gain during CO_2 introduction in the first cycle and expressing the weight gain during subsequent cycles as a percentage of this initial capacity.

In Figure 5.4 the CO_2 uptake capacity is shown with and without inter-cycle H_2-treatment. As evident, the regeneration with added H_2 in between each cycle improves the CO_2 uptake capacity (top curve) relative to the uptake in the absence of the H_2 treatment (bottom curve). A higher CO_2 uptake capacity for the second and third cycle is seen when the catalyst was treated with H_2 at 320°C between each cycle. Recovery of 90% of initial CO_2 uptake capacity upon H_2-treatment shows that the catalyst does not undergo significant irreversible deactivation during CO_2 hydrogenation at 260°C. Although further testing is needed to confirm the link between Ru^0 oxidation and loss of CO_2 chemisorption sites, these results are supportive of our hypothesis that the loss of CO_2 uptake after the first cycle is likely due to re-oxidation of Ru^0 by the O atoms produced during the dissociation of CO_2.

Chapter 6 : The effect of temperature on CO_2 adsorption over Ru/γ-Al_2O_3

The results presented in this chapter are under review for publication in Applied Catalysis B: Environmental in a paper entitled "Kinetics of catalytic CO_2 methanation over Ru/γ-Al_2O_3 and implications for renewable energy storage applications ".

This chapter presents the TGA-DSC adsorption studies performed on 10% Ru/γ-Al_2O_3 to investigate the adsorption of CO_2 at different temperatures. Thermodynamic and kinetic limitations for CO_2 adsorption on catalyst are identified at 140-330^{o}C.

6.1 TGA-DSC Analysis of Chemisorption of CO_2

TGA-DSC studies were performed to understand the mass change and heat flux through the 10% Ru/γ-Al_2O_3 catalyst due to CO_2 chemisorption at different temperatures. The fresh catalyst was saturated with CO_2 at the desired temperature from the range 140-330^{o}C. DSC data for all tests showed negative peaks (exothermic reaction) associated with CO_2 chemisorption.

The total CO_2 uptake and heat release associated with CO_2 chemisorption at all temperatures are plotted in Figure 6.1. From an increasing trend in the amount of CO_2 uptake with increasing temperature, it is apparent that CO_2 chemisorption on 10% Ru/γ-Al_2O_3 is an activated process, which is limited by kinetics up to a temperature of 300^{o}C. At temperatures greater than 300^{o}C the adsorption of CO_2 decreases due to thermodynamic limitations. The heat released and mass uptake values show a direct correlation for CO_2 chemisorption for all experiments. This is a demonstration of the reliability of TGA-DSC data for determining energetics of chemical reactions, even at different temperatures.

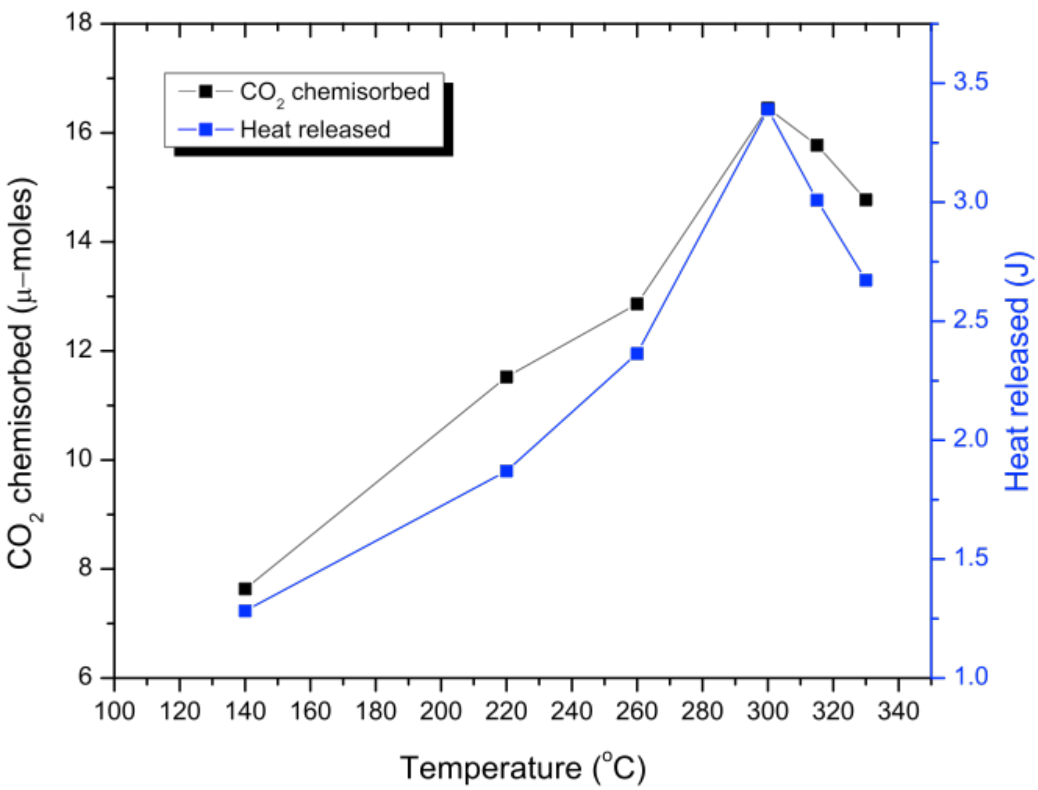

Figure 6.1: Total mass uptake and heat release for CO_2 chemisorption at T=140-330^oC, feed: 0.5% CO_2/N_2

Chapter 7 : The Eley-Rideal Mechanism for CO_2 Hydrogenation over Ru/γ-Al_2O_3 and its determination through TGA-DSC and kinetic studies

The results presented in this chapter are under review for publication in Applied Catalysis B: Environmental in a paper entitled "Kinetics of catalytic CO_2 methanation over Ru/γ-Al_2O_3 and implications for renewable energy storage applications ".

7.1 The impact of changing sequence of adsorption of reactants- E-R mechanism

Figure 7.1 (left) displays results for the Ru catalyst exposed first to CO_2 followed by addition of H_2 at 260°C. It can be seen on the left that when 10% Ru/γ-Al_2O_3 is exposed first to CO_2, there is a sharp rise in mass accompanied by a negative (exothermic) DSC signal indicative of CO_2 adsorption. Upon switching to N_2, a slight variation in mass is seen, believed to be due to buoyancy effects. When H_2 is introduced, a sudden mass decrease and negative DSC peak (exothermic) is observed with the sample mass returning to its initial value. The decrease in weight and corresponding exotherm are assigned to the hydrogenation of adsorbed CO_2 and release as methane.

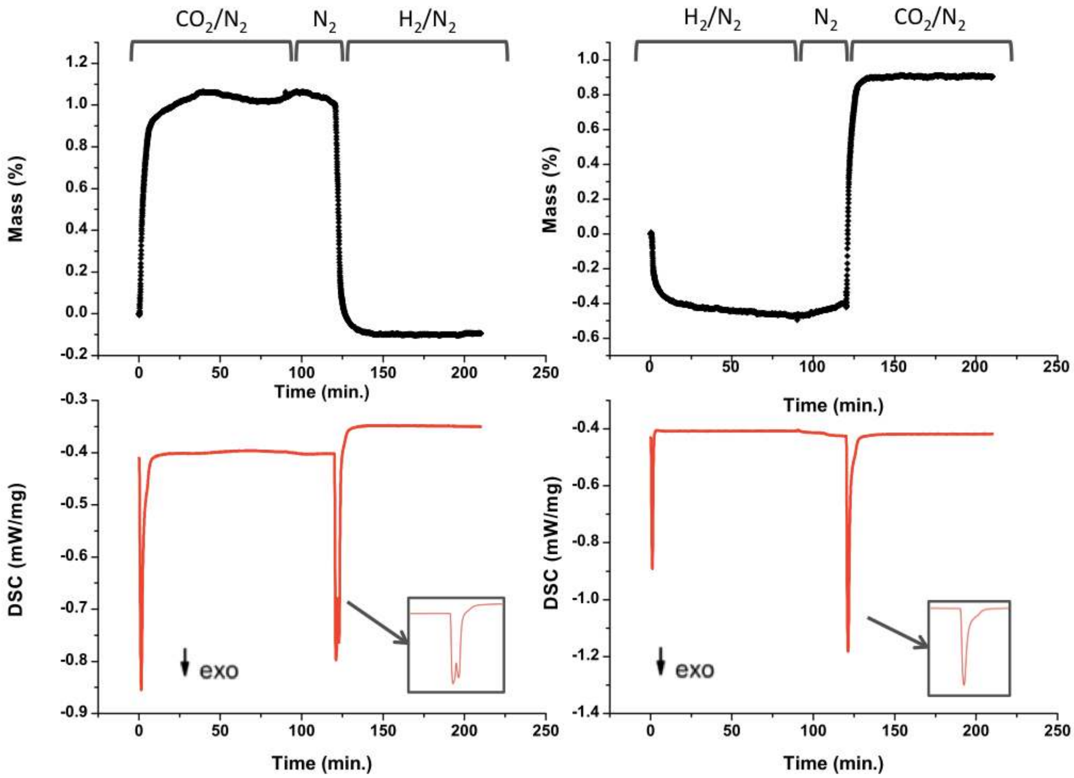

Figure 7.1: TG (top) and DSC (bottom) responses observed during the sequential introduction of reactants over 10% Ru/γ-Al_2O_3. T=260^{o}C

The objective of this study was to understand the influence of sequential addition of both CO_2 and H_2 to the Ru surface. **Figure 7.1** (right) shows that when H_2 is introduced first to a fresh catalyst, a drop in mass accompanied by a negative (exothermic) DSC peak is observed. The drop in mass.indicates a reduction of oxide surface species. Although the catalyst was pre-reduced at 320^{o}C prior to this test, it was observed that a mass uptake equivalent to the mass lost during H_2 introduction at 260^{o}C occurred while the catalyst was cooled down from 320^{o}C to 260^{o}C in N_2. This was assumed to be associated with trace amount of O_2 present in the N_2 gas, which oxidized the catalyst surface. Nevertheless, a mass uptake following reduction of surface species is not observed during the entire H_2 step at 260^{o}C. Moreover, upon subsequent introduction of CO_2, a sharp increase in mass accompanied by an exothermic DSC peak is observed. The value of the mass change was greater than that observed during the test shown in the left panel of **Figure 7.1**, by roughly the same amount of mass lost during the introduction of hydrogen. This is indicative of CO_2 adsorption on a freshly reduced catalyst. The fact that the catalyst weight immediately increases without delay implies that CO_2 hydrogenation does not occur under these conditions. Moreover, the DSC signal reveals that while hydrogenation of adsorbed CO_2 (**Figure 7.1**, left) results in a double peak, introduction of CO_2 over catalyst exposed to H_2 results in a single peak (**Figure 7.1**, right). While this qualitative difference in the exotherms could be indicative of the different nature of reaction taking place on the catalytic surface, it could also be an experimental artifact due to diffusional limitations in the TGA-DSC apparatus. Overall, the data presented in **Figure 7.1** indicate that the processes taking place in the two experiments are distinct from each other. These results point towards an Eley-Rideal mechanism for CO_2 hydrogenation over Ru/γ-Al_2O_3, in which CO_2 adsorbs on the catalyst and reacts with gas phase H_2. Pre-adsorbing H_2 followed by the addition of CO_2 does not result in methanation, as would be the case if a Langmuir-Hinshelwood kinetic model where two adsorbed species react to form the product was operative. As a matter of fact H_2 chemisoption was not observed to occur at these temperatures on bare Ru metal in chemisorption expeirments. Thus H_2 only adsorbs when CO_2 is first adsorbed consistent with the E-R mechanism discussed in the next section.

7.2 Eley-Rideal Rate Expression for CO_2 Hydrogenation

In order to validate the proposed Eley-Rideal mechanism, kinetic experiments were performed below 6 kPa CO_2 partial pressure with a constant P_{H2} of 43 kPa at 230°C and 1 atm total pressure. The results, displayed in Figure 7.2, show that the rate of reaction shows greater dependence on changing CO_2 partial pressure below 1.5 kPa, after which point the slope of the curve decreases. As the CO_2 is further increased, the rate reaches a plateau, consistent with the Eley-Rideal mechanism.

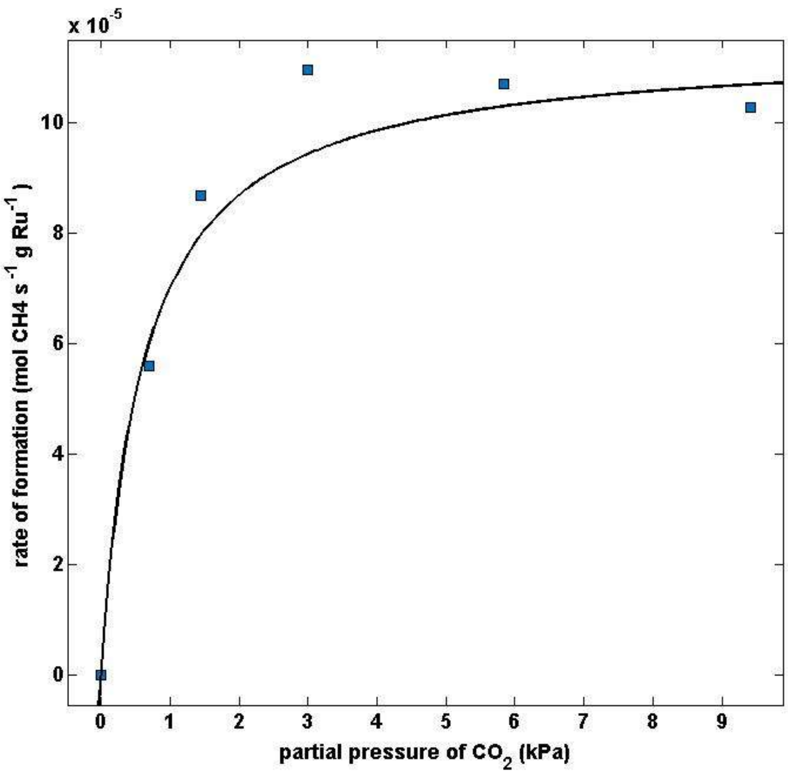

Figure 7.2: Kinetic data at low CO_2 partial pressures and constant H_2 partial pressure (filled squares) and nonlinear regression curve fitting for an Eley-Rideal rate expression (solid line). T=230°C, P_{H2}= 10.422 kPa

Hence it is shown here that the reaction has a variable order with respect to CO_2. An Eley-Rideal rate law takes into account the equilibrium constant for adsorption of CO_2 at a given temperature (K_{eq}) as well as the rate constant for the surface reaction (k) as shown in Eq.12:

$$R_{CH_4,f} = \frac{k \times K_{eq} \times P_{CO_2} \times P_{H_2}}{1 + K_{eq} \times P_{CO_2}} \tag{Eq. 12}$$

Using nonlinear regression in MATLAB kinetic data for varying H_2 and CO_2 partial pressures at 230°C were used to identify Eley-Rideal rate constants. Curve fitting methods are frequently employed in reaction engineering to analyze rate data, identify rate constants and distinguish between different possible mechanisms[95, 96]. Here, the focus is only on fitting an Eley-Rideal rate expression to our kinetic data because we have identified this as the most likely mechanism through TGA-DSC experiments in addition to kinetic measurements. The final rate expression at 230°C was determined as shown in Eq. 13:

$$R_{CH_4,f} = \frac{2.664 \times 10^{-6} \times 1.598 \times P_{CO_2} P_{H_2}}{1 + 1.598 \times P_{CO_2}} \tag{Eq. 13}$$

This expression describes the changing order of reaction for 0-6 kPa CO_2 partial pressure at 230°C. The surface rate constant and equilibrium constant for CO_2 adsorption at 230°C were determined to be 2.664×10^{-6} mol CH_4 s^{-1} gRu^{-1} kPa^{-1} and 1.598 kPa^{-1} respectively from nonlinear regression curve fitting. Clearly at low partial pressures of CO_2 the denominator approximates 1 while at high pressure the rate approaches zero. Changing CO_2 reaction orders occurs in between these two extremes.

In realistic renewable energy storage applications, assuming a stoichiometric H_2/CO_2 of 4 and atmospheric pressure operation, it is expected that the partial pressure of CO_2 will be higher than those investigated in this section. The experiments described in the following chapter investigate kinetic effects of the partial pressure of CO_2 for more realistic values (greater than 8 kPa).

Chapter 8 : Empirical Rate Law for CO_2 Hydrogenation over Ru/γ-Al_2O_3

The results presented in this chapter are under review for publication in Applied Catalysis B: Environmental in a paper entitled "Kinetics of catalytic CO_2 methanation over Ru/γ-Al_2O_3 and implications for renewable energy storage applications ".

Mechanistic observations presented in Chapter 6 demonstrate that the mechanism of CO_2 hydrogenation likely follows an Eley-Rideal model due to the changing order of reaction with respect to CO_2. However, for the design of a methanation reactor for renewable energy storage applications, an empirical rate law is developed in this chapter to describe kinetic behavior at realistic partial pressures of reactants and for a wider range of temperatures. A H_2/CO_2 range of 4-6 was used in developing the empirical rate expressions, closely simulating the ratios expected in a real application.

8.1 Determining kinetic control: eliminating mass transfer limitations

CH_4 formation rates were compared under differential reaction conditions for catalysts of varying particle sizes under identical conditions (space velocity, feed composition, temperature) to determine the effect of pore (intra-particle) diffusion. Measurements were performed at 350^{o}C (largest anticipated operating temperature under realistic conditions) and GHSV of 66480 h^{-1} for a 4% CO_2/16% H_2/80% He feed mixture.

It can be seen from results displayed in Table 8.1 that the rate of CH_4 formation rate is slightly increased for the particle size range 425-600μm. However, since decreasing the particle size even further (to 250-425 μm) results in a slower rate (which is also equal to the rate observed for the particle size range 600-710 μm), it can be concluded that pore diffusion limitations are not rate limiting under any of these conditions.

Table 8.1: Apparent rate of formation for catalyst of varying particle size distributions. T=350°C, Feed: 4% CO_2/16% H_2/ 80% He

Particle size	CH_4 apparent rate of formation (g-mol . s^{-1}. g_{Ru}^{-1})
600-710 μm	2.0E-04
425-600 μm	2.2E-04
250-425 μm	2.0E-04

8.2 Order of reaction with respect to H_2

The rate of CO_2 hydrogenation over Ru/γ-Al_2O_3 shows a strong dependence on H_2 partial pressure in the feed as indicated by results shown in Figure 8.1. In all experimental conditions the H_2 to CO_2 ratio was always greater than 4:1, the stoichiometry for methanation. Each data point represents the average rate for an experiment where H_2 partial pressure varied from 43-63 kPa at a fixed CO_2 partial pressure of 10 kPa, constant temperature (230°C) and ambient total pressure. The linear slope of the best-fit line is equal to the reaction order with respect to H_2, which was determined as 0.88 with a good correlation of 0.995. A reaction order of nearly 1 with respect to hydrogen is consistent with an Eley-Rideal mechanism, as proposed earlier.

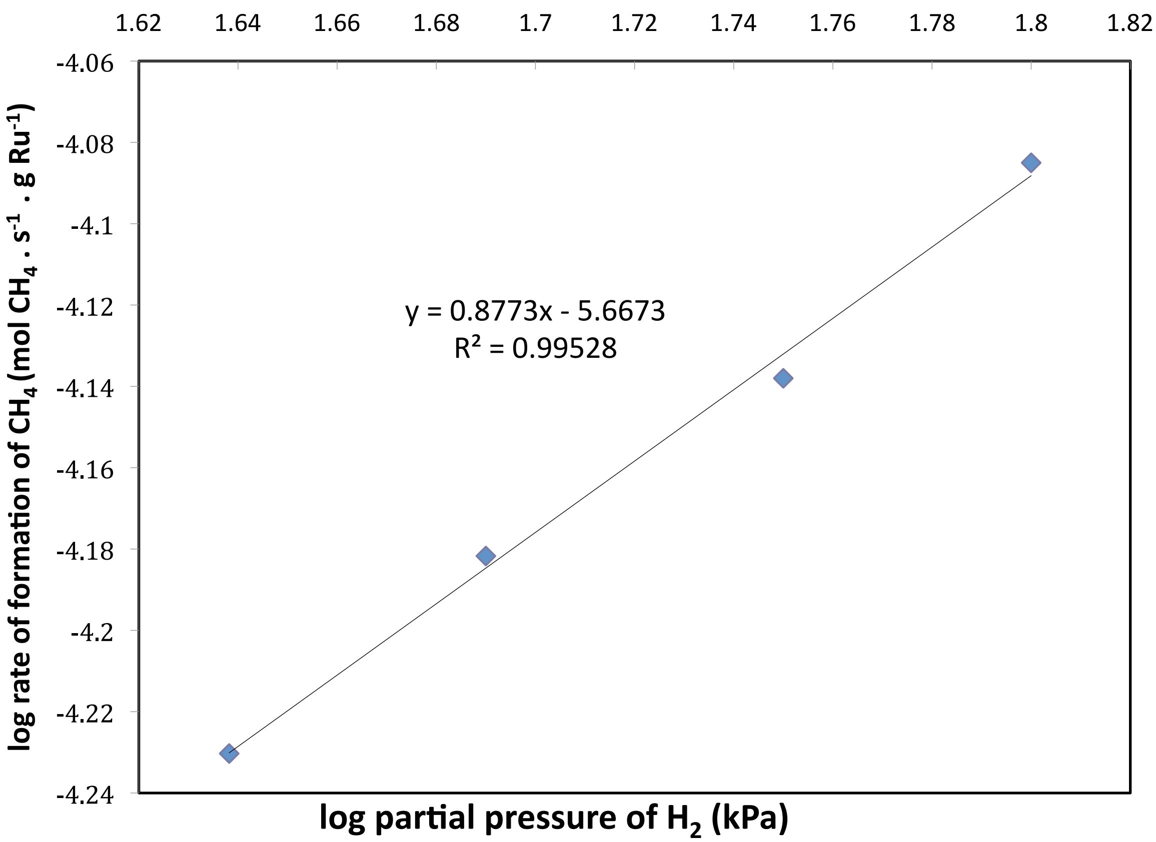

Figure 8.1: Dependence of reaction rate on H_2 concentration. P_{CO2}=10 kPa, P_{H2}=43-63 kPa. T= 230°C, 1 atm total pressure.

8.3 Order of reaction with respect to CO_2

The rate of CO_2 hydrogenation shows a weak dependence on CO_2 concentration, when CO_2 partial pressure is varied from 8-10 kPa at a constant H_2 partial pressure of 40 kPa at 230°C. From the slope of the linear plot shown in Figure 8.2 the order of reaction with respect to CO_2 is 0.34 under these conditions. This is indicative of strong chemisorption of CO_2 onto the catalyst;

The catalyst surface coverage by CO_2 molecules saturates at relatively low partial pressures, consistent with the Eley-Rideal mechanism. This observation is in accordance with previous work by Prairie et al., who have determined that CO_2 methanation over Ru/γ-Al_2O_3 follows zero order kinetics with respect to CO_2 concentration at temperatures less than 200°C[74]. Obviously the reaction order for CO_2 partial pressure is variable for an Eley-Rideal rate law, as discussed in the Chapter 6.

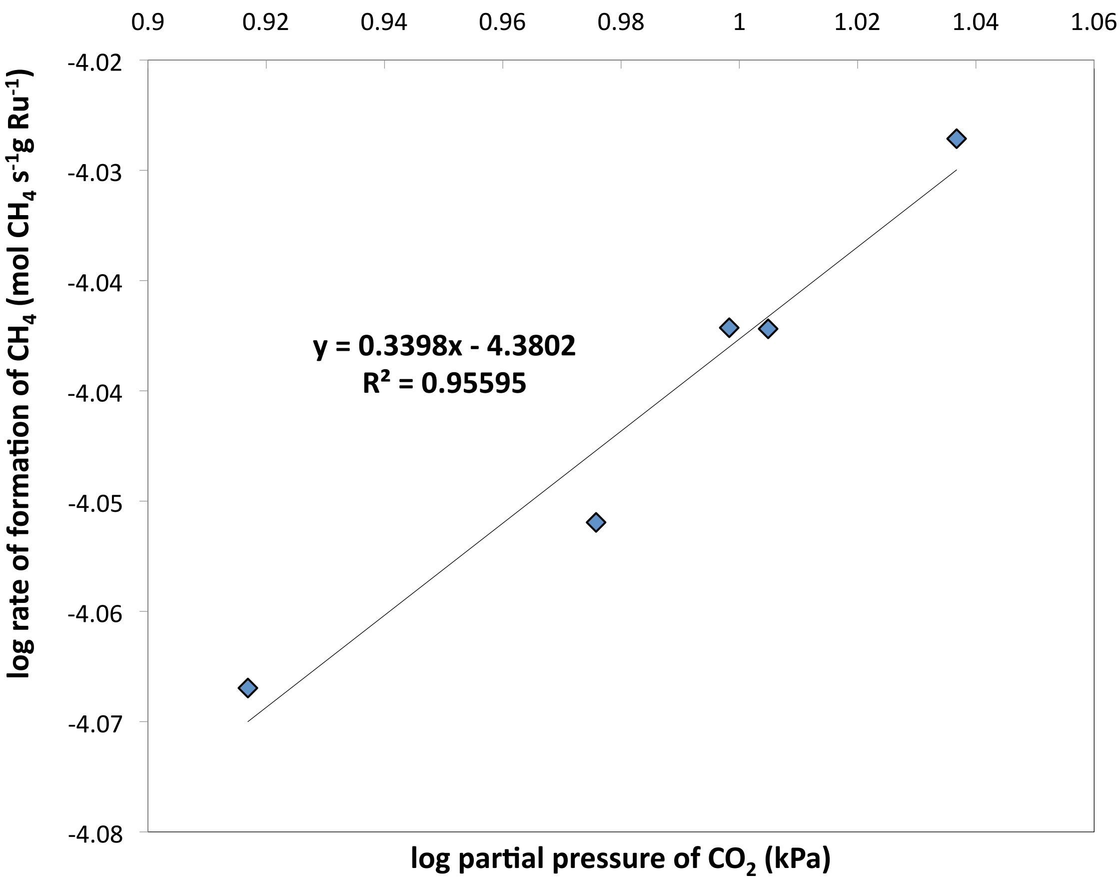

Figure 8.2: Dependence of reaction rate on CO_2 concentration. P_{CO2}=8-10 kPa kPa, P_{H2}=40 kPa. T= 230°C, 1 atm total pressure.

8.4 Order of reaction with respect to CH_4

CO_2 hydrogenation was found to show a very weak dependence on CH_4 concentration, as determined by Figure 8.3. The order of reaction with respect to CH_4 was determined as -0.11. The data show a weak correlation with an R^2 value of nearly 0.4, indicating that the inhibiting effect is negligible and largely affected by experimental fluctuations. This value is representative for methane partial pressures varying from 1 to 25 kPa and CO_2 conversions ranging from 25 to 89%. The negative order reflects the small inhibiting effect of methane on the forward reaction rate, which is not expected to be significant even at high conversions.

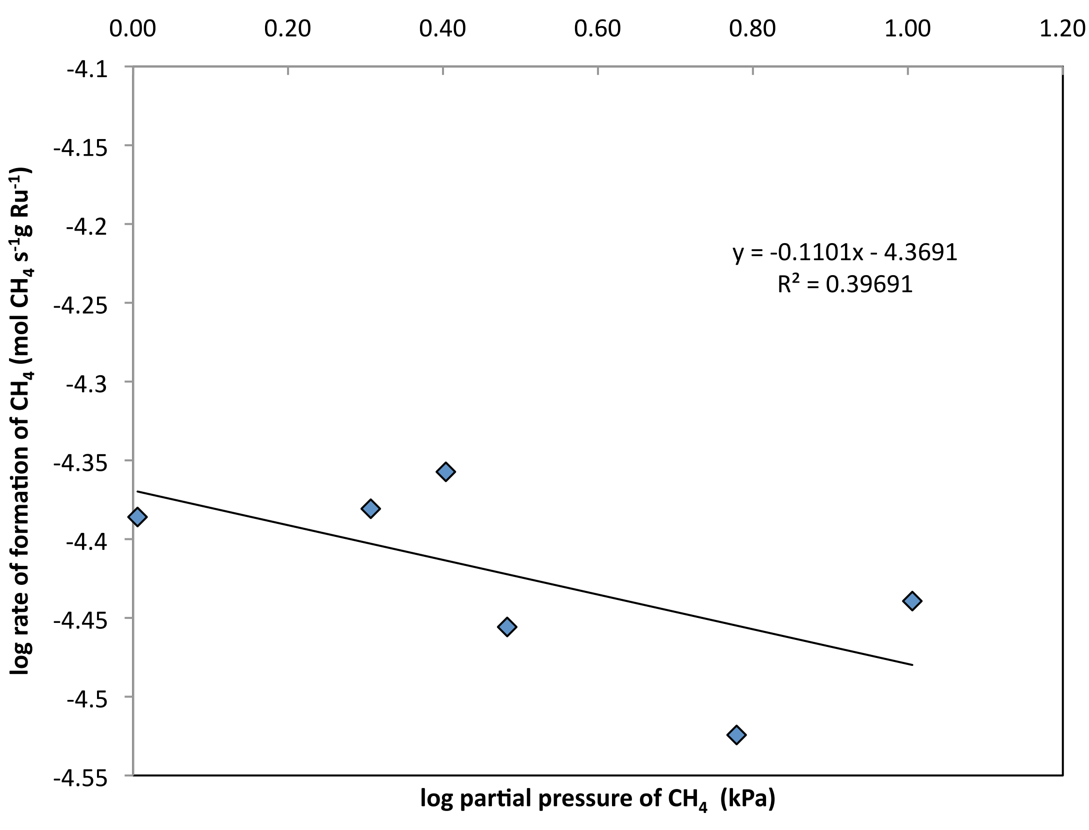

Figure 8.3: Dependence of reaction rate on methane partial pressure. P_{CH4}= 1-25 kPa, T=230^{o}C, 1 atm total pressure

8.5 Order of reaction with respect to H_2O

The order of reaction was determined from results shown in Figure 8.4 to be -0.23 with respect to H_2O during experiments where H_2O partial pressure was varied from 3 to 20 kPa to represent CO_2 conversions in the range 34-77%. The negative order indicates that H_2O produced at the surface during methanation slightly inhibits the reaction. This observation is in line with the existing literature on the kinetics of CO_2 methanation over Ru catalysts. Marwood et al. have previously observed that water has an inhibiting effect on the methanation of CO_2 over Ru/TiO_2[72, 73]. Through DRIFTS they were able to observe that with increasing water partial pressure in the feed, the concentration of $CO_{(a)}$ and $HCOO^-_{(a)}$ decreased[72]. Marwood et al. propose a methanation mechanism which includes to formation of adsorbed CO (which is then methanated) via the reverse water gas shift reaction[73]. This explains the inhibiting effect of water since water is a product of reverse water gas shift as well as methanation. The reaction order for H_2O is slightly more negative compared to CH_4 and could potentially be important at high conversions since twice as much H_2O compared to CH_4 is formed.

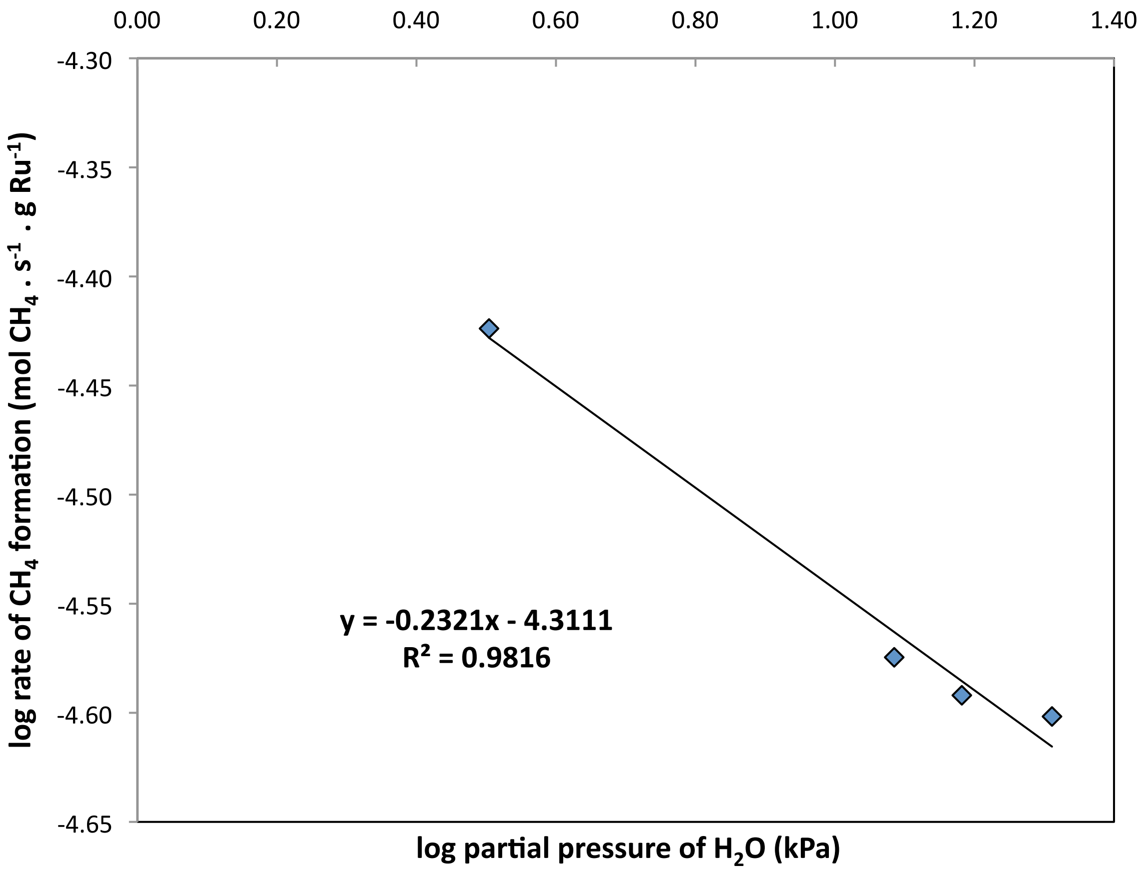

Figure 8.4: Dependence of reaction rate on H_2O partial pressure. P_{H2O}= 3-20 kPa, T=230^{o}C, 1 atm total pressure

8.6 Arrhenius coefficient and energy of activation

Measurements for the determination of activation energy and Arrhenius coefficient were performed at temperatures ranging from 200 to 245^{o}C. The activation energy for CO_2 hydrogenation was calculated as 66.084 kJ/g-mol. This value is consistent with those presented in the existing literature on Ru based catalysts. Kusmiers estimated the true activation energy of methanation over Ru/γ-Al_2O_3 as 60±12kJ/g-mol[77]. Brooks et al. have reported an activation energy of 69.06 kJ/g-mol for CO_2 methanation over Ru/TiO_2 catalysts[97] while Prairie et al. have determined the activation energy for both Ru/TiO_2 and $Ru/\gamma\text{-}Al_2O_3$ to be 79 kJ/mol[74]. Lunde and Kester have reported an activation energy of 70.46 kJ/mol for methanation over $Ru/\gamma\text{-}Al_2O_3$[98]. The Arrhenius plot used for this calculation is shown in Figure 8.5. The Arrhenius coefficient was determined from the y-intercept of the Arrhenius plot, and was equal to 35.495.

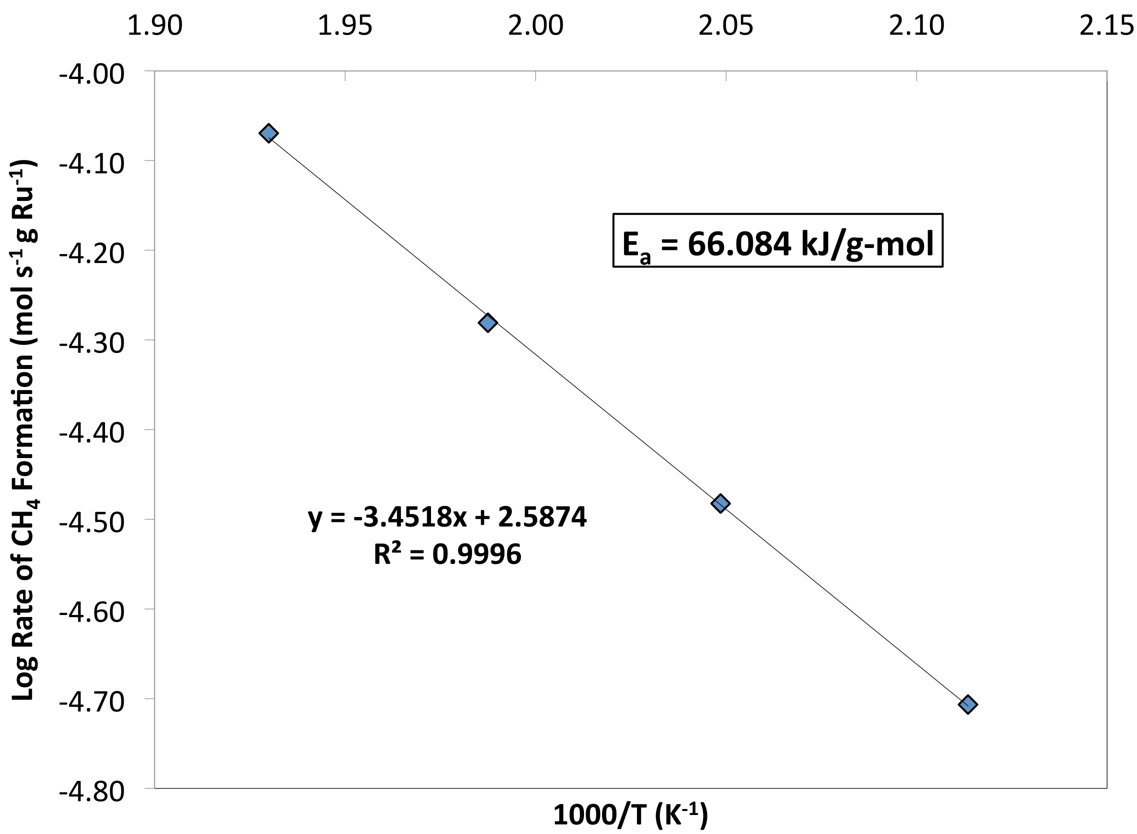

Figure 8.5: Arrhenius plot for CO_2 hydrogenation. T= 230-245^oC

8.7 Empirical rate law

An empirical rate equation for CO_2 hydrogenation has been developed through the differential reactor approach as shown in Eq. 11.This expression was determined for temperatures ranging from 473-573 K and for partial pressures of 43-63 kPa for H_2 and 6-8 kPa for CO_2 and is expected to be valid when conditions are similar to those employed in this study. The ratio of H_2/CO_2 ranged from 4-6 consistent with that expected in a real application.

$$R_{CH_4,f} = 35.495 \times e^{-66084/(RT)} \times p_{H_2}{}^{0.88} \times p_{CO_2}{}^{0.34} \times p_{CH_4}{}^{-0.11} \times p_{H_2O}{}^{-0.23}$$

(Eq. 14)

The empirical rate equation presented here gives the rate of formation of methane ($R_{CH4,f}$) in units of (g-mol $CH_4 \cdot s^{-1} \cdot g_{Ru}{}^{-1}$). In the above equation, R is the universal gas constant with units J/g-mol K and T is temperature in units of K. In order to verify the empirical rate expression, rates of CH_4 formation measured at 473-573 K for a feed consisting of 4% CO_2, 16% H_2 and 80% He were compared to values calculated using the empirical rate law. Results plotted in Fig.8 show the agreement between experimental and calculated rates. The calculated rates are within 1-4% of the experimental rate measurements. It should be noted that the calculated rates are initial rates, which neglect the presence of H_2O and CH_4 in the catalyst bed since measurements were made under differential conditions.

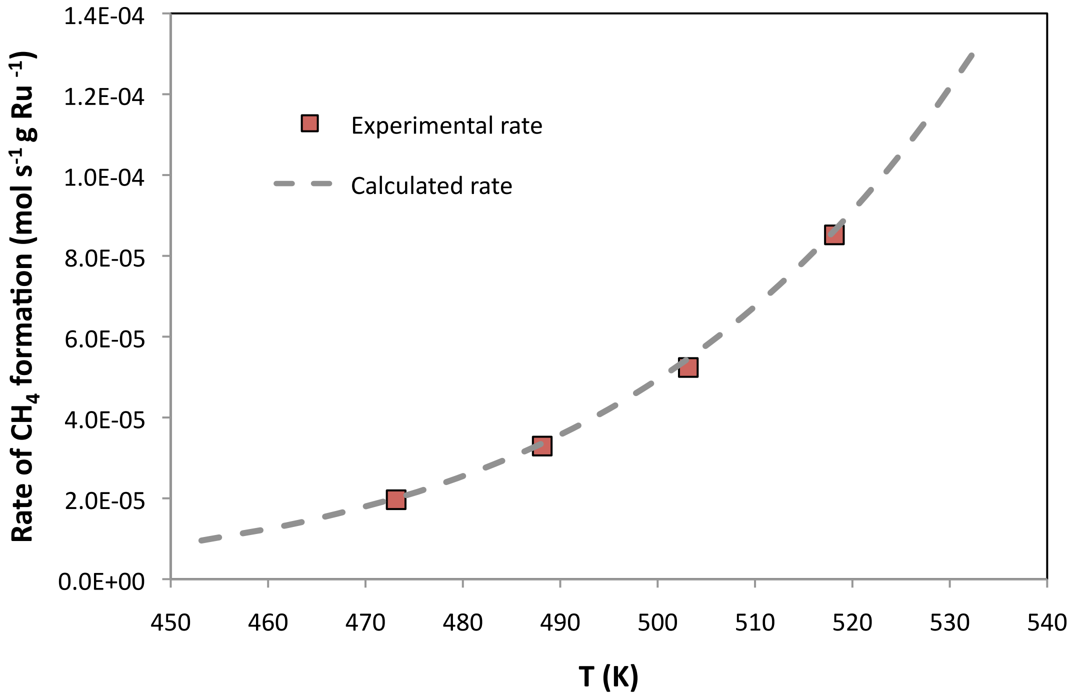

Figure 8.6: Experimental and calculated rates of CH_4 formation.

Feed: 4% CO_2 / 16% H_2 / 80% He.

Chapter 9 : Lessons learned from Ru/γ-Al_2O_3 for the operation of dual function materials

9.1 Process conditions and pretreatment

The variation of catalyst lightoff with changing gas hourly space velocity (GHSV) has been shown by experiments presented in Chapter 4. The dual function material performance will also be similarly affected during the methanation step. The methanation step can be controlled independently of the target application because it only depends on the supply of renewable hydrogen. Since the target application does not present any constraints on the methanation step, it is important to utilize the insight on Ru/γ-Al_2O_3 presented in Chapter 4 in order to optimize operating conditions and pretreatment of dual function materials containing Ru as catalytic component.

The results presented in Chapter 4 show that optimum catalytic performance can be obtained when the methanation step is operated at a GHSV of 4720 h^{-1} or less and at temperatures exceeding 280^{o}C but below 350^{o}C. This will yield suitable thermodynamics and kinetics. It has also been shown in Chapter 4 that pre-reduction of the catalyst at 320^{o}C achieves the maximum metal dispersion due to the complete reduction of RuO_x species. Pre-reduction of the DFMs at 320^{o}C will possibly be needed initially or at intervals to reduce RuO_x (due to air exposure during the capture mode).

Sintering of Ru metal has been identified as a cause of catalyst deactivation in Chapter 4. Since methanation is an exothermic reaction, the reaction heat can build up within the material and cause sintering. Upon optimization of the dual function material in terms of its CaO and Ru composition, excess heat is not expected to present any problems as the endothermic desorption of CO_2 will absorb the heat liberated by methanation.

9.2 Implications of cyclic TGA-DSC studies on Ru/γ-Al_2O_3 for Ru CaO/γ-Al_2O_3 dual function materials

A dual function material will operate under cyclic conditions where CO_2 is captured first, followed by hydrogenation, thus rendering the Ru in DFMs susceptible to deactivation through oxidation. Hence the data presented in Chapter 5 become relevant for identifying factors affecting stability and activity of Ru in dual function materials (Ru CaO/γ-Al_2O_3) due to the cyclic introduction of CO_2 and H_2.

Results from TGA-DSC studies as well as literature sources imply that CO_2 dissociates on the Ru/γ-Al_2O_3 catalyst and deactivates Ru by forming RuO_x. The oxidation of Ru during introduction of CO_2 and its dissociation are particularly relevant for dual function material (DFM) systems used for CO_2 capture and subsequent methanation. The DFMs operate by first chemisorbing CO_2 from the flue gas followed by methanation when renewable H_2 is added in the second step. The data presented in Chapter 5 suggest that RuO_x formed from dissociation of adsorbed CO_2 can be reduced at 320^{o}C in hydrogen. Hence it is likely that performing the hydrogenation step in the cyclic operation of DFMs at 320^{o}C will be sufficient to reduce any

RuO_x species formed during the oxidizing flue gas environment back to Ru^0, the active state for methanation of CO_2. Operation of the DFM at 320^{o}C eliminates this problem completely since Ru---O is reduced when H_2 is introduced and methanation proceeds uninhibited.

9.3 Consequences of Eley-Rideal rate model and other kinetic observations on Ru/γ-Al_2O_3 for development and operation of Ru CaO/γ-Al_2O_3 dual function materials

CO_2 methanation over 10%Ru/γ-Al_2O_3 follows an Eley-Rideal mechanism where gas phase H_2 reacts with strongly adsorbed CO_2. The empirical rate law developed in Chapter 8 confirms a strong dependence on H_2 and weak dependence on CO_2 concentrations expected from an Eley-Rideal reaction model. The strong dependence of methanation rate over Ru/γ-Al_2O_3 on hydrogen partial pressure suggests that in a real dual function CO_2 capture and methanation reactor it may be necessary to introduce excess hydrogen during the methanation step. Increasing the CO_2 partial pressure beyond a certain value saturates the catalyst and will not further increase the rate.

Since increasing temperatures does not favor the equilibrium, increasing the H_2 partial pressure becomes the only process parameter for enhancing the reaction rate. This will constitute a problem if the final synthetic natural gas produced contains more than 6% H_2, which is the upper limit allowed in methane pipelines (by volume) [99]. Excess H_2 above 6% can be removed (and recycled) with a membrane before the SNG enters the pipeline.

Chapter 10 : Nano dispersed CaO/γ-Al_2O_3 as a reversible CO_2 adsorbent at intermediate temperatures

The results presented in this chapter were conducted as partial fullfillment of the requirements for the MS degree in Earth and Environmental Engineering and have been published in Industrial & Engineering Chemistry Research in a paper entitled "In-situ CO_2 capture using CaO/γ-Al_2O_3 washcoated monoliths for sorption enhanced water gas shift reaction".

When dispersed on a porous γ-Al_2O_3 carrier to form nano-sized islands, CaO attains properties differing significantly from bulk CaO. These properties are particularly useful for CO_2 capture at moderate temperatures (300-650^{o}C). The interaction between nano dispersed CaO/γ-Al_2O_3 and CO_2 has previously been investigated for in-situ CO_2 capture to enhance the hydrogen yields from the water gas shift reaction at high temperatures. This chapter presents some of the relevant studies on CO_2 capture by nano dispersed CaO to demonstrate the suitability of this novel adsorbent for dual function material applications. The reversibility of CO_2 capture at intermediate temperatures is discussed and the CO_2 adsorption/desorption over CaO/γ-Al_2O_3 coated ceramic monoliths in the presence of varying amounts of steam is evaluated.

10.1 The unique CO_2 adsorption/desorption behavior over nano dispersed $CaO/\gamma\text{-}Al_2O_3$ compared to bulk CaO

$CaO/\gamma\text{-}Al_2O_3$ has previously been evaluated for its CO_2 capture properties by Gruene et al. using thermogravimetric analysis[86]. Their results comparing bulk CaO and $CaO/\gamma\text{-}Al_2O_3$ are reproduced here to highlight the unique properties of nano dispersed CaO. When comparing the performances of different adsorbents, adsorption efficiency was used as parameter of merit. Adsorption efficiency θ, shown in Eq.15, is defined as the ratio of the moles (n) of CO_2 adsorbed to the moles of CaO that are present in the adsorbent sample, expressed as a percentage. Adsorption efficiency provides a measure of how much of the theoretical CO_2 capture capacity of an adsorbent sample is utilized under a given set of experimental conditions.

$$\theta = \frac{n(CO_{2,\,ads})}{n(CaO)} \times 100\%$$

(Eq. 15)

Gruene et al. performed CO_2 capture over both CaO and nano dispersed $CaO/\gamma\text{-}Al_2O_3$ using the TGA and their findings are presented in Figure 10.1[86]. Both adsorbents were exposed first to a mixture of 15% CO_2 in N_2 for 30 minutes, then to pure N_2 for 30 minutes, with both steps taking place at a temperature of 300^oC. CO_2 capture is indicated by a rise in adsorption efficiency for both adsorbents. Figure 10.1(a) shows that when exposed to CO_2, bulk CaO captures it to form a solid compound, which is stable at 300^oC when the feed is switched to pure N_2. Bulk CaO reacts with CO_2 to form $CaCO_3$, which is a stable product that does not decompose until temperatures around 800^oC. The response of $CaO/\gamma\text{-}Al_2O_3$ to CO_2/N_2 and N_2

feeds is shown in Figure 10.1(b). It is clear that CaO/γ-Al_2O_3 shows a higher overall adsorption efficiency compared to bulk CaO. This is because by dispersing CaO as nanometer sized islands, it is possible to utilize more of the CaO present in the sample; in bulk CaO a small portion of the material is utilized for CO_2 capture because reaction with CO_2 forms a $CaCO_3$ "crust" that makes it difficult for CO_2 to diffuse into the bulk material. What is more remarkable in Figure 10.1(b) is that when the feed is switched to pure nitrogen, the CO_2 saturated CaO/γ-Al_2O_3 releases about 30% of captured CO_2 at 300°C. This clearly indicates weak bond formation between CO_2 and CaO/γ-Al_2O_3.

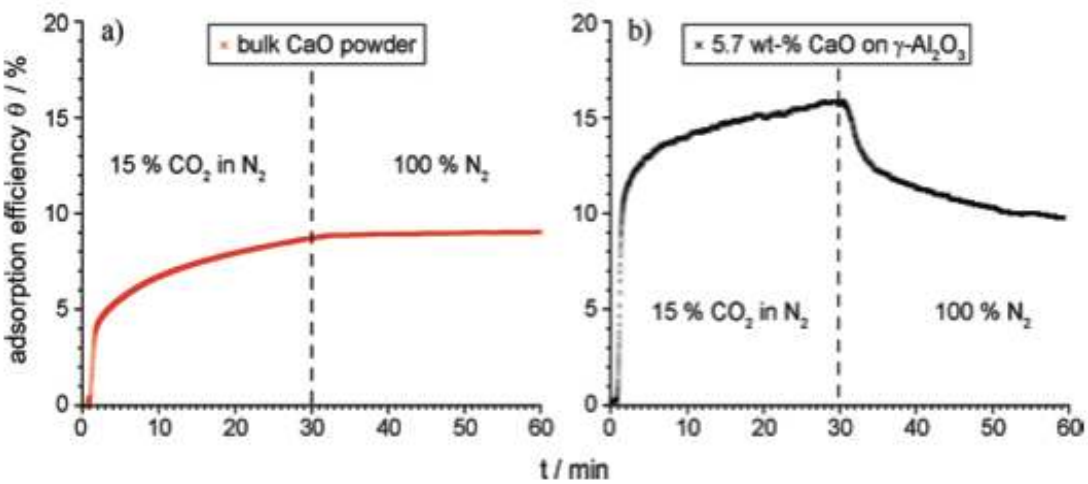

Figure 10.1: Adsorption efficiency Θ at 300°C as a function of time for bulk CaO (a) and CaO/γ Al_2O_3 with 5.7 weight % CaO loading (b)

The interaction of CO_2 with bulk CaO and nano dispersed CaO/γ-Al_2O_3 was investigated by Gruene et al. using in-situ diffuse reflectance infrared fourier transform spectroscopy (DRIFTS) at 300 and 450°C. It was determined through these means that bulk CaO can interact with CO_2 in a number of ways, some of which form strongly bound bridged carbonates and crystalline $CaCO_3$ that require very high temperatures to release CO_2[86]. In contrast, there is only one weak binding interaction that is energetically feasible between CO_2 and nano dispersed $CaO/\gamma\text{-}Al_2O_3$. The DRIFTS results from Gruene et al. show that strongly bound carbonate and crystalline $CaCO_3$ formation is inhibited in $CaO/\gamma\text{-}Al_2O_3$[86]. CO_2 binding on the support was not observed for $CaO/\gamma\text{-}Al_2O_3$ at the temepratures investigated in this study.

10.2: CO_2 capture at 350^oC and determining the temperature for complete adsorbent regeneration using TGA

TGA was used to determine the temperature at which CO_2 adsorbed on $CaO/\gamma\text{-}Al_2O_3$ can be released from the adsorbent. Figure 10.2 displays mass change data from a TGA experiment performed on a powder sample of 10% $CaO/\gamma\text{-}Al_2O_3$. The sample was first saturated with CO_2 at 350^oC and then regenerated in a flow of N_2 while increasing the temperature. Results shown in Figure 10.2 indicate that the saturated adsorbent can be fully regenerated at 390^oC in a flow of nitrogen. The temperature of 390^oC is much lower than that required for decomposition of bulk $CaCO_3$ (>800^oC). This result is consistent with the work by Gruene et al.[86] which has shown that nano dispersed CaO interacts more weakly with CO_2 compared to bulk CaO.

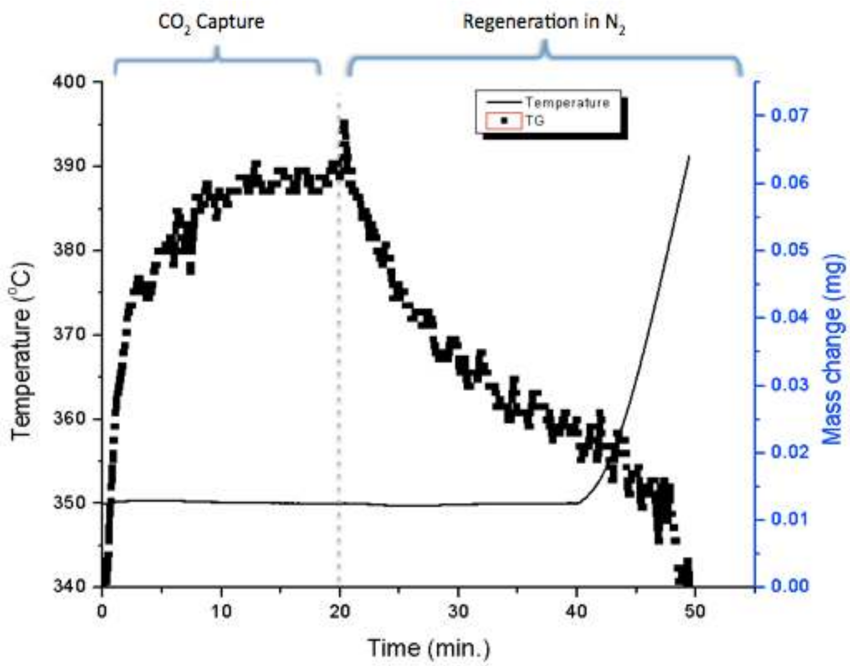

Figure 10.2: TGA response for a $CaO/\gamma\text{-}Al_2O_3$ sample during CO_2 capture (350°C) and regeneration (350-390°C). Feed: 10% CO_2/N_2 for "CO_2 capture", 100% N_2 for "Regeneration"

10.3 The impact of steam on CO_2 capture and release from nano dispersed $CaO/\gamma\text{-}Al_2O_3$

$CaO/\gamma\text{-}Al_2O_3$ was previously studied as a sorbent for enhancing the hydrogen yields from the water gas shift reaction at high temperatures through in-situ CO_2 capture. Since the water gas shift reaction is operated under conditions where steam is present as reactant, the impact of steam on CO_2 adsorption and desorption properties of $CaO/\gamma\text{-}Al_2O_3$ was investigated in a flow reactor using 10% $CaO/\gamma\text{-}Al_2O_3$ coated monoliths and in a TGA using powder 10% $CaO/\gamma\text{-}Al_2O_3$. These results are relevant for dual function materials for CO_2 capture and subsequent methanation since flue gas from combustion of fossil fuels will also contain steam.

Figure 10.3 displays the adsorption and desorption efficiency of 10% $CaO/\gamma\text{-}Al_2O_3$ coated monoliths under conditions of varying steam concentration in the feed. Each sample was exposed to CO_2 capture from a 10% CO_2 stream diluted with a specific mixture of steam and nitrogen. The samples were then exposed to varying amounts of steam and nitrogen during sorbent regeneration. Figure 10.3(a) shows that greater adsorption efficiency is observed when the feed consists of 28% steam. Since the partial pressure of CO_2 is fixed for all experiments, this is interpreted as a beneficial effect of steam on CO_2 uptake capacity of the adsorbent. In a study by Stevens et al., bulk CaO showed increased CO_2 capture capacity compared to untreated CaO, when used in a fixed bed water gas shift reactor[100]. Based on XRD results, it was hypothesized that steam converts CaO to $Ca(OH)_2$ and thus increases the CO_2 capture capacity of the sorbent[100]. The results shown in Figure 10.3 also point to a mechanism where steam interacts with $CaO/\gamma\text{-}Al_2O_3$, possibly via the hydration reaction or weak chemisorption.

Figure 10.3(b) shows that when CO_2 is removed from the feed at 350°C its desorption is enhanced by steam. Exposure of the $CaO/\gamma\text{-}Al_2O_3$ to steam is thought to result in the hydration of CaO sites or chemisorption of H_2O molecules on CaO sites. When CO_2 is present in the feed stream, it replaces these surface species due to its higher affinity towards CaO. Likewise, when CO_2 is removed from the feed and the steam concentration is increased, the chemisorbed CO_2 molecules are displaced due to the interaction of CaO with H_2O molecules. The increase in steam concentration is thought to be responsible for a greater degree of replacement of adsorbed CO_2

molecules, hence a greater extent of regeneration of the sorbent. It should be noted that isothermal desorption of CO_2 was also observed during previous TGA studies where no steam was present although this was not the case with results shown in Figure 10.3. This difference in the detection of desorbed CO_2 in reactor and TGA tests is likely due to the longer sampling time for GC gas analysis (~1 minute) used with the reactor compared to the mass change detection in the TGA (~4 seconds).

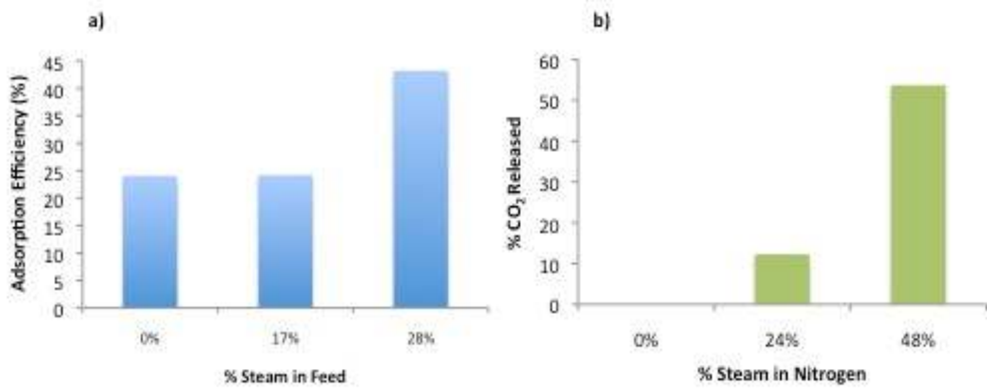

Figure 10.3: (a) Adsorption efficiencies of 10% CaO/γ-Al_2O_3 coated monoliths at 350^oC exposed to different steam concentrations (b) Volume of CO_2 released during regeneration at 350^oC as a percentage of initial volume adsorbed

The following mechanism for interactions between steam, CO_2 and CaO/γ-Al_2O_3 have been proposed in light of the results shown in Figure 10.3:

CaO hydration:

$$CaO_{(s)} + H_2O_{(g)} \rightarrow Ca(OH)_{2(s)} \qquad \text{(Eq. 16)}$$

Chemisorption of H_2O on CaO:

$$CaO_{(s)} + H_2O_{(g)} \rightarrow CaO^{\cdots}H_2O_{(s)} \qquad \text{(Eq. 17)}$$

Possible CO_2 adsorption mechanisms in the presence of steam:

$$Ca(OH)_{2(s)} + CO_{2(g)} \rightarrow CaO^{\cdots}CO_{2(s)} + H_2O_{(g)} \qquad \text{(Eq. 18)}$$

$$CaO^{\cdots}H_2O_{(s)} + CO_{2(g)} \rightarrow CaO^{\cdots}CO_{2(s)} + H_2O_{(g)} \qquad \text{(Eq. 19)}$$

Possible mechanisms for steam regeneration of saturated adsorbent:

$$CaO^{\cdots}CO_{2(s)} + H_2O_{(g)} \rightarrow CaO^{\cdots}H_2O_{(s)} + CO_{2(g)} \qquad \text{(Eq. 20)}$$

$$CaO^{\cdots}CO_{2(s)} + H_2O_{(g)} \rightarrow Ca(OH)_{2(s)} + CO_{2(g)} \qquad \text{(Eq. 21)}$$

The increased adsorption efficiency observed during reactor experiments in the presence of 28% steam corresponds to a capacity of 0.63 moles CO_2/kg CaO/γ-Al_2O_3. 0.5 moles/kg has previously been reported as an economically feasible uptake capacity for CO_2 adsorbents[101]. Therefore, CaO/γ-Al_2O_3 has a potential to be an economically acceptable adsorbent in the presence of steam.

Figure 10.1 shows results from BET analysis performed on 10% CaO/γ-Al_2O_3 powder samples exposed to different treatments. Exposure to 350^{o}C causes a slight decrease in surface area whereas exposure to the same temperature in the presence of steam causes a small increase. Steam might be increasing BET surface area of CaO/γ-Al_2O_3 by chemisorbing on or hydrating the CaO crystallites (forming $Ca(OH)_2$ or $CaO \cdot H_2O$); this may be causing some pores that were previously inaccessible to open and hence causes a small increase in BET area.

Table 10.1: BET analysis for CaO/γ-Al_2O_3 samples exposed to different conditions

Sample	BET surface area (m^2/g)
Fresh 9.4% CaO/Al_2O_3 adsorbent	69.24
9.4% CaO/Al_2O_3, 2 hours at 350°C	64.41
9.4 % CaO/Al_2O_3 350C, 2 hours at 350°C in 66% H_2O	76.72

Figure 10.4 displays results from a TGA test where a powder 10%CaO/γ-Al_2O_3 sample was exposed to steam at 350°C. Results from this test show that 0.12 mg of steam is adsorbed, which supports the hypothesis that steam is chemisorbing or reacting with the surface of the sample.

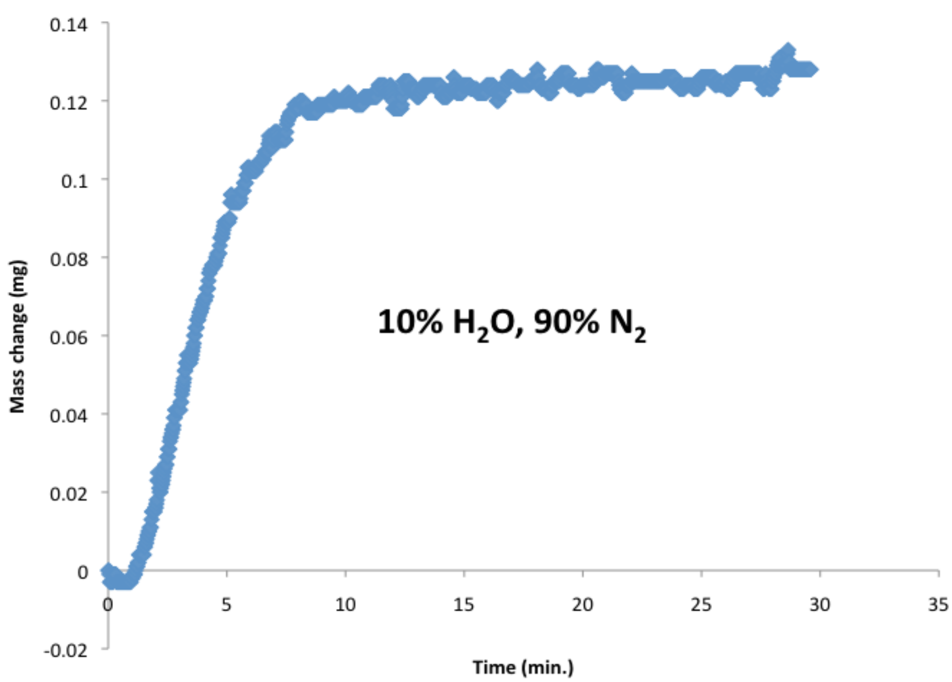

Figure 10.4. TGA signal during the period of exposure of CaO/γ-Al_2O_3 to steam

Figure 10.5 shows adsorption efficiencies for the first minute of CO_2 capture for a sample that has previously been exposed to steam and a sample that has never been exposed to steam. The decreased weight gain for the steam treated sample agrees with the hypothesis that pre-adsorbed H_2O molecules (or hydroxide groups) are being replaced by CO_2. This replacement results in weight decrease due to water molecules (or hydroxide groups) leaving the surface and weight gain due to adsorbing CO_2. After the first 30 seconds of capture, the steam-treated sample follows the same rate of CO_2 uptake as the untreated sample.

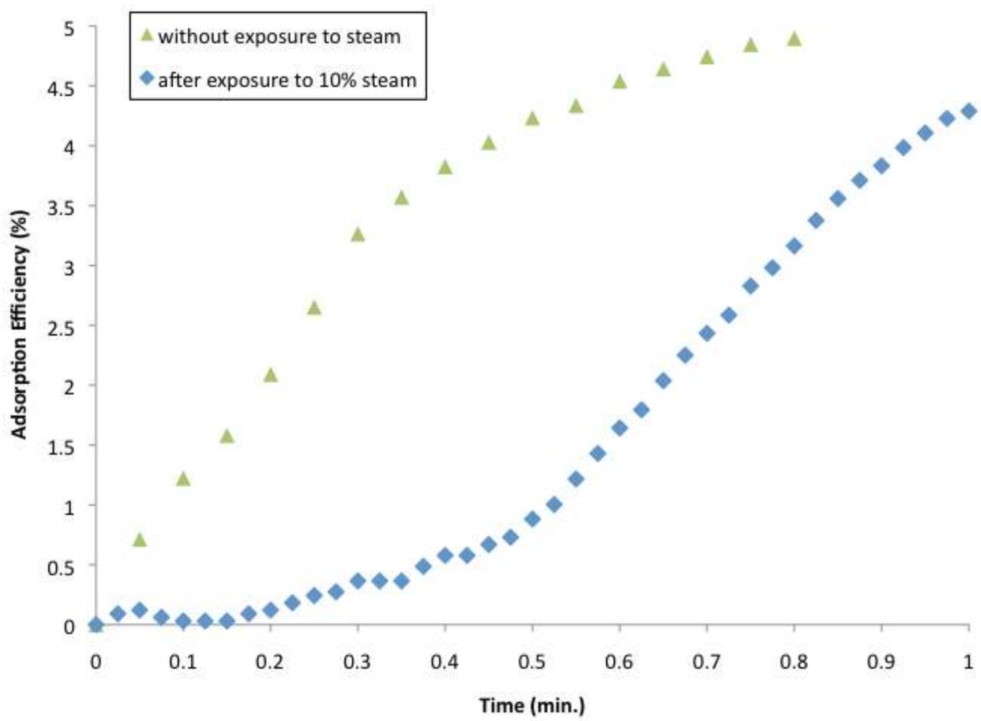

Figure 10.5. Adsorption efficiencies for a steam treated and an untreated sample of CaO/γ-Al_2O_3 in the first minute of CO_2 capture

Chapter 11 : Dual function materials for CO_2 capture and subsequent methanation

A physical mixture of 10% Ru/γ-Al_2O_3 and 10% CaO/γ-Al_2O_3 was investigated through cyclic CO_2 capture and methanation experiments in a flow reactor to provide proof of concept for dual function materials. It was demonstrated that a physical mixture of CaO/γ-Al_2O_3 and Ru/γ-Al_2O_3 could capture CO_2 from a 10% CO_2/N_2 stream and release it as CH_4 upon purging with 40%H_2/N_2. This is a completely unique approach to CO_2 capture and utilization, because a dual function material performing both processes consecutively has not been reported.

11.1 Adsorption studies on a physical mixture of 10% CaO/γ-Al_2O_3 and 10% Ru/Al_2O_3 using TGA-DSC

A physical mixture of 10% CaO/γ-Al_2O_3 and 10% Ru/γ-Al_2O_3 was used to capture CO_2 from a dilute stream (0.5%CO_2 in N_2) and to subsequently generate CH_4 from the adsorbed CO_2 by flowing H_2 (2% in N_2) under isothermal conditions. CaO/γ-Al_2O_3 and Ru/γ-Al_2O_3 were mixed in equal weights. Experiments were performed in the TGA/DSC apparatus (Netszch Jupiter) at 350^{o}C, a temperature where the Ru catalyst could easily be maintained in a reduced state. Figure 11.1 displays TGA and DSC responses during the period of exposure to CO_2, N_2 and H_2. It can be seen from the TGA signal that a slight mass increase occurs upon exposure to CO_2. This mass increase also corresponds to a negative DSC peak, which indicates an exothermic process. These TGA and DSC signals are associated with the adsorption of CO_2. A slight decrease in mass not accompanied by any change in the DSC signal is observed when H_2 is introduced. Upon exposure to H_2, the sample undergoes rapid and significant mass loss (2.5% of initial mass). This mass change is in large excess of the amount corresponding to CO_2 adsorption, distinguishing it from desorption or methanation. The significant mass loss, combined with the corresponding large negative DSC peak, indicates that Ru metal in the Ru/γ-Al_2O_3 catalyst is being reduced.

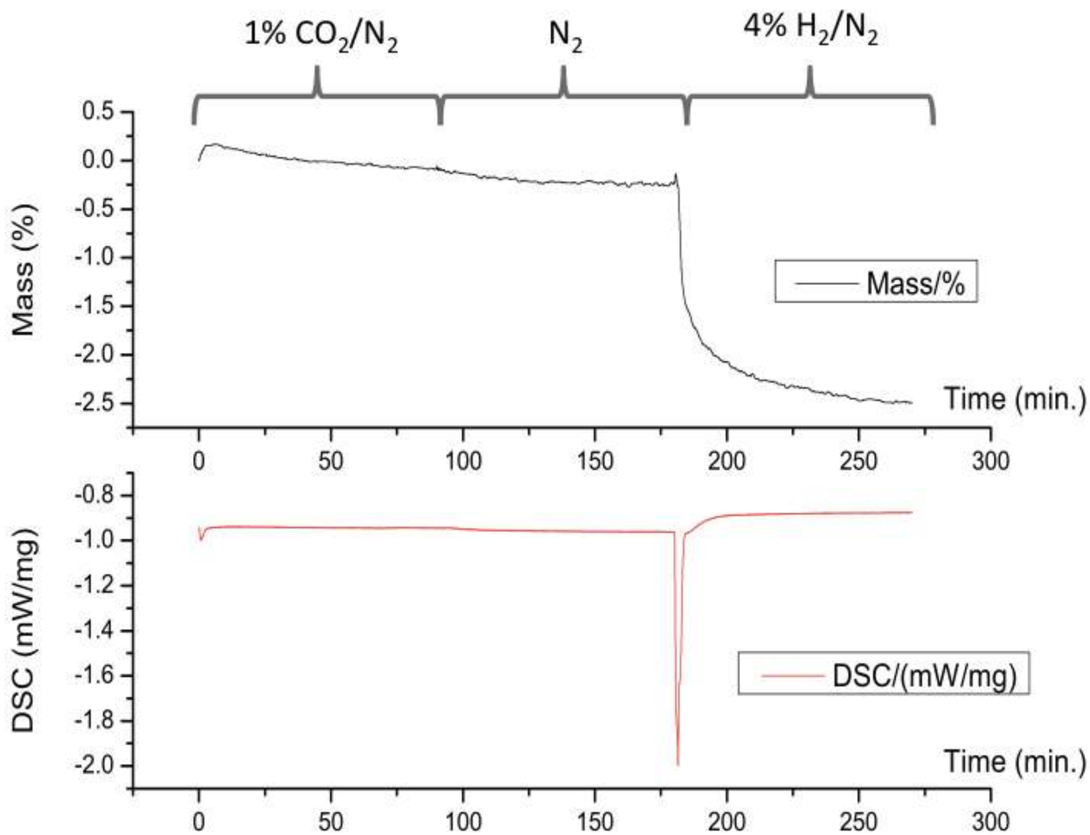

Figure 11.1: $CO_2/N_2/H_2$ cycle for CaO/γ-Al_2O_3 and Ru/γ-Al_2O_3 mixture

In order to observe CO_2 adsorption and hydrogenation without the effects of catalyst reduction, the experiment was repeated, but with an additional reduction step (4% H_2/N_2 at 350°C for 1 hour) at the beginning. Results for this test, plotted in Figure 11.2, display a much larger uptake of CO_2 compared to the first test without initial pre-reduction, as well as a larger exotherm. This increased capacity for CO_2 adsorption indicates that the reduced Ru^0 metal adsorbs CO_2. Hence it can be deduced that in the previous experiment, CaO/γ-Al_2O_3 was the only CO_2 adsorbing species; the pre-reduction step allowed for much greater uptake of CO_2 because it enabled adsorption by Ru in addition to CaO. A slight decrease in mass is observed when the feed is switched to N_2, without any noticeable change in the DSC signal. Upon exposure to H_2, the sample rapidly loses mass and releases heat as can be seen in the TGA and DSC signals shown in Figure 11.2. This process results in the sample mass to stabilize at around -0.4% of its initial value. It is hypothesized that all of the CO_2 that was previously adsorbed by the sample is hydrogenated in this step to produce CH_4.This process is likely followed by further reduction of the metal which could be made more kinetically favorable by the rapid release of heat (as seen from DSC signal in Figure 11.2) in the catalyst/adsorbent powder.

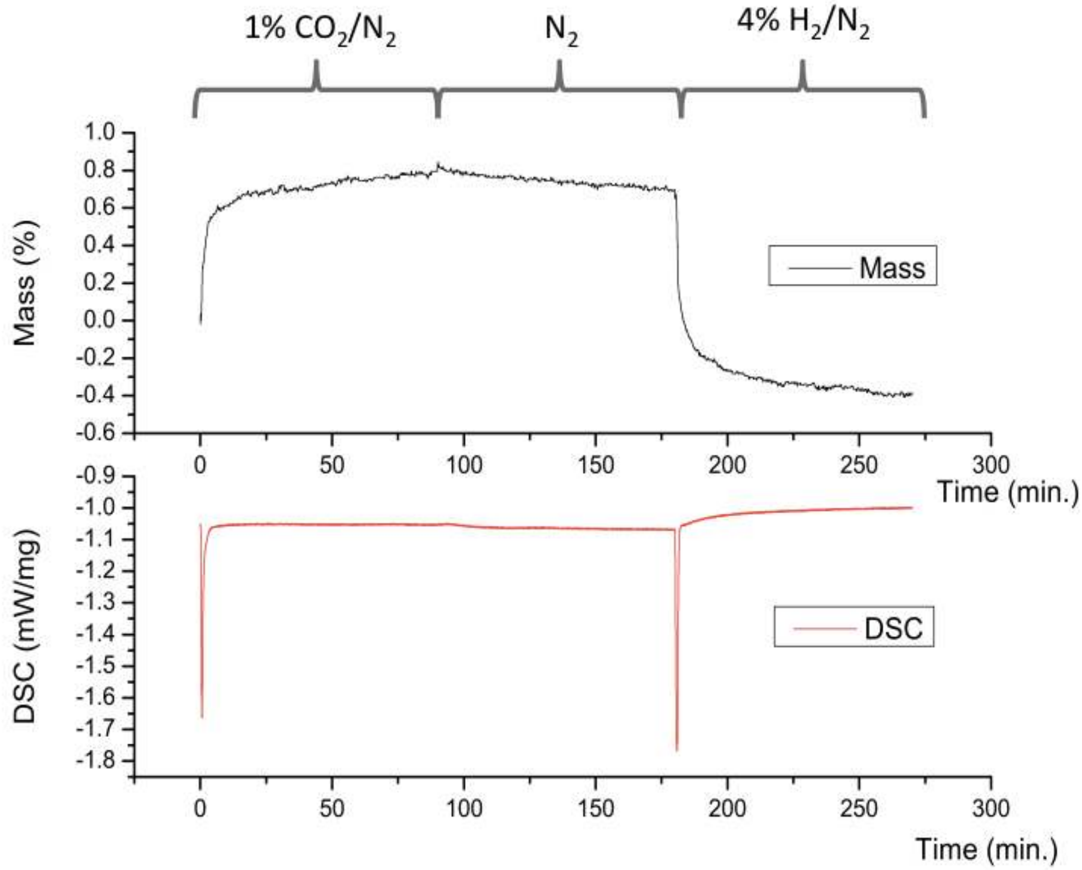

Figure 11.2: CO_2/N_2/H_2 cycle for pre-reduced CaO/γ-Al_2O_3 and Ru/γ-Al_2O_3 mixture

CO_2 adsorption and desorption on CaO/γ-Al_2O_3 was previously studied for the same temperature (350°C) with pure CO_2 and pure N_2 introduction to facilitate adsorption and desorption respectively[87]. It was shown that approximately 40% of adsorbed CO_2 was released from the adsorbent upon exposure to N_2 at 350°C in the same TGA setting. Based on results shown in Figure 11.2 it is assumed that in the presence of Ru/γ-Al_2O_3, which is a good methanation catalyst, all captured CO_2 is released, likely in the form of CH_4. This effect can be due to generation of heat within the sample itself, causing migration of CO_2 strongly adsorbed on

CaO sites to the Ru sites and their subsequent hydrogenation. Hence the addition of Ru to CaO/γ-Al_2O_3 can facilitate complete regeneration of the saturated adsorbent at isothermal conditions, while converting the captured CO_2 to a valuable fuel.

11.2 Proof of concept using a physical mixture of 10% CaO/γ-Al_2O_3 and 10% Ru/γ-Al_2O_3 for CO_2 capture and subsequent methanation in a flow reactor

A physical mixture of 10 wt.% CaO/γ-Al_2O_3 and 10 wt.% Ru/γ-Al_2O_3 was packed into a fixed bed reactor. The reactor was operated in a cyclic manner; 5 cycles each were performed at 260 and 320^{o}C. Each cycle consisted of a 'CO_2 capture' from a 10% CO_2 /N_2 feed, followed by a 'methanation' period, where 10% CO_2/N_2 was discontinued and a stream of 40% H_2/He was introduced. The test included a pre-reduction step (at reaction temperature) only before the first cycle because it was observed in previous TGA studies that the pre-reduced catalyst adsorbs more CO_2 compared to its untreated state. Pre-reduction was not performed before the other cycles because it was assumed that the H_2 -rich stream during methanation would be sufficient to reduce the catalyst prior to the next cycle of CO_2 capture. The reactor was purged with He between each cycle.

Figure 11.3 shows the CO_2 capture period for the first cycle. It can be seen that when the mixture of CaO/γ-Al_2O_3 and Ru/γ-Al_2O_3 is exposed to 10% CO_2/N_2, CO_2 is immediately captured during the first 10 minutes. The period after 10 minutes is termed 'breakthrough' and is characterized by the detection of CO_2. CO_2 flow rate quickly reaches the background value following breakthrough. The total volume of CO_2 captured was 15.7 mL at room temperature (641 μ-moles).

Figure 11.4 displays the methane flow rate during methanation in the 1st cycle. Methane is observed as a pulse in the product stream. This clearly demonstrates that it is possible to convert CO_2 captured in a solid adsorbent/catalyst mixture, to methane. Total amount of methane released during methanation in the first cycle was 18.4 mL (738 μ-moles). Since there are only 397 μ-moles of Ru in the reactor bed, the amount of methane generated in the first cycle is too large to have only been produced from CO_2 adsorbed on Ru sites (assuming 1:1 ratio of adsorption of CO_2 per Ru site). In previous TGA-DSC experiments it was observed that when exposed to a 0.5% CO_2 /N_2 stream, the weight increase by Ru/γ-Al_2O_3 corresponds to 0.8% of the original sample weight (50 mg). From this data, the percentage of Ru sites which adsorb CO_2 is calculated as 18%. This is indicative of a spillover process by which CO_2 molecules adsorbed on CaO sites migrate to Ru sites and are hydrogenated there. The spillover process is likely to be the result of heat generated via the highly exothermic methanation reaction, which drives the endothermic process of CO_2 desorption from CaO sites.

The discrepancy between CO_2 captured and methane released is assumed to be reflective of the experimental error in this measurement; because the micro-GC takes one sample every 2 minutes, integration of data points contains some error. In order to understand whether all of the captured CO_2 was converted to methane, 5 cycles each were performed at 260 and 320^{o}C. Repeatability of these results over many cycles would indicate stable capture capacity, meaning complete regeneration of adsorbent capabilities at each cycle.

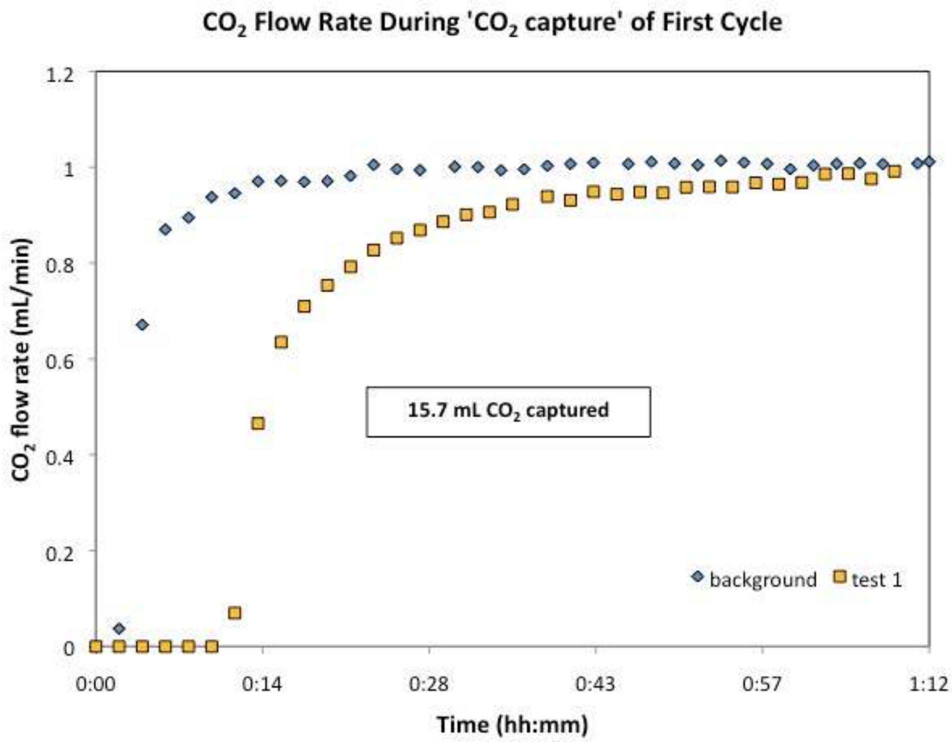

Figure 11.3: CO_2 flow rates during the 'CO_2 capture' period of the first cycle, for background (with γ-Al_2O_3) and test conditions (with CaO/γ-Al_2O_3 + Ru/γ-Al_2O_3). T=260^oC, Feed: 10% CO_2/90%N_2

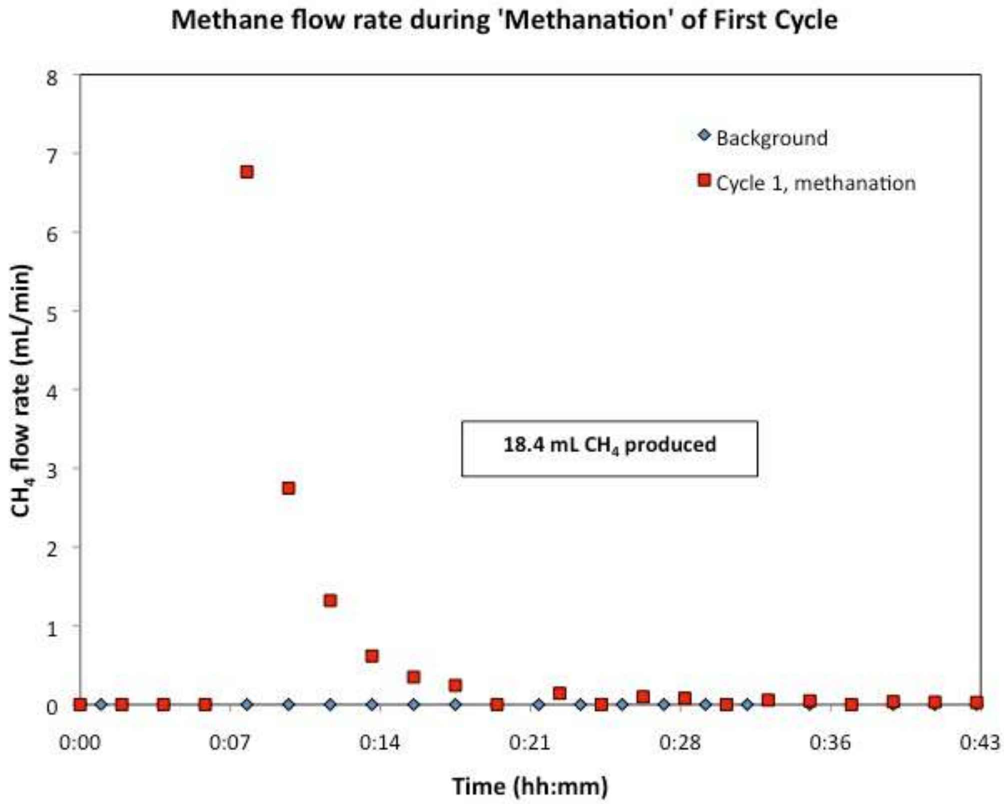

Figure 11.4: CH_4 flow rates during the 'methanation' period of the first cycle, for background (γ-Al_2O_3) with and test conditions (CaO/γ-Al_2O_3 + Ru/γ-Al_2O_3). T=260^oC, Feed: 40% H_2/ 60% He

The conversion for each cycle is calculated as follows:

$$Conversion(\%) = \frac{N_{CH_4 released}}{N_{CO_2 captured}}$$

(Eq. 22)

where N is moles of CO_2 or CH_4. The CO_2 capture, methanation and conversion data for all cycles are summarized in Table 11.1.

Table 11.1: Amounts of CO_2 captured and methanated during cycle test in flow reactor with a physical mixture of 10% CaO/γ-Al_2O_3 and 10% Ru/γ-Al_2O_3

Cycle	Temperature (°C)	CO_2 captured (μ-moles)	CH_4 released (μ-moles)	Conversion to CH_4 (%)
1	260	642	753	100
2	260	429	249	58
3	260	454	290	64
4	260	323	204	63
5	260	356	184	52
6	320	747	247	33
7	320	334	193	58
8	320	411	330	80
9	320	359	287	80
10	320	423	287	68

The data show large fluctuations in CO_2 captured and methane released. This is due to the fact that there is some uncertainty in the measurement of volumes of species captured or released, since the GC sampling time is 2 minutes; a single point can have a dramatic effect on the total volume of CH_4 released, since CH_4 appears as a pulse released over a typical time frame of 6 minutes. Therefore the major conclusion of these cyclic tests is that the activity of the adsorbent and catalyst mixture for CO_2 capture and methanation is maintained and does not appear to be in a diminishing trend at the end of 10 cycles. The fluctuations in the data highlight the need for more frequent measurements of gases (faster sampling times) in future experiments.

Chapter 12 : Optimization of dual function materials containing dispersed Ru and CaO on γ-Al_2O_3

The results presented in this chapter have been published in Applied Catalysis B: Environmental in a paper entitled "Dual function materials for CO_2 capture and conversion using renewable H_2".

Upon successful demonstration of the concept, DFMs consisting of a combination of 1-11% Ru (by weight) and 1-10% CaO (by weight) dispersed on γ-Al_2O_3 carrier were investigated. From previous chapters and prior work on nano dispersed CaO/γ-Al_2O_3 it becomes apparent that the components of the DFM chosen for proof of concept are compatible over a range of operating temperatures. For the studies presented in this chapter, the reaction temperature was fixed at 320^{o}C, because it was determined from mechanistic studies presented in Chapter 6 that at this temperature Ru will remain in a reduced state during methanation of captured CO_2.

12.1 TPR-TPO of dual function materials

3 cycles of TPR-TPO were performed on 10%CaO 10%Ru/Al_2O_3 in a thermal gravimetric analysis - differential scanning calorimetry instrument (TGA-DSC). The mass change (TGA) and heat flux (DSC) data for the TPR-TPO are presented in Figure 12.1. It is apparent that the first cycle of TPR differs significantly in terms of both the TG and DSC signals, whereas the second and third TPR cycles are well aligned, indicating strong consistency in

reduction behavior. In the first TPR cycle, a significant mass loss is accompanied by two distinct DSC exotherms, starting around 200°C and 250°C respectively. When compared with the TPR-TPO profile of 10% Ru/Al_2O_3 (Figure 5.1), which was analyzed in section 5.1 of Chapter 5, it is apparent that the DSC peak at 200°C corresponds to decomposition of Ru precursor species. Therefore the second peak starting at 250°C must be associated with the decomposition of $Ca(NO_3)_2$ to CaO. Based on these TPR-TPO results, pre-reduction with hydrogen at 320°C for 2 hours prior to reaction was deemed appropriate for all dual function materials. The pre-reduction is expected to decompose all precursors, as well as reduce RuO_x species that may be present.

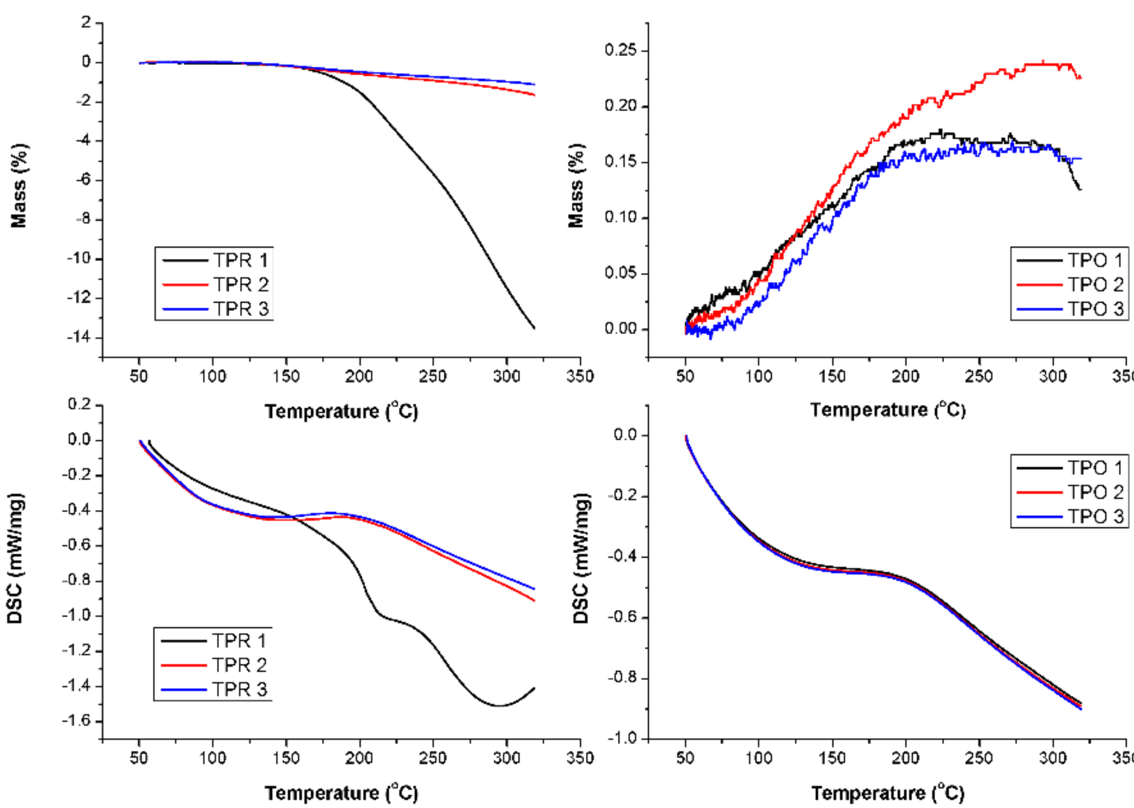

Figure 12.1: TG and DSC signals for 3 consecutive cycles of TPR-TPO performed on 10% CaO 10% Ru/Al_2O_3 using 2% H_2/N_2 as feed during TPR and 2% O_2/N_2 during TPO

12.2 Reactor testing of various DFM compositions

Nine DFMs, as well as a 10%Ru/γ-Al_2O_3 methanation catalyst, were tested in a microreactor where cycles of CO_2 capture and methanation were performed. Methanation of captured CO_2 yielded a characteristic peak of methane observed at the exit of the reactor, as shown in Figure 12.2. The extents of methanation for each material are compared in Table 12.1.

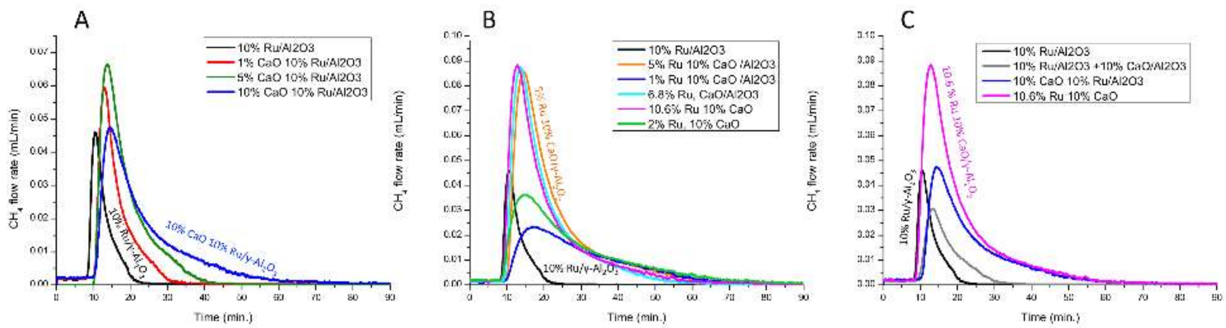

Figure 12.2: Methane produced by DFM samples with CaO impregnated on 10%Ru/γ-Al_2O_3 (A), Ru impregnated on 10%CaO/γ-Al2O3 (B) and a comparative plot for DFMs prepared via different orders of impregnation (C). Feed: 4%H_2/N_2 (26 mL/min), T=320^oC.

Figure 12.2 (A) displays methanation results for materials where 0-10 wt.% CaO was impregnated on 10% Ru/γ-Al_2O_3. It can be seen from Figure 12.2 (A) that all samples with CaO present produce larger methane peaks compared to the 10%Ru/γ-Al_2O_3 catalyst. Figure 12.2 (B) displays methanation results for materials prepared by impregnating 1-10%Ru on 10% CaO/γ-Al_2O_3. It is apparent from the figure that all samples performed significantly better compared to the original catalyst (10% Ru/Al_2O_3) based on methane production. In order to determine whether the order in which the Ru and CaO were loaded onto the γ-Al_2O_3 support affected the methanation performance of the different materials, the sample containing 10% CaO impregnated on 10% Ru/Al_2O_3 was compared with the sample containing 10.6% Ru impregnated on 10%CaO/Al_2O_3. A physical mixture of equal parts 10%Ru/γ-Al_2O_3 and 10%CaO/γ-Al_2O_3 was tested and compared with these samples to determine whether the co-impregnation of CaO and Ru gave any additional benefits over the physical mixture. It can be seen from Figure 12.2 (C) that the performance is significantly enhanced when Ru is impregnated onto the CaO/Al_2O_3.

Table 12.1 displays the methanation capacity (g-mol CH_4 /kg DFM) and the methane turnover (g-mol CH_4/g-mol Ru in DFM) of all samples tested in the microreactor. It can be seen from rows 3-5 in Table 12.1 that the addition of CaO to 10%Ru/γ-Al_2O_3 results in increased methane production; 10%CaO 10%Ru/γ-Al_2O_3 produces 3 times as much CH_4 as 10%Ru/γ-Al_2O_3. CO_2 methanation is not observed on CaO/γ-Al_2O_3 only. This is a clear demonstration of the operation of dual function materials; CO_2 adsorbs on both CaO and reduced Ru sites during CO_2 capture. Upon introduction of H_2, methanation begins with the CO_2 chemisorbed on Ru sites and releases heat, which drives CO_2 desorption from the nano dispersed CaO sites resulting in further methanation.

Table 12.1: Methane turnover (moles CH_4 produced/moles Ru present in sample) and methanation capacity (g-mol CH_4/kg DFM) for all samples during 1 cycle consisting of a CO_2 capture and a methanation step.

Row	Sample	CH_4/Ru	g-mol CH_4/kg DFM
1	γ-Al_2O_3	0.00	0.00
2	10% Ru /γ-Al_2O_3	0.10	0.10
3	1% CaO 10% Ru/γ-Al_2O_3	0.19	0.19
4	5% CaO 10% Ru/γ-Al_2O_3	0.27	0.27
5	10% CaO 10% Ru/γ-Al_2O_3	0.31	0.30
6	1.1% Ru 10% CaO/γ-Al_2O_3	2.46	0.27
7	2%Ru, 10% CaO/γ-Al_2O_3	1.79	0.35
8	5% Ru 10% CaO/γ-Al_2O_3	1.01	0.50
9	6.8% Ru,10%CaO/γ-Al_2O_3	0.65	0.44
10	10.6%Ru, 10% CaO/γ-Al_2O_3	0.44	0.46
11	10% Ru/γ-Al_2O_3 +10% CaO/γ-Al_2O_3	0.25	0.12

Rows 6-10 in Table 1 display methanation results for materials prepared by impregnating 1-10% Ru on 10% CaO/γ-Al_2O_3. It is apparent from Table 12.1 that all such samples performed significantly better compared to our original catalyst (10% Ru/Al_2O_3) based on methane production. As indicated by the CH_4/Ru column the greatest amount of spillover of CO_2 occurs in the sample containing 1.1% Ru and 10% CaO. However, it is the 5%Ru, 10% CaO sample that shows the largest production of CH_4 per kg of material. This indicates that a large CaO:Ru ratio in the DFM is desirable since it increases the amount of methanation. However, low loadings of Ru do not generate sufficient heat to liberate all CO_2 from CaO sites, which likely causes the overall methanation capacity to be lower for the 1.1% Ru 10%, CaO/Al_2O_3 compared to the 5% Ru, 10% CaO /Al_2O_3.

In order to determine whether the order in which the Ru and CaO were loaded onto the γ-Al_2O_3 support affect the methanation performance of the different materials, the sample containing 10% CaO impregnated on 10% Ru/Al_2O_3 (row 5 of Table 12.1) was compared with the sample containing 10.6% Ru impregnated on 10%CaO/Al_2O_3 (row 10 of Table 12.1). A physical mixture of equal parts 10%Ru/γ-Al_2O_3 and 10%CaO/γ-Al_2O_3 was tested and compared with these samples to determine whether the co-impregnation of CaO and Ru gave any additional benefits over the physical mixture. When comparing this to the other samples, CH_4/Ru, which is a measure of CO_2 spillover will be the focus of the discussion. It can be seen from Table 12.1 that the performance is significantly enhanced when Ru is impregnated onto the CaO/γ-Al_2O_3. This is also verified by the increased methane production per Ru sites (CH_4/Ru) shown in Table 12.1. One possible explanation for this is that CaO impregnation on Ru/γ-Al_2O_3 results in some loss of active Ru sites due to masking by the CaO of the Ru. Another possibility is that the presence of CaO on the support during Ru impregnation results in increased dispersion of the Ru in the final DFM. This phenomenon has recently been observed by Munera et al. for Rh impregnated on CaO/SiO_2 supports, although for samples with much higher concentrations of CaO in the support (20-50 wt.%) and much lower Rh loadings (0.6 wt.%) [102]. However, any effects of increased dispersion, while likely, are only secondary to those resulting from spillover of CO_2 from CaO to Ru sites; this is clearly observed when comparing the methane turnover of 10% Ru/γ-Al_2O_3 (Table 12.1, row 2) with those of samples containing 1-10% CaO impregnated on 10% Ru/γ-Al_2O_3 (Table 12.1, rows 3-5) and the physical mixture of 10% CaO/γ-Al_2O_3 with 10% Ru/γ-Al_2O_3 (Table 12.1, row 11). Significant enhancement of methanation capacities are observed in all these cases where CaO cannot have an impact on Ru dispersion, compared to the 10% Ru/γ-Al_2O_3 baseline.

While impregnation of Ru on CaO/γ-Al_2O_3 results in the best observed methanation activity, other synthesis methods can be explored in the future. The physical mixture of 10% Ru/γ-Al_2O_3 and 10% CaO/γ-Al_2O_3 (row 11) showed increased methanation per kg as well as per mole of Ru present in sample compared to the 10% Ru/γ-Al_2O_3, clearly demonstrating that the spillover mechanism proposed is effective regardless of any surface interactions between Ru and CaO. However, the methane produced per Ru site was better for the samples where CaO and Ru were both deposited on the same γ-Al_2O_3 support. This shows that proximity of CaO and Ru sites plays an important role on the performance of DFMs, also consistent with a CO_2 spillover mechanism from the CaO to the Ru.

Based on results shown in Table 12.1, the sample exhibiting the largest methanation activity per kg is 5% Ru, 10% CaO/γ-Al_2O_3 shown as row 8. This sample produced five-times as much methane as our original methanation catalyst, 10%Ru/Al_2O_3 (row 2). Hence it was chosen as a candidate for advanced testing. The best performance was obtained when the Ru precursor salt was impregnated onto the CaO dispersed on the γ-Al_2O_3. This is shown when rows 10 and 3, 8 and 4 are compared. It is also noted that co impregnated samples (row 10) performed better than mechanical mixtures of the same amount of Ru and CaO but on separate particles (row 11).

Although the methanation activity is highest for 5% Ru, 10% CaO/γ-Al_2O_3, it can be seen from Table 12.1 that the highest methane turnover (CH_4/Ru) is observed for 1%Ru, 10% CaO/γ-Al_2O_3. In fact, when the methane turnover is plotted against the weight ratio of CaO to Ru in the material (CaO:Ru) as in Figure 12.3, a direct correlation is observed. Thus CO_2 spillover from

CaO to Ru sites increases with the increasing weight ratio of CaO to Ru. This suggests that individual Ru sites generate more methane due to migration of CO_2 from CaO to Ru. The extent of CO_2 spillover from CaO to Ru sites increases greatly by increasing the CaO content for a given amount of Ru.

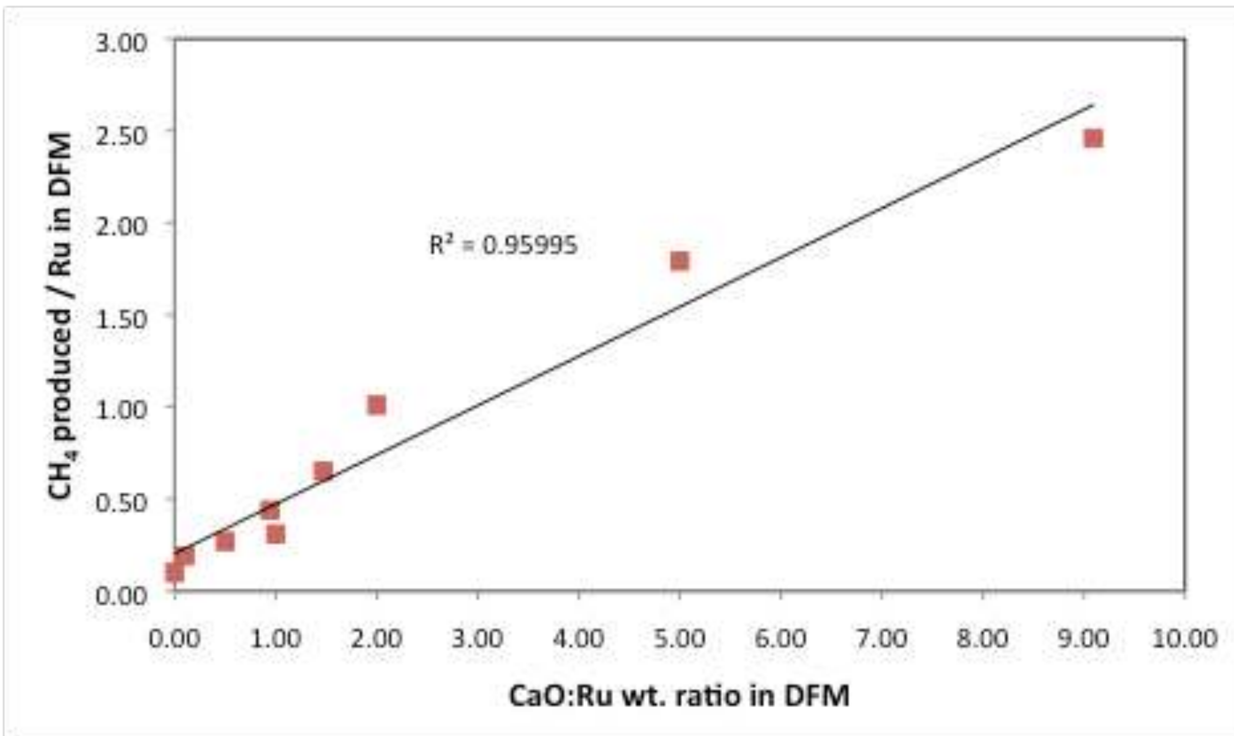

Figure 12.3: Methane turnover for varying CaO:Ru (weight ratio) in the sample.

12.3 Accelerated cyclic testing under post-combustion conditions: CO_2 capture from highly oxidizing streams

The sample demonstrating largest methanation activity per kg DFM (5% Ru, 10% CaO/γ-Al_2O_3) was chosen for further evaluation under more realistic post combustion conditions. In a real post-combustion CO_2 capture application the DFM will have to capture CO_2 in the presence of air over many cycles of operation; a natural gas fired turbine generates a flue gas containing 3-4 vol.% CO_2 and (12-15%) O_2[10]. Post combustion flue gas will also contain steam (6-8% in the case of the natural gas fired turbine). Hence in order to understand the effect of power plant conditions on the performance of DFMs, two cyclic tests were performed using 5%Ru,10%CaO/γ-Al_2O_3. The first cyclic test involved CO_2 capture in the presence of air to investigate the impact of oxygen on the CO_2 capture and hydrogenation performance of the DFM. It also tests the resilience of Ru during redox (reducing and oxidizing) cycles. A second cyclic test (performed with fresh DFM) was performed with CO_2 capture from a mixture containing air, steam and CO_2 to simulate further a power generation effluent. The response of the components of the DFM to oxidizing conditions is a crucial piece of information gathered from these cyclic studies.

Cyclic tests with air (~18% O_2) present were performed from a source of 10% CO_2 /air over 20 cycles of CO_2 capture and methanation in a packed bed reactor. Note that O_2 concentration in this test is above that expected in the effluent and thus can be considered an accelerated test. The results are displayed in Figure 12.4. The hollow diamond points indicate CO_2 capture during the first step of the cycle, and the filled square and triangle data points indicate the CH_4 and CO_2 released during the methanation step associated with each cycle. Due to a mass flow controller related error in the first cycle the first reliable data is from the methanation step in the 2nd cycle. A stable CO_2 and CH_4 release is observed during methanation in the subsequent 19 cycles. However, there is variability in the CO_2 captured during each cycle, which shows a slightly decreasing trend. After the 11th cycle, the reactor was purged with 5% H_2/N_2 overnight at 320^{o}C to see whether this would restore CO_2 capture activity and increase methanation activity by releasing all CO_2 remaining in the DFM. As can be seen from Figure 12.4, this resulted in a significant increase in the CO_2 captured during cycle 12, without any proportional change in the amounts of CH_4 and CO_2 released. This means that while the overnight H_2 purge freed some sites for CO_2 capture, some CO_2 molecules are more strongly bound to these sites and are only slowly removed during methanation. A longer methanation period regenerates those sites. Overall, stable methanation activity was observed for 19 cycles.

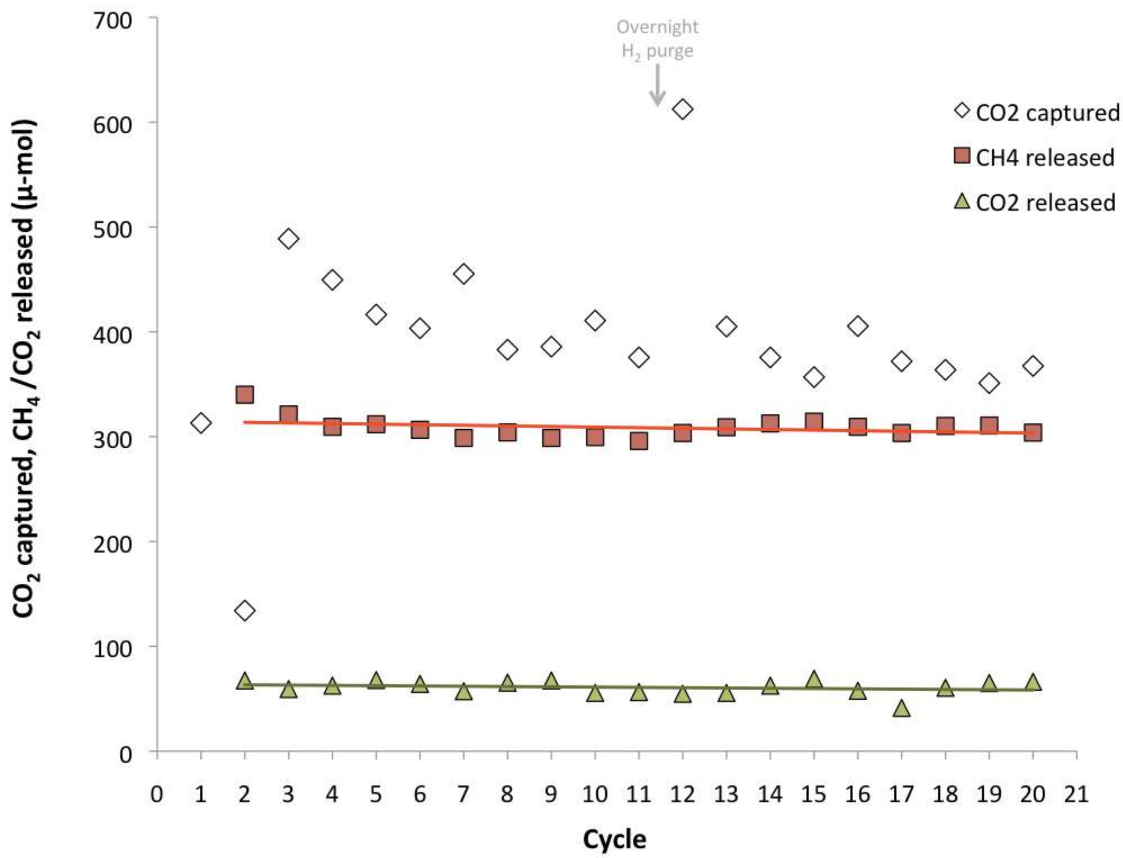

Figure 12.4: CO_2 captured, CH_4 released and CO_2 released for 20 cycles of methanation. One cycle consists of CO_2 capture from a 10% CO_2/air stream for 20 minutes followed by a He purge and subsequent 20 minute methanation by flowing 5%H_2/N_2. T=320°C. An overnight purge with 5% H_2/N_2 was performed after the 11th cycle.

A detailed analysis of results from cyclic experiments performed with 5%Ru 10%CaO/γ-Al_2O_3 is displayed in Table 12.2. It includes the CO_2 capture capacity, conversion of captured CO_2 to CH_4, and the gas phase carbon balance for each cycle. The average carbon balance based on measured gas concentrations for cycles 3-20 was 91.23%. This indicates that most of the CO_2 adsorbed is reversibly released from the material. Thus about 9% of the CO_2 remains on sorbent (CaO) sites. Nevertheless, we do not see a significant change in amounts of CO_2 or CH_4 released from the DFM over 19 cycles (as seen in Figure 12.4), which implies that accumulation of carbon on the surface of the DFM does not take place to an appreciable extent. When 100% H_2 is used in the real application it is expected that most, if not all of these sites, will lead to the formation of CH_4. This method also can be used to achieve a more favorable carbon balance. The average conversion of captured CO_2 to CH_4 was 76.17% over 19 cycles. This is comparable to the results by Rynkowski et al. using 5% Ru/γ-Al_2O_3 where a maximum CO_2 conversion of 72% was observed around 400°C using a mixture of H_2/CO_2 (5:1 volumetric ratio)[103]. Most of the remaining CO_2 is released as a result of the heat generated during methanation, and can be converted to methane in a small downstream catalytic reactor to upgrade the mixture to pure CH_4. The downstream reactor will likely operate at a lower temperature to achieve more favorable equilibrium conversions. We have already shown that 10%Ru/γ-Al_2O_3 allows us to reach equilibrium conversions at 280°C [104]. The average CO_2 capture capacity was 0.41 g-mol CO_2/kg DFM and the average methanation capacity was 0.31 g-mol CH_4/kg DFM over 19 cycles. There is a need to improve the CO_2 capture capacity of the DFM, as it is low compared to those of other state of the art CaO based sorbents that have been evaluated for post-combustion CO_2 capture (>2 g-mol CO_2 /kg sorbent) [105]. One way of increasing CO_2 capture capacity would be by increasing the CaO loading on γ-Al_2O_3. However, it has previously been demonstrated that the reversibility of chemisorption depends on the presence of nano-sized CaO particles, which means that there will be a tradeoff between reversibility of adsorption and capture capacity[86, 87]. For this reason, promoters and other sorbents suitable for operation under catalytic reaction conditions are also being investigated.

Table 12.2: Detailed analysis of the 20 cycle test performed on 5%Ru, 10%CaO/γ-Al_2O_3. One cycle consists of CO_2 capture from a 10% CO_2/air stream for 20 minutes followed by a He purge and subsequent 20 minute methanation by flowing 5%H_2/N_2. T=320^{o}C. An overnight purge with 5% H_2/N_2 was performed after the 11th cycle.

Cycle	CO_2 captured (mL)	CH_4 released (mL)	CO_2 released (mL)	CO_2 captured (μ-mol)	CH_4 released (μ-mol)	CO_2 released (μ-mol)	Gas phase C balance (%)	Conversion to methane (%)	CO_2 capture capacity (g-mol/kg)
1	7.7	NA	NA	313.1	NA	NA	NA	NA	0.3
2	3.3	8.3	1.7	134.1	340.1	67.4	304.0	253.7	0.1
3	12.0	7.9	1.5	488.8	321.3	59.3	77.8	65.7	0.5
4	11.0	7.6	1.5	449.6	309.4	62.5	82.7	68.8	0.4
5	10.2	7.6	1.7	416.5	311.9	67.8	91.2	74.9	0.4
6	9.9	7.5	1.6	403.4	306.6	64.2	91.9	76.0	0.4
7	11.1	7.3	1.4	455.3	298.8	57.2	78.2	65.6	0.5
8	9.4	7.4	1.6	383.0	304.1	65.4	96.5	79.4	0.4
9	9.4	7.3	1.7	385.8	298.8	67.4	94.9	77.4	0.4
10	10.1	7.3	1.4	410.8	299.6	55.6	86.5	72.9	0.4
11	9.2	7.2	1.4	375.6	295.9	56.4	93.8	78.8	0.4
12	15.0	7.4	1.3	612.4	303.5	54.8	58.5	49.6	0.6
13	9.9	7.6	1.4	405.1	309.0	55.6	90.0	76.3	0.4
14	9.2	7.7	1.5	375.6	312.7	62.5	99.9	83.2	0.4
15	8.7	7.7	1.7	356.8	314.3	69.1	107.4	88.1	0.4
16	9.9	7.6	1.4	405.5	309.4	57.6	90.5	76.3	0.4
17	9.1	7.4	1.0	371.9	303.5	41.3	92.7	81.6	0.4
18	8.9	7.6	1.5	363.8	310.2	60.5	101.9	85.3	0.4
19	8.6	7.6	1.6	351.1	310.6	65.0	107.0	88.5	0.4
20	9.0	7.4	1.6	367.5	303.9	66.2	100.7	82.7	0.4

In order to evaluate the performance the 5% Ru 10%CaO/γ-Al_2O_3 upon exposure to steam, another cycle test was performed where the simulated flue gas used for CO_2 capture cycles consisted of 8%CO_2, 21%H_2O, and balance air. The concentration of steam in this test far exceeds what would be typical for a natural gas (methane) power plant (6-8%) and thus constitutes an extreme oxidizing/sintering condition for the use of DFMs. The results showing CH_4 and CO_2 released during each methanation cycle are plotted in Figure 12.5. For this experiment, the background measurements for the CO_2 capture cycles (using γ-Al_2O_3) showed significant variation in residence time of the flue gas in the reactor, which has prevented the accurate measurement of CO_2 captured during the cycle test. This is attributed to the fluctuating flow rate of steam due to the use of a syringe pump for its generation (explained in Chapter 3). However, the CH_4 and CO_2 released can be used to understand the effect of high concentrations of steam on this system. While an overnight H_2 purge was also performed after the 11th cycle of this test, it did not result in a significant change in methane production. CH_4 produced during methanation portions of these cycles fluctuates around a mean value of 283 μ-mol, which translates to an average methanation capacity of 0.27 g-mol CH_4/kg DFM, about 10% lower than in the absence of steam (0.31 g-mol CH_4/kg DFM over 19 cycles). While this may not be a significant difference, the composition of the gas released during methanation has changed in a positive direction in that very little CO_2 was detected with 99.9% methane released on average. In no cases was CO present. In the absence of steam, methanation produced a gas mixture containing on average 83.6% CH_4 and 16.4% CO_2 by volume. The increased purity of methane released creates the advantage of simplicity in overall process design. A high purity methane yield will eliminate the need for downstream catalytic treatments to prepare the gas for injection to natural gas pipelines.

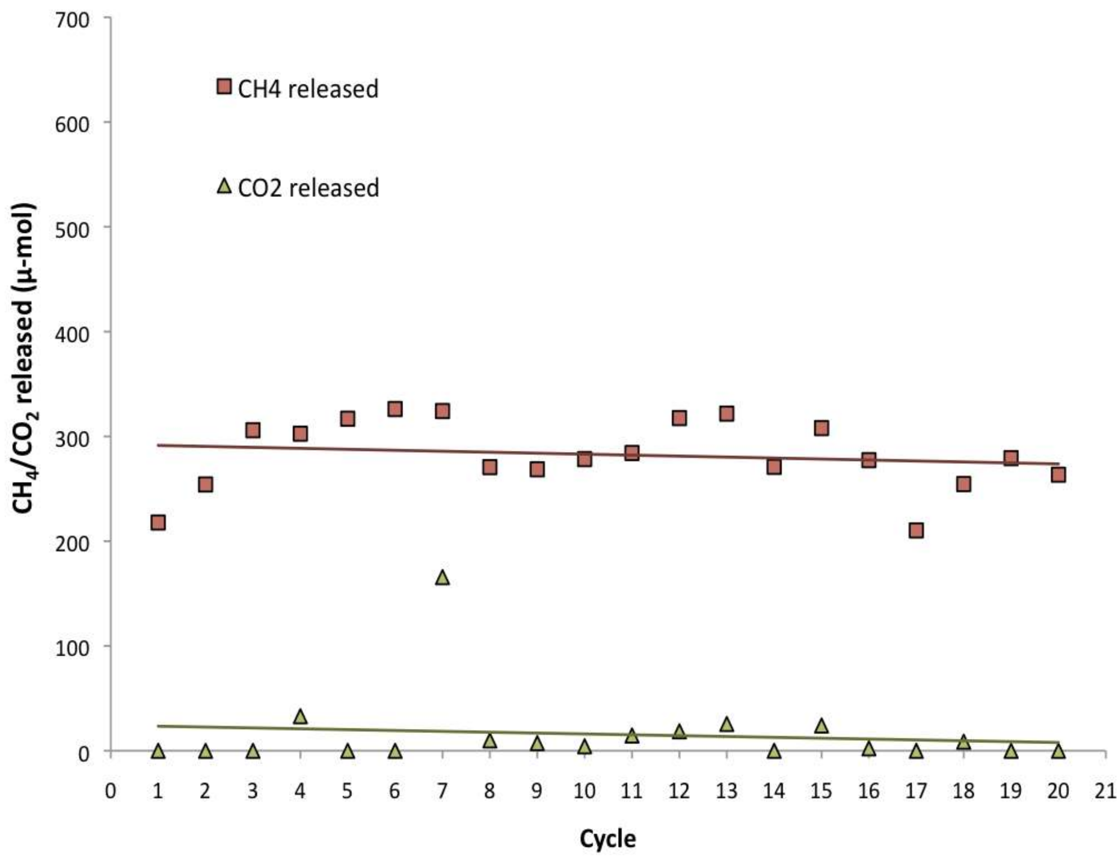

Figure 12.5: CH_4 and CO_2 released upon H_2 introduction during the 20-cycle test with steam exposure. Feed during CO_2 capture: 8%CO_2/21%H_2O/Air (22.1 mL/min), Feed during H_2 introduction: 5% H_2/N_2 (90.5 mL/min)

Fresh 5%Ru, 10%CaO/γ-Al_2O_3 and spent DFM samples from both cyclic tests were characterized via BET surface area analysis as well as H_2 and CO_2 chemisorption to determine Ru and CaO dispersions. The dispersion values indicate the percentage of Ru or CaO actively participating in CO_2 adsorption or catalysis. Results shown in Table 12.3 indicate that BET surface area has not been affected as a result of aging cycle tests, The dispersions of both Ru and

CaO (also shown in Table 12.3) decrease by no more than 20% after 20 cycles of CO_2 capture and methanation, when the simulated flue gas only contains air and CO_2. Where steam was present, the Ru dispersion was similar to that after the test with air only (about 24% lower than fresh). However, the CaO dispersion is greatly reduced; the dispersion of CaO drops by 87% after the cyclic test with steam.

Table 12.3: Characterization of 5%Ru 10%CaO/γ-Al_2O_3 before and after 20 cycles of CO_2 capture and methanation at 320°C

Sample	Ru dispersion	CaO dispersion	BET surface area (m^2/g)
Fresh DFM (5% Ru 10% CaO/γ-Al_2O_3)	26.29%	13.59%	83.87
DFM after 20-cycle test with simulated dry flue gas	21.00%	10.01%	92.69
DFM after 20-cycle test with simulated wet flue gas	20.05%	1.74%	88.99

Although CaO dispersion of the DFM shows a significant decrease after the accelerated cycle test involving steam, the methanation capacity is not drastically affected. Furthermore, in Figure 12.5 the amount of methane produced does not show a significant decreasing trend over time. One explanation is that the DFM contained a number of excess or "inactive" CaO sites in the fresh state and losing those sites did not affect material performance during the test. When compared to the values presented in Table 12.1, methanation capacity of 5% Ru, 10%CaO/γ-Al_2O_3 is lower for both cycle tests compared to the measurements made in the absence of oxygen or steam. This can easily be attributed to some oxidation of Ru. However, the methanation capacities for both cycle tests are nevertheless much higher than that of 10%Ru/γ-Al_2O_3 (Table 12.1, row 2) which indicates that the methanation is still being enhanced by the presence of CaO.

Temperature programmed desorption (TPD) was performed on the spent DFM sample thinking that perhaps some carbonate had formed leading to a lower CO_2 chemisorption. The TPD results showed that a total of 7.7201 μ-moles of CO_2 were remaining on a 0.1001 g sample (77.1240 μ-moles/g). However, CO_2 desorption is observed only below 60°C, which indicates that these are weakly adsorbed molecules taken up by the sample after it was removed from the reactor. Since no carbonate decomposition was observed the decrease in CaO dispersion is attributed to sintering mainly due to the accelerated test with 21% steam. It is therefore necessary to understand the rate of CaO sintering in the presence of the more realistic 6-8% steam in the flue gas. Further feasibility studies to understand mechanisms and rates of deactivation of DFMs over prolonged periods of testing under realistic conditions will be the subject of future experimentation.

Chapter 13 : Identification of other catalytic components for DFMs

13.1 Methanation activity of different metals

Precious and base metal catalysts were screened for their methanation activity and selectivity in a fixed bed flow reactor within a temperature range of 150-350^{o}C. All catalyst metals were supported on γ-Al_2O_3 and were prepared via incipient wetness impregnation to reach a metal loading of 10% by weight. All catalysts were calcined at 500^{o}C in air with the exception of Ru/γ-Al_2O_3, which underwent a much lower temperature calcination step to prevent the formation of volatile oxides as is described in section 3.1. The catalyst weight was identical (0.1000 ± 0.0002 g) in all test runs and gas hourly space velocity (GHSV) was fixed at 4000 h^{-1}. Only base metal catalysts (Co/γ-Al_2O_3 and Ni/γ-Al_2O_3) received pre-reduction at the beginning of the test to ensure reduction of the metals to their active states. This pre-reduction was performed at 450^{o}C for 3 hours in pure hydrogen. It was assumed based on experience with Ru/γ-Al_2O_3 that the precious metal catalysts would be reduced during startup by the reactant feed, which contains 16% H_2.

Figure 13.1 shows the variability in CO_2 conversion to methane with increasing temperature for all candidate hydrogenation catalysts, tested within the temperature range of interest (150-350^{o}C). Rh/γ-Al_2O_3 begins to show methanation activity at 150^{o}C. However, in the temperature range of 175-250^{o}C Ru/γ-Al_2O_3, showed the highest methanation activity. In order to be consistent with previous experiments, the methanation activity at 320^{o}C was compared and was found to follow the trend Rh>Ru>Ni>Pd>Co>Pt, although the lightoff temperature was best for Ru. Based on this study, Rh and Ni were identified as the leading candidates for methanation catalyst alternatives to Ru in dual function materials for CO_2 capture and methanation.

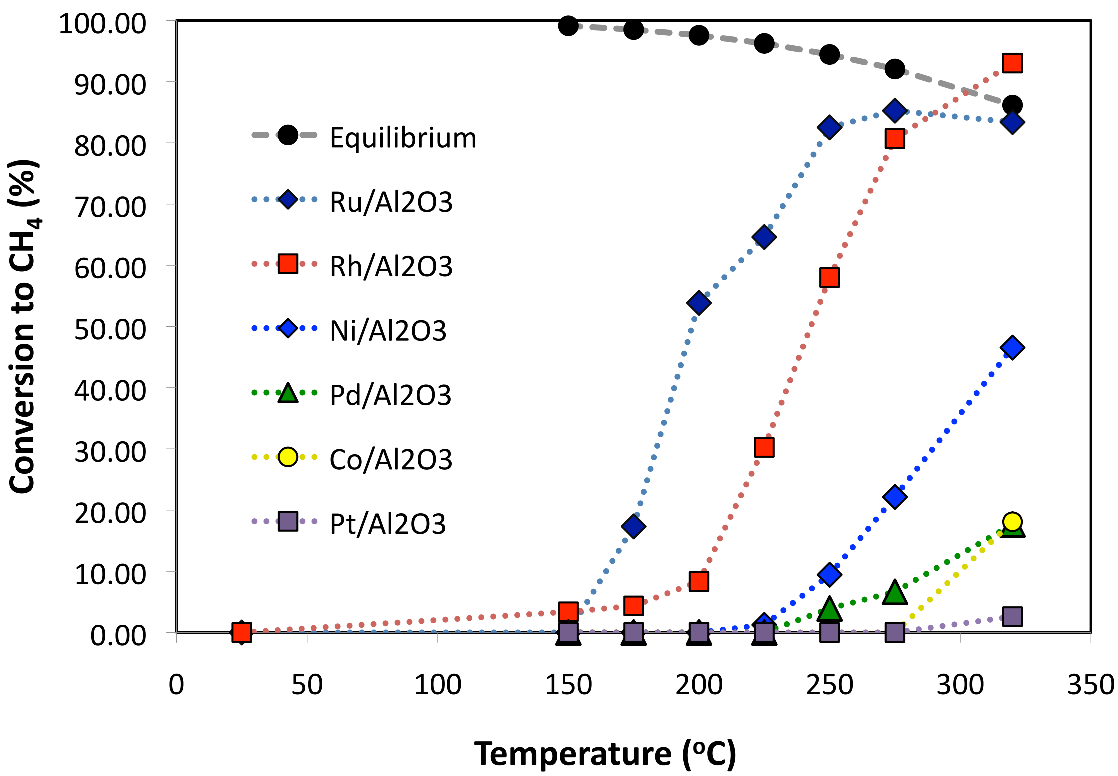

Figure 13.1: Conversion of CO_2 to CH_4 for various supported metal catalysts. Feed: 4% CO_2/ 16% H_2/He

13.2 Optimization of new DFM with Rh as the methanation catalyst component

6 dual function materials consisting of 0.1-10% Rh impregnated on 10% CaO/γ-Al_2O_3 were prepared to evaluate the suitability of Rh as a methanation catalyst for new DFM

formulations. 10% Rh/γ-Al_2O_3 was used as a baseline. All materials were tested in the Quantachrome microreactor used for previous optimization studies (section 12.2) and the experimental protocol followed was identical to that explained in section 3.7.4.

Results from optimization studies with Rh, CaO/γ-Al_2O_3 DFMs are presented in Table 13.1. Based on these results it is clear that all DFMs significantly outperformed the 10% Rh/γ-Al_2O_3 baseline in terms of both methane turnover (CH_4/Rh) and total methanation capacity (g-mol CH_4/kg DFM). The highest methanation capacity observed for Ru based DFMs tested under the same conditions was 0.50 g-mol CH_4/kg DFM, as is discussed in section 12.2 of Chapter 12. Hence it is also apparent from Table 13.1 some Rh based DFMs have much higher methanation capacities compared to the optimized Ru based DFM. Hence this study shows that the methanation activity of the DFMs can be improved by changing the catalyst component.

Table 13.1: Methane turnover (moles CH_4 produced/moles Rh present in sample) and methanation capacity (g-mol CH_4/kg DFM) for all samples during 1 cycle consisting of a CO_2 capture and a methanation step.

Row	Sample	CH_4/Rh	g-mol CH_4/kg DFM
1	10% Rh/γ-Al_2O_3	0.13	0.13
2	10% Rh 10% CaO/γ-Al_2O_3	0.72	0.70
3	8.5% Rh 10% CaO/γ-Al_2O_3	1.14	1.11
4	5% Rh 10% CaO/γ-Al_2O_3	1.15	0.56
5	1% Rh 10% CaO/γ-Al_2O_3	10.12	0.98
6	0.5% Rh 10% CaO/γ-Al_2O_3	3.87	0.38
7	0.1% Rh 10% CaO/γ-Al_2O_3	5.94	0.58

In the case of Rh based DFMs, it can be seen from Table 13.1 that the matter of choosing an optimum is complicated by multiple factors. The data in Table 13.1 have been plotted in Figure 13.2 to reveal the complicated relationship between methanation capacity and Rh loading. The oscillating behavior of methanation capacity with increased Rh loading observed is likely due to the mixed effects of two factors. While reduced loading results in fewer overall Rh atoms on the catalyst, it is expected to increase dispersion of the Rh, thus creating more accessible sites for reaction to occur. Hence there is a tradeoff between reduced metal loading and increased dispersion. This is an expected result, since Munera et al. have already shown that for Rh impregnated on CaO/SiO_2 supports have increased dispersions compared to Rh/SiO_2, for 20-50 wt.% CaO in the support and 0.6 wt.% Rh [102]. More detailed studies on surface characterization need to be undertaken and the relationship between catalyst structure and activity in the context of a DFM need to be established in order to optimize Rh based dual function materials.

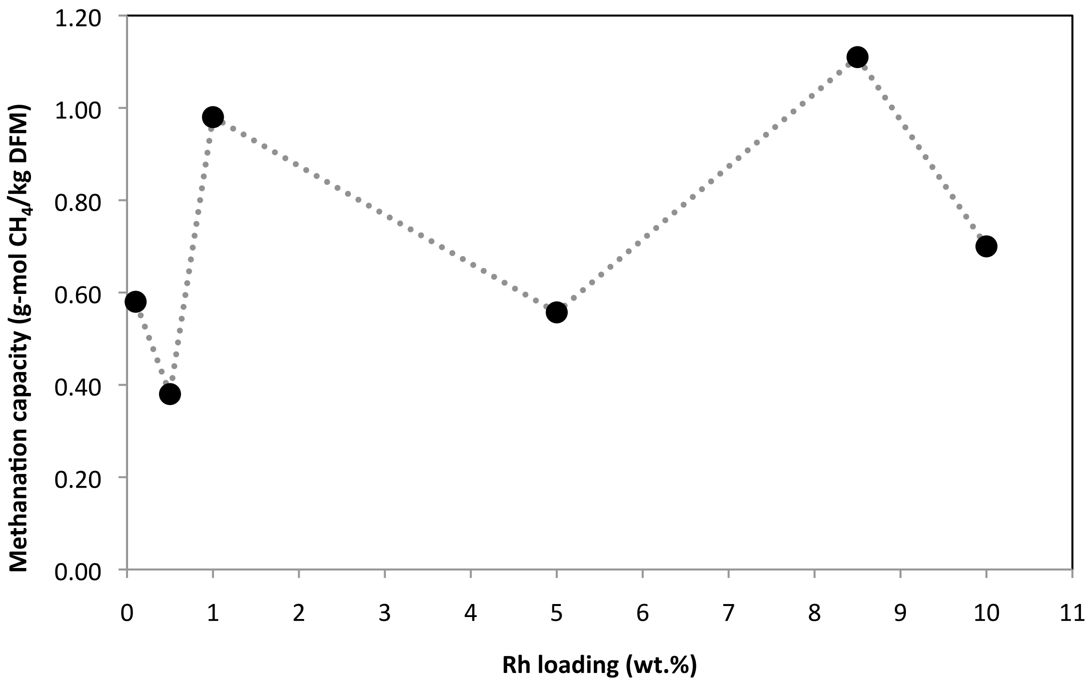

Figure 13.2: Variation of methanation capacity as a function of Rh loading on DFMs

It can be seen from row 7 in Table 13.1 that the DFM with the lowest loading of Rh, 0.1% Rh 10% CaO produces a comparable yet higher amount of methane than 5% Ru 10% CaO/γ-Al_2O_3. Hence this is a reasonable choice for the optimum material since a superior performance for methanation has been achieved with a much lower metal loading compared to Ru based DFMs.

Rhodium is an attractive substitute metal for Ru because of its higher activity at low temperatures[48, 49, 106, 107]. The initial findings with Rh suggest that it may be possible to decrease Rh loading even further to achieve a higher methanation activity in the DFM. Moreover, it has been suggested that the presence of oxygen in the feed during methanation over Rh catalysts has a positive effect on CO_2 methanation. This makes Rh particularly suitable as methanation catalyst in DFMs because of the presence of O_2 in industrial flue gas streams[49, 106]. Hence Rh based DFMs are promising for the development of DFMs that operate at temperatures lower than 320^{o}C and provide superior methanation performance compared to Ru upon exposure to oxygen.

It is also important to factor in the high cost of Rh compared to Ru when designing new dual function materials. Current prices of ruthenium and rhodium are 1650 $/kg and 36500 $/kg respectively. 0.1% Rh 10% CaO/γ-Al_2O_3 DFM shows higher methanation activity compared to the optimum Ru based DFM (5% Ru 10% CaO/γ-Al_2O_3). It is expected that Rh content of DFMs can be further reduced while still maintaining a methanation activity close to or higher than the optimum observed for Ru based DFMs. Since the metal loading has been successfully reduced by a factor of 50 and the price of Rh is higher than Ru by a factor of 22, it is not unreasonable that Rh based DFMs can be optimized to have reduced costs compared to Ru based DFMs.

Chapter 14 : Conclusions and future work

14.1 Conclusions

A dual function material (DFM) consisting of solid adsorbent and catalyst (nano-dispersed CaO and Ru) has been developed and demonstrated to capture CO_2 in the presence of air and steam (power plant effluent). The addition of stored renewable H_2 (from renewable electricity used to electrolyze water) to the CO_2-saturated DFM produces synthetic natural gas at high efficiencies. The synthetic natural gas can then be recycled to supply fuel for the process while minimizing CO_2 release. This feasibility study represents a major departure from carbon capture and sequestration technology currently being investigated for decreasing greenhouse gas emissions. By capturing and releasing CO_2 in the same reactor and at the same temperature using the DFM approach, the energy intensive sorbent regeneration step of existing CO_2 capture technologies is eliminated. Additionally, the technical and infrastructure-related problems associated with CO_2 storage and transportation are also avoided because CO_2 is converted to a fuel that can be consumed at ideally at the same location.

Adsorption studies were performed on Ru/γ-Al_2O_3 to better understand the catalytic component to be used in DFM via TGA-DSC. These studies suggest that CO_2 methanation over 10% Ru/γ-Al_2O_3 follows an Eley-Rideal mechanism. Based on the existing literature and the adsorption studies presented in this work CO_2 exists as dissociated CO and O on Ru. Using nonlinear regression, an Eley-Rideal rate expression has been developed based on kinetic data at 230^oC in a differential reactor. The rate expression is consistent with gas phase H_2 reacting with adsorbed species (CO and O) on Ru in accordance to the E-R rate law. Kinetics of CO_2

methanation over a 10% Ru/γ-Al_2O_3 catalyst were further examined using a differential reactor approach and an empirical rate law developed. The rate of methanation of CO_2 shows significant dependence on H_2 partial pressure with a reaction order being 0.88 and a much weaker dependence on CO_2 partial pressure with order of reaction being 0.34. The order of reaction with respect to the products CH_4 and H_2O were determined to be -0.11 and -0.23 respectively showing small inhibition effects.

In view of a renewable energy storage application, the kinetic information related to CO_2 hydrogenation was used to identify potential challenges for scale-up. A major constraint in a realistic renewable energy storage application is the low operating temperature (<300^oC) requirement to achieve favorable equilibrium distributions. While kinetics can be made favorable at lower temperatures with the use of excess hydrogen in the feed, unconverted hydrogen presents an explosion hazard for any application in which the product (SNG) will be injected into the natural gas pipelines. This can be addressed by using a H_2-permeable membrane for recycling excess H_2 before the SNG enters the pipeline.

For samples containing equal amounts of Ru, the addition of CaO increased methane yield, demonstrating that CO_2 spillover from CaO to Ru sites is occurring in DFMs. It was observed that increasing CaO:Ru ratio results in a greater extent of spillover of CO_2 and hydrogenation to CH_4. However there is an optimum composition around 5% Ru 10% CaO/γ-Al_2O_3. Impregnation of Ru on CaO/γ-Al_2O_3 results in better performance compared to materials where CaO is impregnated on Ru/γ-Al_2O_3. 5%Ru, 10%CaO/γ-Al_2O_3 was tested under simulated post combustion conditions where CO_2 capture was performed from a dry gas mixture consisting of 10%CO_2 in air and under accelerated aging conditions using a mixture consisting of 8%CO_2/21%H_2O/air. DFM also showed stable adsorption and methanation performance over both cyclic tests with up to 99.9% methane purity obtained in the cycle test where steam in addition to air was present during CO_2 capture.

Other precious and base metal candidates were evaluated in order to investigate their methanation activity and selectivity. Rh/γ-Al_2O_3 showed excellent activity and selectivity for CO_2 methanation. DFMs consisting of Rh and nano dispersed CaO were evaluated in terms of their cyclic CO_2 capture and methanation performance. Rh based DFMs showed higher methanation capacity on average compared to Ru based DFMs. An optimum Rh based DFM was identified as 0.1% Rh 10% CaO/γ-Al_2O_3. Cost must be considered for the final DFM system to be used.

14.2 Future work

A completely novel approach to capturing and converting CO_2 from emissions sources has been presented in this thesis. Dual function materials capable of capturing and converting CO_2 to methane in a single cyclic reactor operating isothermally using excess renewable H_2 have been conceptually developed and successfully demonstrated. By providing proof of concept for such systems, this work opens up many new areas of research.

14.2.1 Increasing sorption capacity of DFMs by using different adsorbent materials

Nano dispersed $CaO/\gamma\text{-}Al_2O_3$ was chosen as adsorbent component for DFMs in the present work mainly due to simplicity in preparation, previous experience with $CaO/\gamma\text{-}Al_2O_3$ in catalytic systems [87], its well characterized surface and reversible adsorption behavior[86]. Since we have shown that $CaO/\gamma\text{-}Al_2O_3$ reversibly adsorbs CO_2 between 200-600^oC, it was a natural candidate for integration into catalytic systems and was a good starting material for demonstrating the feasibility of DFMs[86]. However, the capture capacity of 10% $CaO/\gamma\text{-}Al_2O_3$ is a major constraint in designing real systems for CO_2 capture and conversion. Since the reactor operates in cycles, the overall methane conversion in each methanation cycle is determined by how much CO_2 can be adsorbed, and the percentage of CO_2 captured that can be converted. In the Ru $CaO/\gamma\text{-}Al_2O_3$ system, up to 76% of captured CO_2 was converted to methane. Hence increasing CO_2 capture capacity for this system will have the most significant influence on increasing overall performance. This will require improved CO_2 adsorbents with reversible behavior.

Moreover, when designing an industrial scale reactor, increasing CO_2 capture capacity becomes an important practical issue that needs to be resolved. The flow rate of CO_2 containing flue gas of a process is an inherent design constraint. The DFM capture capacity determines the duration of the CO_2 capture cycle, because the methanation cycle needs to be initiated when the DFM surface is saturated with CO_2. Increasing CO_2 capture capacity will result in longer cycle times and/or reduced reactor volumes, which make the overall process easier to integrate into industrial applications. Since the proof of concept for DFMs has been established and their feasibility demonstrated under accelerated aging conditions, future research should focus on improving the CO_2 capture capacity of dual function materials to enhance their performance and make their integration into industry seamless.

14.2.2 Tuning DFM activity and selectivity by using different support materials

γ-Al_2O_3 has been used in this study because it is an inexpensive and widely available catalyst carrier used in industry. The role of the support for Ru CaO/γ-Al_2O_3 materials apart from achieving a nano dispersion of catalytic and adsorbent components has been assumed to be negligible due to previous experience with Ru/γ-Al_2O_3 and CaO/γ-Al_2O_3. However, an important area of future work is the investigation of other carrier materials such as activated carbon, CeO_2, SiO_2, ZrO_2, zeolites and MOFs. Supports can tune CO_2 capture and catalytic activity by providing sites for adsorption, better dispersion of DFM components and participating in the methanation reaction pathway. Preliminary results suggest ceria-containing materials are promising to enhance CO_2 capacity.

14.2.3 Investigating other catalytic materials for use in DFMs

It has been shown in Chapter 1 that other precious and base metal catalysts are active for CO_2 methanation. Rh has been identified as a suitable but expensive methanation catalyst component and Rh CaO/γ-Al_2O_3 DFMs have been developed, demonstrated and initially optimized. Future work should focus on undertaking similar approaches to identify more inexpensive substitutes for Ru and Rh in DFMs for methanation. This will make it significantly easier to implement DFM technologies as a CO_2 emission mitigation option.

For proof of concept purposes, Ru has been used as the catalyst in DFMs due to its relatively labile redox properties compared to less expensive Ni; While nickel is a base metal catalyst that has good CO_2 methanation activity, it is converted to its inactive NiO form under power plant flue gas conditions containing oxygen. However, Ni DFMs that achieve high dispersions of Ni can potentially create small enough sized islands of Ni that can easily be reduced upon exposure to H_2 during the methanation cycle. Similarly, base metal methanation catalysts that are resistant to deactivation through oxidation can be developed for use in DFMs as part of future work. Furthermore, some applications may be free of O_2 in the effluent such as CO_2 rich gases from breweries.

14.2.4 Proof of concept and optimization of DFMs making other bulk chemicals from captured CO_2

The demonstration that CO_2 can be captured and released as concentrated CH_4 leads the way to designing dual function materials that can produce other bulk chemicals. Theoretically, the synergy between adsorbent and catalyst components that has been demonstrated in this thesis can be achieved by coupling any exothermic reaction of CO_2 with desorption from adsorbent sites. A suitable area of future research can be the production of methanol and ethanol from captured CO_2. These chemicals are widely used in the chemical industry and can also be used as fuel additives. The reactions are exothermic, and hence can facilitate the spillover of CO_2 from adsorbent sites to catalyst sites. In order to make such DFM processes work, it is expected that hydrogenation of CO_2 will be performed under high pressure. Partial oxidation reactions such as production of ethylene oxide or formaldehyde may be achieveable using dissociated CO_2 on other metals or oxides such as Ag or BiMo.

14.2.5 Detailed characterization of DFM surfaces

In situ and ex situ methods of characterization should be used to aid in the development of more active and selective DFMs as well as DFMs that produce chemicals other than CH_4. XPS can be used to understand the interaction of DFM components with each other and to optimize material preparation methods. In situ infrared and other methods can be used to understand bond formation on catalyst and adsorbent components in DFMs as well as the processes taking place during spillover of CO_2 from adsorbent to catalytic sites. This kind of approach will particularly be useful for guiding the development of DFMs producing other chemicals and to understand whether a synergy exists between novel catalyst and adsorbent components developed in the future. Characterization of active sites through TEM in addition to CO chemisorption may need to be employed for new catalyst formulations where the active sites are not necessarily reduced metals.

14.2.6 Scale up of dual function materials

Scale up of Ru CaO/γ-Al_2O_3 is critical for commercialization of this technology. Ru based dual function materials have been optimized and tested in a laboratory scale reactor using up to 1 gram of material in fine powder form. Demonstration of DFMs in any industrial setting will require much larger quantities of DFM (kg scale), in addition to different catalyst geometry. Catalyst geometry must be changed to increase particle size of the catalyst because fine particulates cause pressure drop in reactors operating at high flow rates. It is important to adopt a geometry that prevents pressure drop while still allowing the capture and reaction of CO_2 on the material without introducing significant mass transfer resistance to the system. There are many options for the scale up of catalysts, which can be explored for their suitability for dual function materials. For example, it is possible to support Ru and CaO on alumina pellets, which are spherical or cylindrical in shape, or to extrude Ru $CaO/\gamma\text{-}Al_2O_3$ into any desired shape.

Scale up of catalysts is not a trivial matter. When changing the catalyst size and shape, an important step will be to devise experiments to understand the effects of particle size and shape on pressure drop, effectiveness factor and mechanical stability. Moreover, the preparation protocol of DFMs must also be optimized; Different precursors (such as chloride or acetate salts rather than nitrates), preparation techniques (wet impregnation compared with incipient wetness impregnation) and temperature programs for drying, calcination and pre-reduction are some aspects that can be modified to yield enhanced activity for CO_2 capture and conversion to CH_4. Lessons learned from the scale up of Ru $CaO/\gamma\text{-}Al_2O_3$ will be applicable to any new DFM that is discovered in the future and scaled up to pilot plant scale. Finally pilot plant studies of DFM in real flue gas effluents (slip-stream testing) will have to be conducted with the cooperation of suitable industrial partners. This will help understand effects of trace gas phase components and real process conditions on DFM operation and to take preventative measures for DFM deactivation.

Works Cited

1. *IPCC 2013: Summary for Policymakers.* , in *Climate Change 2013: The Physical Science Basis. Contribution of Working Group I to the Fifth assessment Report of the Intergovernmental Panel on Climate Change*, T.F. Stocker, et al., Editors.: Cambridge University Press, Cambridge, United Kingdom and New York, NY, USA.
2. Hoeven, M.V.d., *CO_2 Emissions from Fuel Combustion Highlights*, M.V.d. Hoeven, Editor 2014, International Energy Agency: France.
3. Lewis, N.S. and D.G. Nocera, *Powering the planet: Chemical challenges in solar energy utilization.* Proceedings of the National Academy of Sciences, 2007. **104**(50): p. 15729-15735.
4. Rochelle, G.T., *Amine Scrubbing for CO_2 Capture.* Science, 2009. **325**: p. 1652-1654.
5. Pires, J.C.M., F.G. Martins, M.C.M. Alvim-Ferraz, and M. Simoes, *Recent developments on carbon capture and storage: An overview.* Chemical Engineering Research and Design, 2011. **89**: p. 1446-1460.
6. Leung, D.Y.C., G. Caramanna, and M.M. Maroto-Valer, *An overview of current status of carbon dioxide capture and storage technologies.* Renewable and Sustainable Energy Reviews, 2014. **39**: p. 426-443.
7. Solomon, S., G.-K. Plattner, R. Knutti, and P. Friedlingstein, *Irreversible climate change due to carbon dioxide emissions.* Proceedings of the National Academy of Sciences, 2014. **106**(6): p. 1704-1709.
8. Sadler, T.R., *Carbon Capture and a Commercial Market for CO_2.* Int Adv Econ Res, 2013. **19**: p. 189-200.

9. Lanzafame, P., G. Centi, and S. Perathoner, *Catalysis for biomass and CO_2 use through solar energy: opening new scenarios for a sustainable and low-carbon chemical production.* Chem. Soc. Rev., 2014. **43**: p. 7562-7580.

10. Samanta, A., A. Zhao, G.K.H. Shimizu, P. Sarkar, and R. Gupta, *Post-Combustion CO_2 Capture Using Solid Sorbents: A review.* Industrial & Engineering Chemistry Research, 2012. **51**: p. 1438-1463.

11. Lackner, K.S., S. Brennan, J.M. Matter, A.-H.A. Park, A. Wright, and B. van der Zwaan, *The urgency of the development of CO_2 capture from ambient air.* Proceedings of the National Academy of Sciences, 2012. **109**(33): p. 13156-13162.

12. Hicks, J.C., J.H. Drese, D.J. Fauth, M.L. Gray, G. Qi, and C.W. Jones, *Designing Adsorbents for CO_2 Capture from Flue Gas-Hyperbranched Aminosilicas Capable of Capturing CO_2 Reversibly.* Journal of the American Chemical Society, 2008. **130**(10): p. 2902-2903.

13. Padurean, A., C.-C. Cormos, and P.-S. Agachi, *Pre-combustion carbon dioxide capture by gas–liquid absorption for Integrated Gasification Combined Cycle power plants.* International Journal of Greenhouse Gas Control, 2012. **7**(0): p. 1-11.

14. Kunze, C. and H. Spliethoff, *Assessment of oxy-fuel, pre- and post-combustion-based carbon capture for future IGCC plants.* Applied Energy, 2012. **94**(0): p. 109-116.

15. Veawab, A., A. Aroonwilas, and P. Tontiwachwuthikul, *CO_2 absorption performance of aqueous alkanolamines in packed columns.* Fuel Chemistry Division Reprints, 2002. **47**(1): p. 49-50.

16. Dubois, L. and D. Thomas, *Screening of Aqueous Amine-Based Solvents for Postcombustion CO_2 capture by Chemical Absorption.* Chemical Engineering & Technology, 2012. **35**(3): p. 513-524.

17. Mason, J.A., K. Sumida, Z.R. Herm, R. Krishna, and J.R. Long, *Evaluating metal-organic frameworks for post-combustion carbon dioxide capture via temperature swing adsorption.* Energy & Environmental Science, 2011. **4**(8): p. 3030-3040.

18. Webley, P.A., *Adsorption technology for CO_2 separation and capture: a perspective.* Adsorption, 2014. **20**: p. 225-231.

19. Li, W., P. Bollini, S.A. Didas, S. Choi, J.H. Drese, and C.W. Jones, *Structural Changes of Silica Mesocellular Foam Supported Amine-Functionalized CO_2 Adsorbents Upon Exposure to Steam.* ACS Applied Materials & Interfaces, 2010. **2**(11): p. 3363-3372.

20. Zhang, Z., X. Ma, D. Wang, C. Song, and Y. Wang, *Development of silica-gel-supported polyethylenimine sorbents for CO2 capture from flue gas.* AIChE Journal, 2012. **58**(8): p. 2495-2502.

21. Rezaei, F. and C.W. Jones, *Stability of Supported Amine Adsorbents to SO_2 and NO_x in Postcombustion CO_2 Capture. 2. Multicomponent Adsorption.* Industrial & Engineering Chemistry Research, 2014. **53**(30): p. 12103-12110.

22. Chaikittisilp, W., R. Khunsupat, T.T. Chen, and C.W. Jones, *Poly(allylamine)–Mesoporous Silica Composite Materials for CO_2 Capture from Simulated Flue Gas or Ambient Air.* Industrial & Engineering Chemistry Research, 2011. **50**(24): p. 14203-14210.

23. Chen, Z., S. Deng, H. Wei, B. Wang, J. Huang, and G. Yu, *Polyethylenimine-Impregnated Resin for High CO_2 Adsorption: An Efficient Adsorbent for CO_2 Capture*

from Simulated Flue Gas and Ambient Air. ACS Applied Materials & Interfaces, 2013. **5**(15): p. 6937-6945.

24. Liu, Y., Q. Ye, M. Shen, J. Shi, J. Chen, H. Pan, and Y. Shi, *Carbon Dioxide Capture by Functionalized Solid Amine Sorbents with Simulated Flue Gas Conditions.* Environmental Science & Technology, 2011. **45**(13): p. 5710-5716.

25. McDonald, T.M., W.R. Lee, J.A. Mason, B.M. Wiers, C.S. Hong, and J.R. Long, *Capture of Carbon Dioxide from Air and Flue Gas in the Alkylamine-Appended Metal–Organic Framework mmen-Mg2(dobpdc).* Journal of the American Chemical Society, 2012. **134**(16): p. 7056-7065.

26. McDonald, T.M., D.M. D'Alessandro, R. Krishna, and J.R. Long, *Enhanced carbon dioxide capture upon incorporation of N,N[prime or minute]-dimethylethylenediamine in the metal-organic framework CuBTTri.* Chemical Science, 2011. **2**(10): p. 2022-2028.

27. Demessence, A., D.M. D'Alessandro, M.L. Foo, and J.R. Long, *Strong CO2 Binding in a Water-Stable, Triazolate-Bridged Metal−Organic Framework Functionalized with Ethylenediamine.* Journal of the American Chemical Society, 2009. **131**(25): p. 8784-8786.

28. Schrag, D.P., *Preparing to Capture Carbon.* Science, 2007. **315**(5813): p. 812-813.

29. Faisal, T.F., S. Chevalier, Y. Bernabe, R. Juanes, and M. Sassi, *Quantitative and qualitative study of density driven CO_2 mass transfer in a vertical Hele-Shaw cell.* International Journal of Heat and Mass Transfer, 2015. **81**(0): p. 901-914.

30. Liu, H., Z. Hou, P. Were, Y. Gou, L. Xiong, and X. Sun, *Modelling CO_2-brine-rock interactions in the Upper Paleozoic formations of Ordos Basin used for CO_2 sequestration.* Environmental Earth Sciences, 2015. **73**(5): p. 2205-2222.

31. Lackner, K.S., C.H. Wendt, D.P. Butt, E.L. Joyce Jr, and D.H. Sharp, *Carbon dioxide disposal in carbonate minerals.* Energy, 1995. **20**(11): p. 1153-1170.

32. Lackner, K.S., D.P. Butt, and C.H. Wendt, *Progress on binding CO_2 in mineral substrates.* Energy Conversion and Management, 1997. **38, Supplement**(0): p. S259-S264.

33. Kelemen, P.B. and J. Matter, *In situ carbonation of peridotite for CO_2 storage.* Proceedings of the National Academy of Sciences, 2008. **105**(45): p. 17295-17300.

34. Mervine, E.M., S.E. Humphris, K.W.W. Sims, P.B. Kelemen, and W.J. Jenkins, *Carbonation rates of peridotite in the Samail Ophiolite, Sultanate of Oman, constrained through 14C dating and stable isotopes.* Geochimica et Cosmochimica Acta, 2014. **126**(0): p. 371-397.

35. Preston, C., M. Monea, W. Jazrawi, K. Brown, S. Whittaker, D. White, D. Law, R. Chalaturnyk, and B. Rostron, *IEA GHG Weyburn CO_2 monitoring and storage project.* Fuel Processing Technology, 2005. **86**(14–15): p. 1547-1568.

36. Torp, T.A. and J. Gale, *Demonstrating storage of CO_2 in geological reservoirs: The Sleipner and SACS projects.* Energy, 2004. **29**(9–10): p. 1361-1369.

37. de Coninck, H. and S.M. Benson, *Carbon Dioxide Capture and Storage: Issues and Prospects.* Annual Review of Environment and Resources, 2014. **39**(1): p. 243-270.

38. Centi, G. and S. Perathoner, *Opportunities and prospects in the chemical recycling of carbon dioxide to fuels.* Catalysis Today, 2009. **148**(3–4): p. 191-205.

39. Xiaoding, X. and J.A. Moulijn, *Mitigation of CO2 by Chemical Conversion: Plausible Chemical Reactions and Promising Products.* Energy & Fuels, 1996. **10**(2): p. 305-325.

40. Turner, J., G. Sverdrup, M.K. Mann, P.-C. Maness, B. Kroposki, M. Ghirardi, R.J. Evans, and D. Blake, *Renewable hydrogen production.* International Journal of Energy Research, 2008. **32**(5): p. 379-407.

41. Centi, G., E.A. Quadrelli, and S. Perathoner, *Catalysis for CO_2 conversion: a key technology for rapid introduction of renewable energy in the value chain of chemical industries.* Energy & Environmental Science, 2013. **6**: p. 1711-1731.

42. Hashimoto, K., M. Yamasaki, K. Fujimura, T. Matsui, K. Izumiya, M. Komori, A.A. El-Moneim, E. Akiyama, H. Habazaki, N. Kumagai, A. Kawashima, and K. Asami, *Global CO_2 recycling—novel materials and prospect for prevention of global warming and abundant energy supply.* Materials Science and Engineering: A, 1999. **267**(2): p. 200-206.

43. *Energy Turnaround in the Tank*. 2014 [cited 2014; Available from: http://www.audi.com/com/brand/en/vorsprung_durch_technik/content/2013/10/energy-turnaround-in-the-tank.html#vdt-button-enrich.

44. Tropschuh, P.F. and E. Pham, *Audi Future Energies: Balancing Business and Environmental Concerns*, in *Sustainable Automotive Technologies 2013 Proceedings of the 5th International Conference ICSAT 2013*. 2013, Springer International Publishing. p. 185-190.

45. da Silva, D.C.D., S. Letichevsky, L.E.P. Borges, and L.G. Appel, *The Ni/ZrO_2 catalyst and the methanation of CO and CO_2.* International Journal of Hydrogen Energy, 2012. **37**(11): p. 8923-8928.

46. Van Herwijnen, T., H. Van Doesburg, and W.A. De Jong, *Kinetics of the methanation of CO and CO_2 on a nickel catalyst.* Journal of Catalysis, 1973. **28**(3): p. 391-402.

47. Lunde, P.J. and F.L. Kester, *Carbon Dioxide Methanation on a Ruthenium Catalyst.* Industrial & Engineering Chemistry Process Design and Development, 1974. **13**(1): p. 27-33.

48. Karelovic, A. and P. Ruiz, *Mechanistic study of low temperature CO_2 methanation over Rh/TiO_2 catalysts.* Journal of Catalysis, 2013. **301**(0): p. 141-153.

49. Karelovic, A. and P. Ruiz, *CO_2 hydrogenation at low temperature over $Rh/\gamma\text{-}Al_2O_3$ catalysts: Effect of the metal particle size on catalytic performances and reaction mechanism.* Applied Catalysis B: Environmental, 2012. **113–114**(0): p. 237-249.

50. Deleitenburg, C. and A. Trovarelli, *Metal-Support Interactions in Rh/CeO_2, Rh/TiO_2, and Rh/Nb_2O_5 Catalysts as Inferred from CO_2 Methanation Activity.* Journal of Catalysis, 1995. **156**(1): p. 171-174.

51. Park, J.-N. and E.W. McFarland, *A highly dispersed Pd–Mg/SiO_2 catalyst active for methanation of CO_2.* Journal of Catalysis, 2009. **266**(1): p. 92-97.

52. Schild, C., A. Wokaun, and A. Baiker, *Surface species in CO_2 methanation over amorphous palladium/zirconia catalysts.* Journal of Molecular Catalysis, 1991. **69**(3): p. 347-357.

53. Erdöhelyi, A., M. Pásztor, and F. Solymosi, *Catalytic hydrogenation of CO_2 over supported palladium.* Journal of Catalysis, 1986. **98**(1): p. 166-177.

54. Hwang, S., U.G. Hong, J. Lee, J.G. Seo, J.H. Baik, D.J. Koh, H. Lim, and I.K. Song, *Methanation of carbon dioxide over mesoporous Ni–Fe–Al2O3 catalysts prepared by a coprecipitation method: Effect of precipitation agent.* Journal of Industrial and Engineering Chemistry, 2013(0).

55. Zhou, G., T. Wu, H. Xie, and X. Zheng, *Effects of structure on the carbon dioxide methanation performance of Co-based catalysts.* International Journal of Hydrogen Energy, 2013(0).

56. Srisawad, N., W. Chaitree, O. Mekasuwandumrong, A. Shotipruk, B. Jongsomjit, and J. Panpranot, *CO_2 hydrogenation over Co/Al_2O_3 catalysts prepared via a solid-state reaction of fine gibbsite and cobalt precursors.* Reaction Kinetics, Mechanisms and Catalysis, 2012. **107**(1): p. 179-188.

57. Aksoylu, A.E., A.N. Akin, Z.İ. Önsan, and D.L. Trimm, *Structure/activity relationships in coprecipitated nickel-alumina catalysts using CO_2 adsorption and methanation.* Applied Catalysis A: General, 1996. **145**(1–2): p. 185-193.

58. Falconer, J.L. and A.E. Zağli, *Adsorption and methanation of carbon dioxide on a nickel/silica catalyst.* Journal of Catalysis, 1980. **62**(2): p. 280-285.

59. Cai, M., J. Wen, W. Chu, X. Cheng, and Z. Li, *Methanation of carbon dioxide on Ni/ZrO2-Al2O3 catalysts: Effects of ZrO_2 promoter and preparation method of novel ZrO2-Al2O3 carrier.* Journal of Natural Gas Chemistry, 2011. **20**(3): p. 318-324.

60. Sharma, S., Z. Hu, P. Zhang, E.W. McFarland, and H. Metiu, *CO_2 methanation on Ru-doped ceria.* Journal of Catalysis, 2011. **278**(2): p. 297-309.

61. Song, H., J. Yang, J. Zhao, and L. Chou, *Methanation of Carbon Dioxide over a Highly Dispersed Ni/La2O3 Catalyst.* Chinese Journal of Catalysis, 2010. **31**(1): p. 21-23.

62. Takezawa, N., H. Terunuma, M. Shimokawabe, and H. Kobayashib, *Methanation of carbon dioxide: preparation of Ni/MgO catalysts and their performance.* Applied Catalysis, 1986. **23**(2): p. 291-298.

63. Spinicci, R. and A. Tofanari, *Comparative study of the activity of titania- and silica-based catalysts for carbon dioxide methanation.* Applied Catalysis, 1988. **41**(0): p. 241-252.

64. Chang, F.-W., M.-T. Tsay, and S.-P. Liang, *Hydrogenation of CO_2 over nickel catalysts supported on rice husk ash prepared by ion exchange.* Applied Catalysis A: General, 2001. **209**(1–2): p. 217-227.

65. Borgschulte, A., N. Gallandat, B. Probst, R. Suter, E. Callini, D. Ferri, Y. Arroyo, R. Erni, H. Geerlings, and A. Zuttel, *Sorption enhanced CO_2 methanation.* Physical Chemistry Chemical Physics, 2013. **15**(24): p. 9620-9625.

66. Campbell, T.K. and J.L. Falconer, *Carbon dioxide hydrogenation on potassium-promoted nickel catalysts.* Applied Catalysis, 1989. **50**(1): p. 189-197.

67. Liu, H., X. Zou, X. Wang, X. Lu, and W. Ding, *Effect of CeO_2 addition on Ni/Al2O3 catalysts for methanation of carbon dioxide with hydrogen.* Journal of Natural Gas Chemistry, 2012. **21**(6): p. 703-707.

68. Zhang, Z.L., A. Kladi, and X.E. Verykios, *Effects of Carrier Doping on Kinetic Parameters of CO_2 Hydrogenation on Supported Rhodium Catalysts.* Journal of Catalysis, 1994. **148**(2): p. 737-747.

69. Eckle, S., H.-G. Anfang, and R.J. Behm, *Reaction intermediates and side products in the methanation of CO and CO_2 over supported Ru catalysts in H2-rich reformate gases* J. Phys. Chem. C, 2011. **115**: p. 1361-1367.

70. Yaccato, K., R. Carhart, A. Hagemeyer, A. Lesik, P. Strasser, A.F. Volpe Jr, H. Turner, H. Weinberg, R.K. Grasselli, and C. Brooks, *Competitive CO and CO_2 methanation over*

supported noble metal catalysts in high throughput scanning mass spectrometer. Applied Catalysis A: General, 2005. **296**(1): p. 30-48.

71. Takeishi, K. and K.-i. Aika, *Comparison of carbon dioxide and carbon monoxide with respect to hydrogenation on Raney ruthenium catalysts.* Applied Catalysis A: General, 1995. **133**: p. 31-45.

72. Marwood, M., R. Doepper, and A. Renken, *In-situ surface and gas phase analysis for kinetic studies under transient conditions The catalytic hydrogenation of CO_2.* Applied Catalysis A: General, 1997. **151**: p. 223-246.

73. Marwood, M., R. Doepper, M. Prairie, and A. Renken, *Transient DRIFT Spectroscopy for the Determination of the Surface Reaction Kinetics of CO_2 Methanation.* Chemical Engineering Science, 1994. **49**(24A): p. 4801-4809.

74. Prairie, M.R., A. Renken, J.G. Highfield, K.R. Thampi, and M. Gratzel, *A Fourier Transform Infrared Spectroscopic Study of CO_2 Methanation on Supported Ruthenium.* Journal of Catalysis, 1991. **129**: p. 130-144.

75. Prairie, M.R., J.G. Highfield, and A. Renken, *Diffuse-Reflectance FTIR Spectroscopy for Kinetic and Mechanistic Studies of CO_2 Hydrogenation in a Continuous Recycle Reactor.* Chemical Engineering Science, 1991. **46**(1): p. 113-121.

76. Tada, S., O.J. Ochieng, R. Kikuchi, T. Haneda, and H. Kameyama, *Promotion of CO_2 methanation activity and CH4 selectivity at low temperatures over $Ru/CeO_2/Al_2O_3$ catalysts.* International Journal of Hydrogen Energy, 2014. **39**: p. 10090-10100.

77. Kuśmierz, M., *Kinetic study on carbon dioxide hydrogenation over $Ru/\gamma\text{-}Al_2O_3$ catalysts.* Catalysis Today, 2008. **137**(2-4): p. 429-432.

78. Jimenez, V., P. Sanchez, P. Panagiotopoulou, J.L. Valverde, and A. Romero, *Methanation of CO, CO_2 and selective methanation of CO, in mixtures of CO and CO_2, over ruthenium carbon nanofibers catalysts.* Applied Catalysis A: General, 2010. **390**: p. 35-44.

79. Marwood, M., F.V. Vyve, R. Doepper, and A. Renken, *Periodic operation applied to the kinetic study of CO_2 methanation.* Catalysis Today, 1994. **20**: p. 437-448.

80. Veselovskaya, J.V., V.S. Derevschikov, T.Y. Kardash, O.A. Stonkus, T.A. Trubitsina, and A.G. Okunev, *Direct CO_2 capture from ambient air using K_2CO_3/Al_2O_3 composite sorbent.* International Journal of Greenhouse Gas Control, 2013. **17**: p. 332-340.

81. Derevschikov, V.S., J.V. Veselovskaya, T.Y. Kardash, D.A. Trubitsyn, and A.G. Okunev, *Direct CO2 capture from ambient air using K_2CO_3/Y_2O_3 composite sorbent.* Fuel, 2014. **127**: p. 212-218.

82. Xie, Y., T.-T. Wang, X.-H. Liu, K. Zou, and W.-Q. Deng, *Capture and conversion of CO_2 at ambient conditions by a conjugated microporous polymer.* Nature Communications, 2013. **4**: p. 1-7.

83. Yang, Z.-Z., L.-N. He, J. Gao, A.-H. Liu, and B. Yu, *Carbon dioxide utilization with C-N bond formation: carbon dioxide capture and subsequent conversion.* Energy & Environmental Science, 2012. **5**: p. 6602-6639.

84. Bhatia, S.K. and D.D. Perlmutter, *Effect of the product layer on the kinetics of the CO_2-lime reaction.* AIChE Journal, 1983. **29**(1): p. 79-86.

85. Belova, A.A.G., T.M. Yegulalp, and C.T. Yee, *Feasibility study of In Situ CO_2 capture on an integrated catalytic CO_2 sorbent for hydrogen production from methane.* Energy Procedia, 2009. **1**(1): p. 749-755.

86. Gruene, P., A.G. Belova, T.M. Yegulalp, R.J. Farrauto, and M.J. Castaldi, *Dispersed Calcium Oxide as a Reversible and Efficient CO_2-Sorbent at Intermediate Temperatures.* Industrial & Engineering Chemistry Research, 2011. **50**: p. 4042-4049.

87. Duyar, M.S., R.J. Farrauto, M.J. Castaldi, and T.M. Yegulalp, *In Situ CO_2 Capture Using CaO/γ-Al_2O_3 Washcoated Monoliths for Sorption Enhanced Water Gas Shift Reaction.* Industrial & Engineering Chemistry Research, 2014. **53**(3): p. 1064-1072.

88. Galletti, C., S. Specchia, G. Saracco, and V. Specchia, *CO-selective methanation over Ru–γAl2O3 catalysts in H2-rich gas for PEM FC applications.* Chemical Engineering Science, 2010. **65**(1): p. 590-596.

89. Panagiotopoulou, P., D.I. Kondarides, and X.E. Verykios, *Selective methanation of CO over supported Ru catalysts.* Applied Catalysis B: Environmental, 2009. **88**(3–4): p. 470-478.

90. Panagiotopoulou, P., D.I. Kondarides, and X.E. Verykios, *Selective methanation of CO over supported noble metal catalysts: Effects of the nature of the metallic phase on catalytic performance.* Applied Catalysis A: General, 2008. **344**: p. 45-54.

91. Solymosi, F., A. Erdohelyi, and M. Kocsis, *Methanation of CO_2 on Supported Ru Catalysts.* Journal of the Chemical Society, Faraday Transactions 1, 1981. **77**(1003-1012).

92. Zagli, E. and J.L. Falconer, *Carbon Dioxide Adsorption and Methanation on Ruthenium.* Journal of Catalysis, 1981. **69**: p. 1-8.

93. Panagiotopoulou, P., D.I. Kondarides, and X.E. Verykios, *Mechanistic Study of the Selective Methanation of CO over Ru/TiO_2 Catalyst: Identification of Active Surface Species and Reaction Pathways.* Journal of Physical Chemistry, 2011. **115**: p. 1220-1230.

94. Shalabi, M.A., S.A. Zaidi, and M.A. Al-Saleh, *EFFECT OF REDUCTION CONDITIONS ON THE ACTIVITY OF Ni/γAl_2O_3 CATALYST FOR METHANATION REACTION.* Chemical Engineering Communications, 1997. **157**(1): p. 23-33.

95. Altiokka, M.R. and A. Citak, *Kinetics study of esterification of acetic acid with isobutanol in the presence of amberlite catalyst.* Applied Catalysis A: General, 2003. **239**: p. 141-148.

96. Graaf, G.H., E.J. Stamhuis, and A.A.C.M. Beenackers, *Kinetics of low-pressure methanol synthesis.* Chemical Engineering Science, 1988. **43**(12): p. 3185-3195.

97. Brooks, K.P., J. Hu, H. Zhu, and R.J. Kee, *Methanation of carbon dioxide by hydrogen reduction using the Sabatier process in microchannel reactors.* Chemical Engineering Science, 2007. **62**: p. 1161-1170.

98. Lunde, P.J. and F.L. Kester, *Rates of methane formation from carbon dioxide and hydrogen over a ruthenium catalyst.* Journal of Catalysis, 1973. **30**(3): p. 423-429.

99. De Saint Jean, M., P. Baurens, and C. Bouallou, *Parametric study of an efficient renewable power-to-substitute-natural-gas process including high-temperature steam electrolysis.* International Journal of Hydrogen Energy, 2014. **39**: p. 17024-17039.

100. Stevens Jr, R.W., A. Shamsi, S. Carpenter, and R. Siriwardane, *Sorption-enhanced water gas shift reaction by sodium-promoted calcium oxides.* Fuel, 2010. **89**(6): p. 1280-1286.

101. Lee, K.B., M.G. Beaver, H.S. Caram, and S. Sircar, *Reversible Chemisorbents for Carbon Dioxide and Their Potential Applications.* Industrial & Engineering Chemistry Research, 2008. **47**(21): p. 8048-8062.

102. Munera, J., B. Faroldi, E. Frutis, E. Lombardo, L. Cornaglia, and S.G. Carrazan, *Supported Rh nanoparticles on CaO-SiO2 binary systems for the reforming of methane*

by carbon dioxide in membrane reactors. Applied Catalysis A: General, 2014(474): p. 114-124.

103. Rynkowski, J., T. Paryjczak, A. Lewicki, M.I. Szynkowska, T.P. Maniecki, and W.K. Jozwiak, *Characterization of Ru/CeO_2-Al_2O_3 catalysts and their performance in CO_2 methanation.* React. Kinet. Catal. Lett., 2000. **71**(1): p. 55-64.

104. Janke, C., M.S. Duyar, M. Hoskins, and R. Farrauto, *Catalytic and adsorption studies for the hydrogenation of CO_2 to methane.* Applied Catalysis B: Environmental, 2014. **152-153**: p. 184-191.

105. Wang, J., L. Huang, R. Yang, Z. Zhang, J. Wu, Y. Gao, Q. Wang, D. O'Hare, and Z. Zhong, *Recent advances in solid sorbents for CO_2 capture and new development trends.* Energy & Environmental Science, 2014(7): p. 3478-3518.

106. Beuls, A., C. Swalus, M. Jacquemin, G. Heyen, A. Karelovic, and P. Ruiz, *Methanation of CO_2: Further insight into the mechanism over Rh/γ-Al_2O_3 catalyst.* Applied Catalysis B: Environmental, 2012. **113-114**: p. 2-10.

107. Jacquemin, M. and P. Ruiz, *Catalytic production of methane from CO_2 and H_2 at low temperature: Insigth on the reaction mechanism.* Catalysis Today, 2010. **157**: p. 462-466.

Appendix: List of Publications

Duyar, M.S., Ramachandran, A., Wang, C., Farrauto, R.J. (2015). Kinetics of catalytic CO_2 methanation over Ru/γ-Al_2O_3 and implications for renewable energy storage applications. - Submitted to Applied Catalysis B: Environmental, in review

Duyar, M.S., Arellano-Trevino, M.A., and Farrauto, R.J. (2015). Dual function materials for CO_2 capture and conversion to synthetic natural gas using renewable hydrogen. *Applied Catalysis B: Environmental, 168,* 370-376.

Janke, C., **Duyar, M.S.,** Hoskins, M., & Farrauto, R. (2014). Catalytic and adsorption studies for the hydrogenation of CO_2 to methane. *Applied Catalysis B: Environmental, 152-153*, 184-191.

Duyar, M.S., Farrauto, R.J., Castaldi, M.J. and Yegulalp, T.M. (2014). In-Situ CO_2 Capture Using CaO/γ-Al_2O_3 Washcoated Monoliths for Sorption Enhanced Water Gas Shift Reaction. *Industrial & Engineering Chemistry Research* 53(3), 1064-1072.